EFFECTS OF SYSTEM CYCLING, EVAPORATOR AIRFLOW, AND

CONDENSER COIL FOULING ON THE PERFORMANCE OF RESIDENTIAL

SPLIT-SYSTEM AIR CONDITIONERS

A Thesis

by

JEFFREY BRANDON DOOLEY

Submitted to the Office of Graduate Studies of
Texas A&M University
in partial fulfillment of the requirements for the degree of

MASTER OF SCIENCE

December 2004

Major Subject: Mechanical Engineering

EFFECTS OF SYSTEM CYCLING, EVAPORATOR AIRFLOW, AND CONDENSER COIL FOULING ON THE PERFORMANCE OF RESIDENTIAL SPLIT-SYSTEM AIR CONDITIONERS

A Thesis

by

JEFFREY BRANDON DOOLEY

Submitted to Texas A&M University
in partial fulfillment of the requirements
for the degree of

MASTER OF SCIENCE

Approved as to style and content by:

Dennis L. O'Neal (Chair of Committee)	John A. Bryant (Member)
Charles H. Culp (Member)	Dennis L. O'Neal (Head of Department)

December 2004

Major Subject: Mechanical Engineering

ABSTRACT

Effects of System Cycling, Evaporator Airflow, and Condenser Coil Fouling on the

Performance of Residential Split-System Air Conditioners. (December 2004)

Jeffrey Brandon Dooley, B.S., Texas A&M University

Chair of Advisory Committee: Dr. Dennis L. O'Neal

Three experimental studies were conducted to quantify the effects of system cycling, evaporator airflow, and condenser coil fouling on the performance of residential air conditioners. For all studies, the indoor dry-bulb (db) temperature was 80°F (26.7°C) db. The cycling study consisted of twelve transient tests conducted with an outdoor temperature of 95°F (35°C) db for cycle times of 6, 10, 15, and 24 minutes. Indoor relative humidities of 40%, 50%, and 60% were also considered. The evaporator airflow study consisted of twenty-four steady-state tests conducted with an indoor condition of 67°F (19.4°C) wet-bulb (wb) for evaporator airflows ranging from 50% below to 37.5% above rated airflow. Outdoor temperatures of 85°F (29.4°C) db, 95°F (35°C) db, and 105°F (40.6°C) db were also considered. The coil fouling study used a total of six condensers that were exposed to an outdoor environment for predetermined amounts of time and tested periodically. Three of the condensers were cleaned and retested during the periodic testing cycles. Testing consisted of thirty-three steady-state tests conducted with an indoor condition of 67°F (19.4°C) wb for outdoor exposure times of 0, 2000, 4000, and 8000 hours. Outdoor temperatures of 82°F (27.8°C) db and 95°F (35°C) db were also considered.

The results of the cycling study indicated that cycle time did not significantly affect the instantaneous dehumidification performance of the test air conditioner. Absolute dehumidification began 3 to 30 seconds after startup and net positive dehumidification began 5 to 55 seconds after startup, depending on indoor humidity conditions. Cyclic total and latent capacity and cyclic coefficient of performance (COP) decreased with increasing cycle time. Cyclic sensible capacity and cyclic sensible heat factor (SHF) increased with cycle time. Results of the evaporator airflow study indicated that SHF, total capacity, and sensible capacity increased with airflow. Latent capacity decreased with increasing airflow. In general, efficiency was not affected by evaporator airflow. The results of the coil fouling study indicated that outdoor runtime did not significantly affect the performance of the test units. Cleaning consistently improved performance and efficiency, but the benefit in each case was small and statistically insignificant.

TABLE OF CONTENTS

TABLE OF CONTENTS (Continued)

TABLE OF CONTENTS (Continued)

Page

LIST OF FIGURES

LIST OF FIGURES (Continued)

LIST OF FIGURES (Continued)

LIST OF TABLES

LIST OF TABLES (Continued)

LIST OF TABLES (Continued)

TABLE   Page

CHAPTER I

INTRODUCTION

In hot and humid climates, the use of air conditioning systems account for approximately 10% of the total energy consumed in the residential sector (EIA, 1999). With the rising cost of energy, many homeowners appreciate the benefits of owning energy efficient appliances. Today, residential air conditioners are more efficient than ever, using 30% to 50% less energy to produce the same amount of cooling as air conditioners manufactured in the 1970s (DOE, 1999). If even the most efficient systems have not been properly installed or maintained, operation at peak efficiency will likely not occur. This can ultimately lead to greater energy consumption, negating the potential benefits of owning a high efficiency air conditioner. The benefits associated with properly installing and maintaining residential air conditioning systems include better comfort control in the conditioned space and prolonged life of the air conditioning equipment.

Common air conditioning performance parameters such as the energy efficiency ratio (EER), sensible heat factor (SHF), and overall system capacity can be measured using standard steady-state tests in controlled environmental conditions (ARI, 2003). While these performance parameters provide a convenient way of rating and comparing residential air conditioners, they do not necessarily provide an accurate indication of how a system will perform in the field. In practice, most residential air conditioners are designed to cycle off and on in response to the cooling required by the residence. If a system is configured properly and in good operating condition, the length of a given on-

---

The format of this thesis conforms to that of the *ASHRAE Transactions.*

cycle will be just long enough to provide the minimum amount of sensible and latent cooling needed to maintain a space at a set condition. However, if a system cycles too frequently or not frequently enough, drops in performance, efficiency, and comfort level can occur. The transient variations in the instantaneous sensible and latent capacities during startup can affect the ability of a system to cool and dehumidify conditioned air over the course of a cycle. Current test procedures provide a way to quantify performance variables that account for the overall loss in efficiency of a system due to cycling, but these variables do not differentiate between sensible and latent capacities during startup (ARI, 2003).

The overall performance of an air conditioning system depends strongly on the performance of its individual components. Improperly configured evaporators can be a source of inefficiencies in an air conditioning system. Of particular interest is the airflow rate over the evaporator coil. The airflow rate through an evaporator can affect both the sensible and latent cooling capacities of an air conditioner, which, in turn, can affect the overall system efficiency.

The condition of the condenser can also affect the performance of an air conditioner. Unlike the indoor evaporator, the condenser is directly exposed to unfiltered outdoor air and is subject to fouling. Fouling can often be observed on the coil surfaces in the form of clogging and galvanic corrosion. Left untreated, debris can reduce airflow over the coils and hinder the heat transfer processes required for the proper operation of a condenser. Such occurrences can lead directly to an overall decrease in the capacity and efficiency of an air conditioning system.

The purpose of this research is to experimentally quantify the effects of cycling, evaporator airflow, and condenser coil fouling on the performance of split-system residential air conditioners. The variables used to quantify and compare the performance of the systems are sensible and latent capacity, overall capacity, energy efficiency ratio (EER), sensible heat factor (SHF), cyclic SHF, cyclic coefficient of performance (COP), moisture removal rate, and total moisture removed. For the cycling experiments, the independent variables include the run time of the cycles and the humidity of the indoor environment. For the evaporator airflow experiments, the independent variables are the airflow rate through the evaporator unit and the temperature of the outdoor environment. For the condenser coil fouling experiments, the independent variable is the time the coils are exposed to an outdoor environment.

Of particular interest for the cycling experiments is the instantaneous dehumidification capacity of the air conditioner during transient startup. Various studies have been performed to investigate the operating characteristics of air conditioners during the startup period (Murphy and Goldschmidt, 1984; Mulroy and Didion, 1985; Katipamula, 1989; Judge and Radermacher, 1995; Kim and Bullard, 2001; Henderson, Shirey, and Raustad, 2003). However, the majority of the research reviewed for this study focused on the refrigerant dynamics associated with transient startup. Only two studies focused on the effects of startup on dehumidification capacity, but one studied a heat pump and the other presented mostly field measurements of residential air conditioners. Several investigators have studied the overall performance of air conditioners under reduced evaporator airflow (Palani, O'Neal, and Haberl, 1992; Rodriguez, O'Neal, Davis, and Kondepudi, 1996; Wheeler, 2003). Of the literature reviewed, there is a lack of data that quantifies the sensible and latent capacities of

systems over a broad range of evaporator airflow rates, particularly excessive airflow rates. Also, some research has been conducted that focuses on the fouling of heat exchangers typically encountered in heating, ventilating, and air conditioning (HVAC) applications (Greig, 1998; Muyshondt, Nutter, and Gordon, 1998; Siegel and Nazaroff, 2002). But of those reviewed, all investigations focused on the deposition mechanisms of small particles on heat exchanger surfaces and none quantified the effects of coil fouling on system performance. The research for this thesis addresses these issues by providing the experimental data and subsequent analyses necessary to understand the effects of system cycling, evaporator airflow, and condenser coil fouling on the performance of residential air conditioning systems.

The details of this research are provided in eight chapters. Chapter II presents a literature review, followed by a detailed explanation of the experimental apparatus and the experimental procedure in Chapters III and IV, respectively. The results of the cycling experiments are presented in Chapter V, those of the evaporator airflow experiments in Chapter VI, and those of the condenser coil fouling experiments in Chapter VII. Chapter VIII includes the summary and conclusions in addition to recommendations for future work.

CHAPTER II

LITERATURE REVIEW

The typical residential split system air conditioner consists of four main components: a compressor, an outdoor heat exchanger section (a condenser), an expansion device, and an indoor heat exchanger section (an evaporator). The placement of these components in a typical residential air conditioner is shown in the cycle of Figure 2.1.
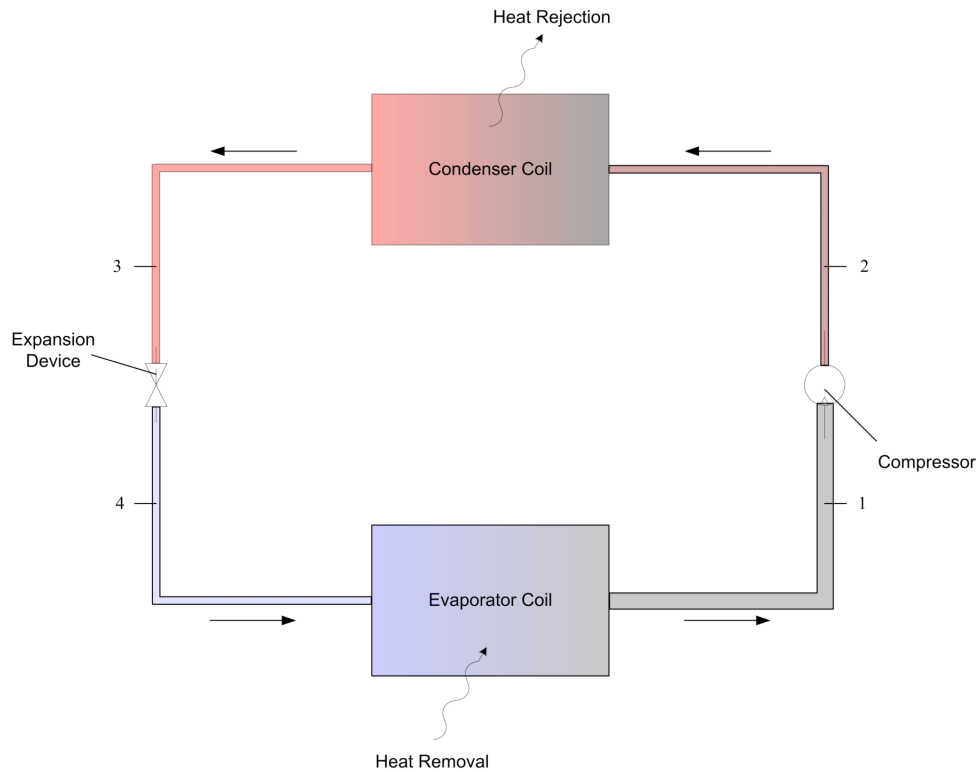
Figure 2.1 – Schematic of a Conventional Air Conditioning Cycle and Major System Components.

The thermodynamic processes for the refrigerant-side of the cycle in Figure 2.1 are shown on the pressure-enthalpy diagram of Figure 2.2.
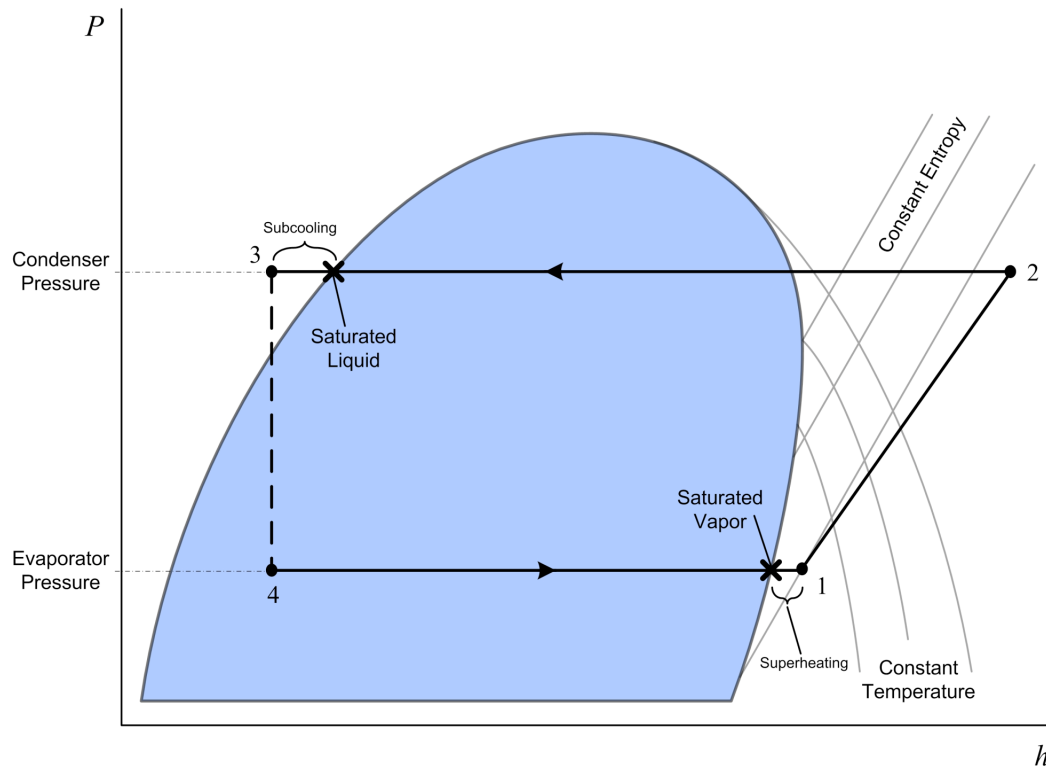
Figure 2.2 – Pressure-Enthalpy Diagram for the Cycle Shown in Figure 2.1.

The processes between the state points shown in Figure 2.2 are as follows:

- Process 1-2: superheated refrigerant vapor at the evaporator pressure is compressed to superheated vapor at the condenser pressure.

- Process 2-3: superheated vapor is condensed into subcooled liquid at constant pressure.

- Process 3-4: subcooled liquid is throttled to a saturated liquid-vapor mixture at the evaporator pressure.

- Process 4-1: two-phase refrigerant is evaporated and superheated at constant pressure.

Superheating or subcooling occurs when the refrigerant temperature rises above or falls below the saturation temperature at the local pressure, respectively. This is shown in Figure 2.2 as the departure of states 1 and 3 from the saturation dome.

During normal operation, the evaporator provides two functions: the transfer of heat energy from the warmer indoor air to the cooler two-phase refrigerant (sensible cooling) and the dehumidification of the indoor air by condensation (latent cooling) on the cold evaporator coil surface. The evaporator is often designed so that the refrigerant leaving this section has a small degree of superheating. The sensible heat energy removed from the indoor air, along with additional heat energy from the energy input into the compressor, is rejected from the superheated refrigerant to the outdoor environment through the condenser coil. A fan is typically used to move air across the evaporator coil and throughout the indoor ductwork. A fan is also used in the condenser to increase heat transfer from the coil to the outdoor environment. Aside from the compressor, the condenser and evaporator coils are the major cost items in a system and they often take up the most space (McQuiston *et al.,* 2000).

SYSTEM CYCLING AND DEHUMIDIFICATION CAPACITY

In normal operation, most residential air conditioners will cycle on and off in response to the cooling load of the residence. The length of time between cycles can vary from a few minutes up to an hour or more. Cycle time depends on several factors, including operator settings, indoor, and outdoor conditions. During steady-state operation, the evaporator continuously removes moisture from the conditioned air stream as long as the evaporator coil surface temperature is below the air dew point temperature. When a system is shut off, dehumidification stops as airflow over the coil

ceases and the surface temperature of the coil increases above the air dew point temperature. Immediately after shut-off, the coil is not dry; in fact, the last bit of moisture that was condensed out of the air stream during the previous cycle can remain on the surface of the coil for quite some time after the unit is shut off (Katipamula, 1989). Unless the air conditioner remains off for a prolonged period of time (many hours or longer) the evaporator coil will likely be partially wet when the system starts up again (Henderson *et al.*, 2003). When airflow is reestablished through the evaporator at the onset of the next cycle, this retained moisture can be evaporated by the air stream and transported throughout the ductwork. This process of "re-evaporation" will occur until the surface temperature of the coil has once again fallen below the air dew point temperature or all of the moisture has been evaporated from the coil surface. Until one of the aforementioned occurs, the net effect of the air conditioner is *humidification* of the space. Any useful dehumidification is delayed until the air conditioner can remove the moisture that has been "re-evaporated" back into the space during start-up.

Investigating the cyclic behavior of air conditioning systems continues to be an area of ongoing research. Many investigators have focused on the overall system performance resulting from the refrigerant dynamics associated with the start-up and shut-down of a system. Murphy and Goldschmidt (1984) showed that refrigerant migration from the condenser to the evaporator caused noticeable power differences and capacity losses immediately after start-up. They also noted that this migration of refrigerant contributed to heating in the evaporator coil during the off-cycle and the thermal mass of the evaporator coil was observed to be an important factor in the start-up performance of the system. Similarly, experimental work by Mulroy and Didion (1985) indicated that immediately following start-up, the overall capacity of a generic

split system with an accumulator was seen to be comparable to its steady-state capacity. According to their interpretation, the rapid boiling of refrigerant in the evaporator immediately after startup results in near steady-state capacity. They also pointed out that as soon as this refrigerant leaves the evaporator coil following start-up, the overall capacity drops accordingly since the expansion device inherently prevents the immediate replenishment of refrigerant in the coil. Judge and Radermacher (1995) studied the transient and steady-state performance of two common refrigerants and showed that as the compressor discharge pressure increased, their test system reached steady-state capacity faster.

Kim and Bullard (2001) showed that the transient cooling capacity and coefficient of performance (COP) of a residential split system could be mathematically represented as a combination of two exponential functions of time. Results of their experimentation showed that the latent capacity of their test system was negative during the first one to two minutes of start-up. Katipamula (1989) developed a model for analyzing the cyclic performance degradation of a standard single speed heat pump in cooling mode. Results of his experimental work showed that the moisture removal rate reached steady-state faster with increasing indoor relative humidity. Henderson *et al.* (2003) presented laboratory and field results that characterized the part-load dehumidification performance of residential air conditioners. They showed that the sensible heat factor (SHF) decreased for increasing cycle run-time fractions in systems operating in the AUTO fan mode (i.e. evaporator fans that cycle on and off with the compressor).

EVAPORATOR AIRFLOW

Improper airflow through the evaporator can result in system inefficiencies. Airflow can be adjusted in residential evaporators that have fans with multiple speed settings. A properly configured evaporator will employ a fan speed setting that yields an airflow rate which provides the right balance between the sensible and latent cooling required for comfort. For airflow rates that are lower than the rated airflow, the sensible capacity of the system can decrease while the latent capacity can increase. For airflow rates that are excessively low, much of the surface of the evaporator coil can become saturated with condensed water, impeding airflow over the coil. Conversely, airflow rates that are higher than the rated airflow may increase the sensible capacity, but lower the latent capacity. For airflow rates that are excessively high, there may be little or no dehumidification (Wheeler, 2003).

Several researchers have studied the effects of evaporator airflow on the overall performance of air conditioners. However, of the studies reviewed, all have focused on how a reduction in evaporator airflow affects overall system performance. Palani *et al.* (1992) quantified the effect of reduced evaporator airflow on the coefficient of performance (COP) and the overall capacity of a standard residential air conditioner. They showed that for a 50% and 75% reduction in evaporator airflow, the overall system capacity can drop by as much as 15% and 45%, respectively. One conclusion from their analysis was that to maintain a reasonable amount of cooling, an evaporator should operate with at least 50% of the rated airflow. Rodriguez *et al.* (1996) showed that the high temperature performance of residential sized air conditioners is similarly affected by reductions in evaporator airflow. Their study showed that a 50% drop in evaporator airflow decreased overall capacity and SHF by 15% and 7%, respectively. A qualitative

analysis by Wheeler (2003) discussed the implications of excessive airflow in the evaporator. He explained that for airflow rates higher than the rated airflow, overall capacities can drop and moisture present on the coil can be blown off. He added that condensate blowoff can cause microbial growth in adjoining downstream ductwork, decreasing indoor air quality.

CONDENSER COIL FOULING

The coils of most condensing units consist of horizontal refrigerant tubes attached to sequential thin vertical plate fins. These thin fins increase the heat transfer area between the refrigerant and the outdoor environment. The refrigerant tubes are often made from copper and the plate fins from aluminum. Under normal circumstances, a condenser will operate in a harsher environment than an evaporator. Since condensers are usually located outdoors, the coils are subject to contamination by dirt and debris. Corrosive degradation of the copper-aluminum bonds and the fin surfaces can also occur (Greig, 1998). In many unitary residential applications, the condenser is often located near the residence lawn or a bedded area where it will be exposed to a wide assortment of contaminants. These contaminants may include biological particles and spores from submicron size all the way up to grass clippings and trash at the macroscopic level.

Although the condenser fan enhances heat transfer, it also draws airborne contaminants deep into the coil where they can deposit on the surface of the fins and tubes. The buildup of these contaminants is commonly referred to as fouling and it can reduce heat transfer by insulating the fins and restricting airflow. Deterioration of the coil surface by corrosion can also reduce heat transfer due to increases in thermal contact

resistance at the copper-aluminum bonds. The net results include higher discharge pressures and higher electrical power consumption for the compressor, decreased capacity, and decreased efficiency.

Theoretical models have been proposed that predict particle deposition on heat exchanger surfaces. Siegel and Nazaroff (2002) explored various mechanisms that cause contaminant deposition on plate fin and tube heat exchanger surfaces, including impaction, diffusion, gravitational settling, and deposition resulting from turbulence effects. Their study considered heat exchangers used in heating, ventilating, and air conditioning (HVAC) systems with coil fin densities ranging between 6 to 18 fins/inch (2.4 to 7.1 fins/cm) and particles with an aerodynamic diameter ranging from 1 to 100 μm. They noted that the factors affecting the probability of a given particle depositing on the surface of the coil includes the size of the particle, the fin density (spacing), and the surface characteristics of the refrigerant tubes and plate fins.

Computer models have been developed to predict particulate deposition on heat exchanger surfaces. Muyshondt *et al.* (1998) utilized a computational fluid dynamics code to numerically model particle deposition on HVAC heat exchangers. They used a 45,008-point three-dimensional mesh to simulate a simplified plate fin and tube coil and considered fin densities between 10 and 14 fins/inch (3.9 and 5.5 fins/cm). Their simulations showed that coil orientation can have a significant impact on fouling potential, with horizontal coils experiencing up to 50% more deposition than vertical coils. They also concluded that fouling potential was less sensitive to fin density and air velocity.

SUMMARY OF LITERATURE REVIEW

  Several conclusions can be drawn from the literature review:

1. Refrigerant migration in the off-cycle can cause capacity losses immediately after start-up.

2. The thermal mass of the evaporator coil plays an important role in the transient performance of an air conditioner.

3. The discharge pressure and type of expansion device can affect the time it takes a system to reach steady-state.

4. Moisture removal rate reaches steady-state faster with increasing indoor relative humidity.

5. Systems operating the in AUTO fan mode are subject to latent degradation at part load conditions.

6. Low evaporator airflow can reduce the overall capacity and efficiency of an air conditioner.

7. High evaporator airflow may reduce the latent capacity of an air conditioner.

8. Fin density (spacing) and orientation can significantly affect the fouling potential of coils.

  Although a number of researchers have studied the transient behavior of air conditioners, most have focused on refrigerant dynamics. Two of the studies reviewed considered the effects of cycling on dehumidification performance, but one was for an older heat pump with a thermostatic expansion valve (TXV) and a reciprocating compressor. The other study presented little data for part-load dehumidification performance in the AUTO fan mode and did not report the specifications of the

experimental apparatus. Only one qualitative analysis was reviewed that discussed the effects of excessive evaporator airflow on performance. All literature reviewed pertaining to coil fouling explored various fouling mechanisms, but no quantitative analyses were reviewed that addressed the effects of condenser coil fouling and degradation on system performance. Further studies are required to enhance the understanding of the three areas considered in this literature review. Therefore, the present study was conducted to quantify:

1. the effects of cycling on the dehumidification performance of a modern air conditioner with an orifice expansion device and a scroll compressor,

2. the effects of low and high evaporator airflow on overall performance, and

3. the effects of coil fouling on overall performance.

CHAPTER III

EXPERIMENTAL APPARATUS

Three main objectives for this research were to quantify:

1. the effects of cyclical operation on the dehumidification capacity of a system,

2. the effects of evaporator airflow on overall system performance, and

3. the effects of condenser coil fouling and degradation on system performance.

The experimental apparatus used to accomplish these objectives consisted of four main components: (1) psychrometric rooms, (2) test air conditioners, an (3) outdoor runtime area, and (4) instrumentation and data acquisition. A detailed breakdown of each component of the experimental apparatus is presented below.

PSYCHROMETRIC ROOMS

The experiments were conducted in the psychrometric facilities of the Energy Systems Laboratory at Texas A&M University. These facilities consisted of two insulated and equally sized adjacent rooms. As shown in Figure 3.1, one room served as the test area for indoor air conditioner components while the other served the same purpose for outdoor equipment. The wet and dry bulb air temperature could be maintained to within ± 0.2°F (± 0.11°C) of a set condition in each room. These rooms were designed to test systems with capacities of up to 10 tons (105.5 kW).

Testing conditions in each room were maintained by a control system, which called upon a combination of cooling, heating, and humidity control equipment. Cooling in each room was provided by a 70 ton (738.5 kW) chiller and a 1000 gallon (3.79 m^3)
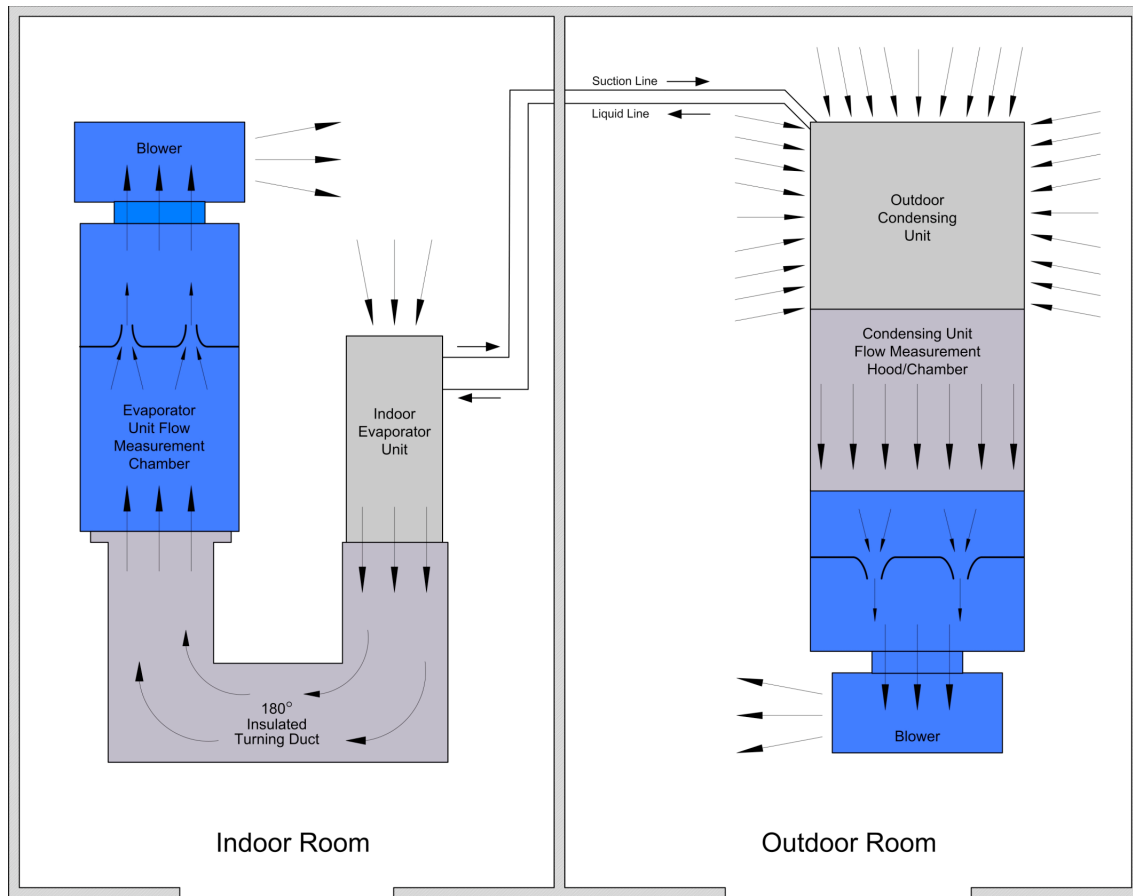
Figure 3.1 – General Layout of the Psychrometric Rooms.

insulated ethylene glycol tank. Chilled glycol was routed through a set of primary

cooling coils in the overhead ductwork of each room. Heating was provided with four

banks of 9.9 kW electrical resistance heaters located in the overhead ductwork.

Dehumidification was achieved with a set of secondary chilled glycol coils or by a

rotating drum air desiccant dehumidifier. Humidification was provided by an electric

steam generator that injected 15 psig (2.05 bar) steam into the overhead ductwork of

each room. The capacity of each cooling and dehumidification coil was controlled by

adjusting the glycol flow rate through each coil. Glycol was supplied to each coil

through an independent circuit and the flow rate was controlled by variable speed pumps. The electrical resistance heaters were controlled by a bank of electrical contactors and the humidifying steam was controlled by a set of electronic valves.

TEST AIR CONDITIONERS

The cycling and evaporator airflow experiments were conducted with one standard three ton (10.5 kW) split-system residential air conditioner consisting of a condenser with a scroll compressor and a factory-matched evaporator with a fixed orifice expansion device. The condenser coil fouling study used a total of six condensers divided into three groups, with each group consisting of two units that were identical in brand, make, and model. Each group was comprised of units made by a different manufacturer. A naming convention of groups A, B, and C was used, with each group consisting of a #1 unit and #2 unit. All six units were rated at three tons (10.5 kW) and were otherwise comparably rated. All testing was completed using the same evaporator and expansion device as used in the cycling and evaporator airflow experiments. More detailed specifications on the evaporator and condensing units used in this research can be found in Table 3.1. Note that unit D represents the condensing unit used in the cycling and evaporator airflow experiments; it is identical to units A.

OUTDOOR RUNTIME AREA

An outdoor area was created where the six condensers used in the coil fouling study could experience fouling and degradation in an actual outdoor environment. The intention was to provide an environment where occurrences brought about by seasonal weather conditions and routine lawn maintenance could contribute to the coil fouling process. A 15 by 76 foot (4.57 by 23.2 m) section at the south end of the Riverside

Table 3.1 – Selected Specifications for Test Air Conditioners.

Specification	Evaporator Unit			
Expansion Device	0.071 inch (1.8 mm) Orifice			
Evaporator Coil Type	Plate Fin			
Evaporator Coil Configuration	Diagonal Updraft			
Testing Orientation	Horizontal Left			
Evaporator Coil Density, fins/in. (fins/cm)	14 (5.51)			
Evaporator Coil Face Area, ft^2 (m^2)	2.86 (0.266)			
Rated Evaporator Fan Power, hp (kW)	1/3 (0.25)			
Rated Evaporator Airflow, ft^3/min (m^3/min)	1200 (34)			
------------------------------------	Condensing Unit			
Specification	**Unit A**	**Unit B**	**Unit C**	**Unit D**
	1 **2**	**1** **2**	**1** **2**	--------
Nominal Capacity, tons (kW)	3 (10.5)	3 (10.5)	3 (10.5)	3 (10.5)
Compressor Type	Scroll	Scroll	Scroll	Scroll
Condenser Coil Fin Type	Pin	Plate	Plate	Pin
Condenser Coil Density, fins/in. (fins/cm)	24 (9.45)	25 (9.84)	22 (8.66)	24 (9.45)
Condenser Coil Face Area, ft^2 (m^2)	15.86 (1.47)	14.90 (1.38)	11.41 (1.06)	15.86 (1.47)
Condenser Fan Capacity ft^3/min (m^3/min)	2500 (70.8)	2800 (79.3)	2510 (71.1)	2500 (70.8)
Rated SEER	11.5	12.0	10.0	11.5
Tests Performed[†]	*3*	*3*	*3*	*1, 2*

[†]Test (1) = Cycling Tests || Test (2) = Evaporator Airflow Tests || Test (3) = Condenser Coil Fouling Tests

building of the Energy Systems Laboratory was fenced off for this area. This area was selected because it was in close proximity to the psychrometric rooms, its turf consisted of mostly perennial grasses that required frequent mowing in the warmer months, drainage was acceptable, and electrical power was easily accessible. Within this area, the six condensers were placed on individual pads that were set ten feet (3.05 m) apart while the backs of each unit were placed within 18 inches of the building wall. The fence was approximately four feet (1.22 m) high and made of galvanized chain-link. A 10 foot (3.05 m) gate on the west end of the outdoor runtime area provided access to the units. The general layout of this area is shown in Figure 3.2.

Part of the coil fouling experiment required the fans in each condenser to run continuously in the outdoor environment for predetermined periods of time. During these runtime periods, the compressors in each unit were disconnected and electrical power was supplied to the fans only. Each unit was provided with an individual fault protected circuit sized appropriately for the condenser fans. The electrical usage of each unit was monitored and recorded hourly with a data logger.
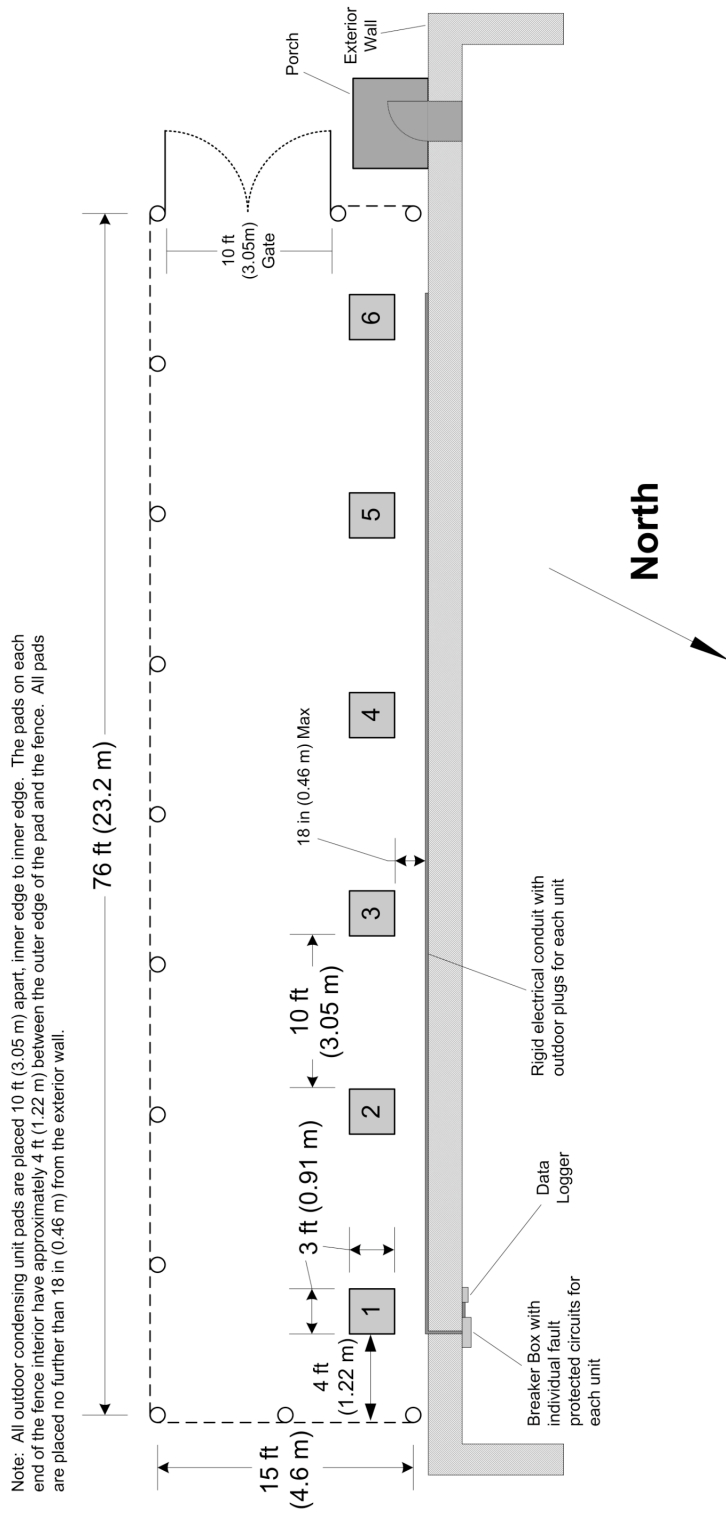
Figure 3.2 – General Layout of the Outdoor Runtime Area.

INSTRUMENTATION AND DATA ACQUISITION

The airflow rate through each air conditioner component was measured by an airflow test section in each room. The airflow test section in the indoor room connected to the outlet of the evaporator unit, as shown in Figure 3.1. It consisted of a 180° turning duct connected to an airflow measurement chamber. An assist blower located on the downstream end of the airflow measurement chamber was used to modulate airflow through the test section. A damper on the exhaust of the assist blower was used to adjust the airflow rate through the evaporator unit and test section. During a test, conditioned air from the indoor room was drawn into the inlet of evaporator where the dry-bulb temperature was measured with a 9-element thermocouple grid. Depending on the type of experiment being conducted, a chilled mirror hygrometer or a relative humidity sensor made a moisture measurement here as well. After passing through the evaporator coil and fan, the temperature of the exiting air was measured with another 9-element thermocouple grid placed over the outlet of the evaporator. The moisture content of the air was measured here by another chilled mirror hygrometer or relative humidity sensor. After passing through the turning duct, the air entered the airflow measurement chamber[*] where it was accelerated through a combination of ASME long radius nozzles. The resulting pressure differential was used to determine the airflow rate through the evaporator. After leaving the test section, the air was re-circulated and reconditioned in the indoor room.

The airflow test section in the outdoor room was similar to that in the indoor room, but with a few notable differences. It consisted of a vertical flow hood that captured air leaving the condenser and was connected to another airflow measurement

---

[*] Chamber was constructed according to ANSI/AMCA Standard 210 (1999).

chamber. An assist blower was used to facilitate airflow through the sealed test section.

A variable speed drive controlled the speed of the assist blower. During an experimental

run for this set-up, conditioned air from the outdoor room was drawn in through the

sides of the condenser. Here, the temperature of the entering air was measured by an air

sampling device[†]. After passing through the condenser coil and fan, the air was

discharged out of the top of the unit and entered into the sealed flow measurement hood.

Here the temperature of the exiting air was measured by a 12-element thermocouple

grid. A relative humidity sensor in this section of the duct measured the moisture

content of the air. A differential pressure transducer was used at this point to measure

the air static pressure referenced to the outdoor room pressure. For all of the

experiments conducted in this research, the static pressure of the condenser fan exhaust

was maintained at zero to achieve the rated free air capacity of the condenser fan. To

maintain zero static pressure, the speed of the assist blower was adjusted accordingly.

After passing through the flow hood, the air was directed into an airflow measurement

chamber, where it accelerated through a combination of ASME long radius nozzles. The

resulting pressure differential generated was used to determine the airflow rate through

the condenser. After leaving the test section, the air was re-circulated and reconditioned

in the outdoor room.

On the refrigerant side, temperature and pressure measurements were made for

the refrigerant entering and exiting the evaporator and condensing units. The refrigerant

temperature measurements were made with soldered thermocouple wells placed near the

centerline of the refrigerant tubing and oriented into the refrigerant flow, as shown in the

schematic of Figure 3.3. A type-T thermocouple was completely inserted into each well.

[†] Air sampling device was built in accordance with ANSI/ASHRAE Standard 41.1 (1986).
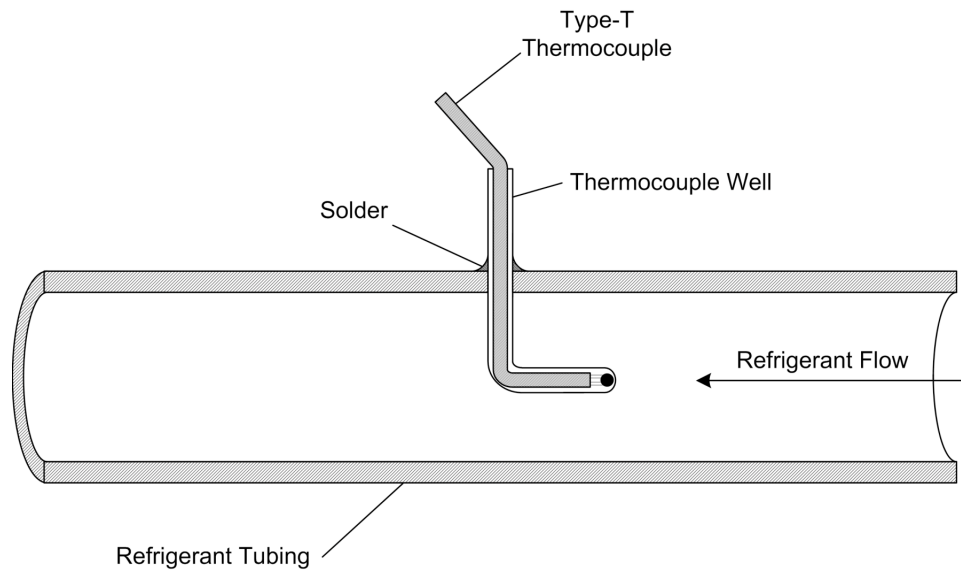
Figure 3.3 – Schematic of Refrigerant Line Thermocouple Well.

The refrigerant pressure measurements were made with pressure transducers connected to standard T-fittings soldered into the refrigerant tubing just downstream of the thermocouple well, as shown in the schematic of Figure 3.4. A standard ball-valve placed between the pressure transducers and T-fittings allowed the pressure transducers to be completely isolated from a pressurized refrigerant line.

The mass flow rate of the refrigerant was measured with a Coriolis-type mass flow meter placed between the condenser and evaporator units in the liquid line. Refrigerant temperatures and pressures were measured at both the inlet and outlet of the mass flow meter. Standard sight-glasses where placed in the liquid line near the condensing unit, the inlet and outlet of the mass flow meter, and near the evaporator unit.
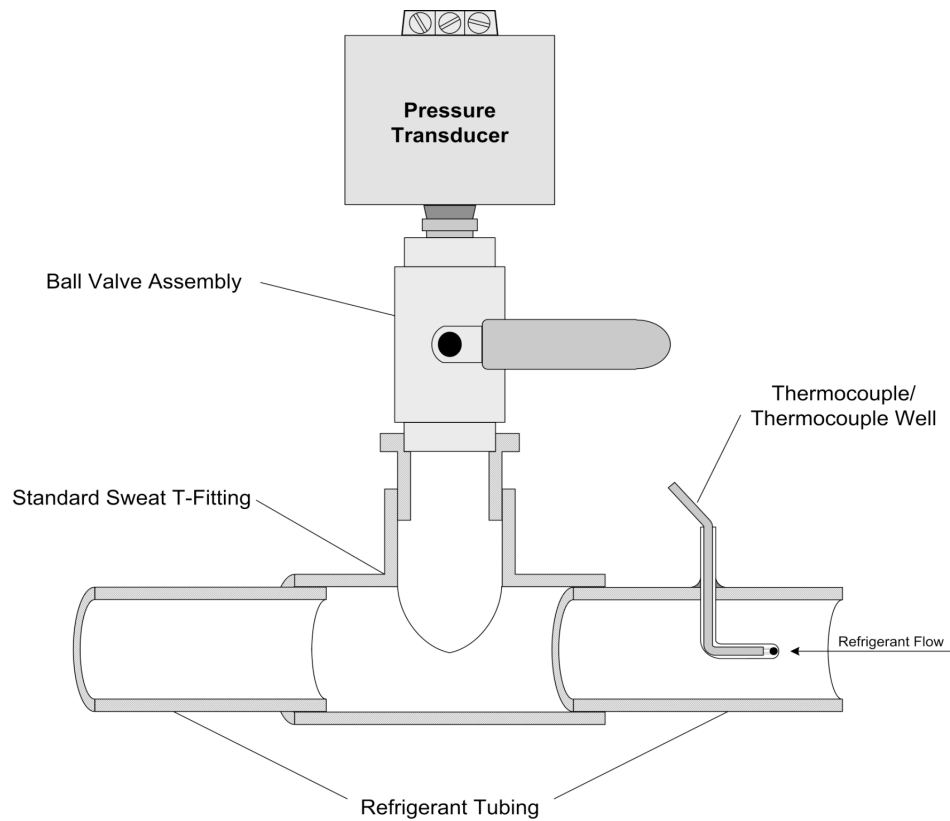
Figure 3.4 – Schematic of Refrigerant Line Pressure Transducer.

 A computerized data acquisition system was used to monitor and record data from 26 test points. Data were recorded in one second intervals and archived in a standard file format. The layout of the instrumentation test points used for all testing in this research is shown in Figure 3.5. A tabular listing and brief description of each test point is presented in Table 3.2.
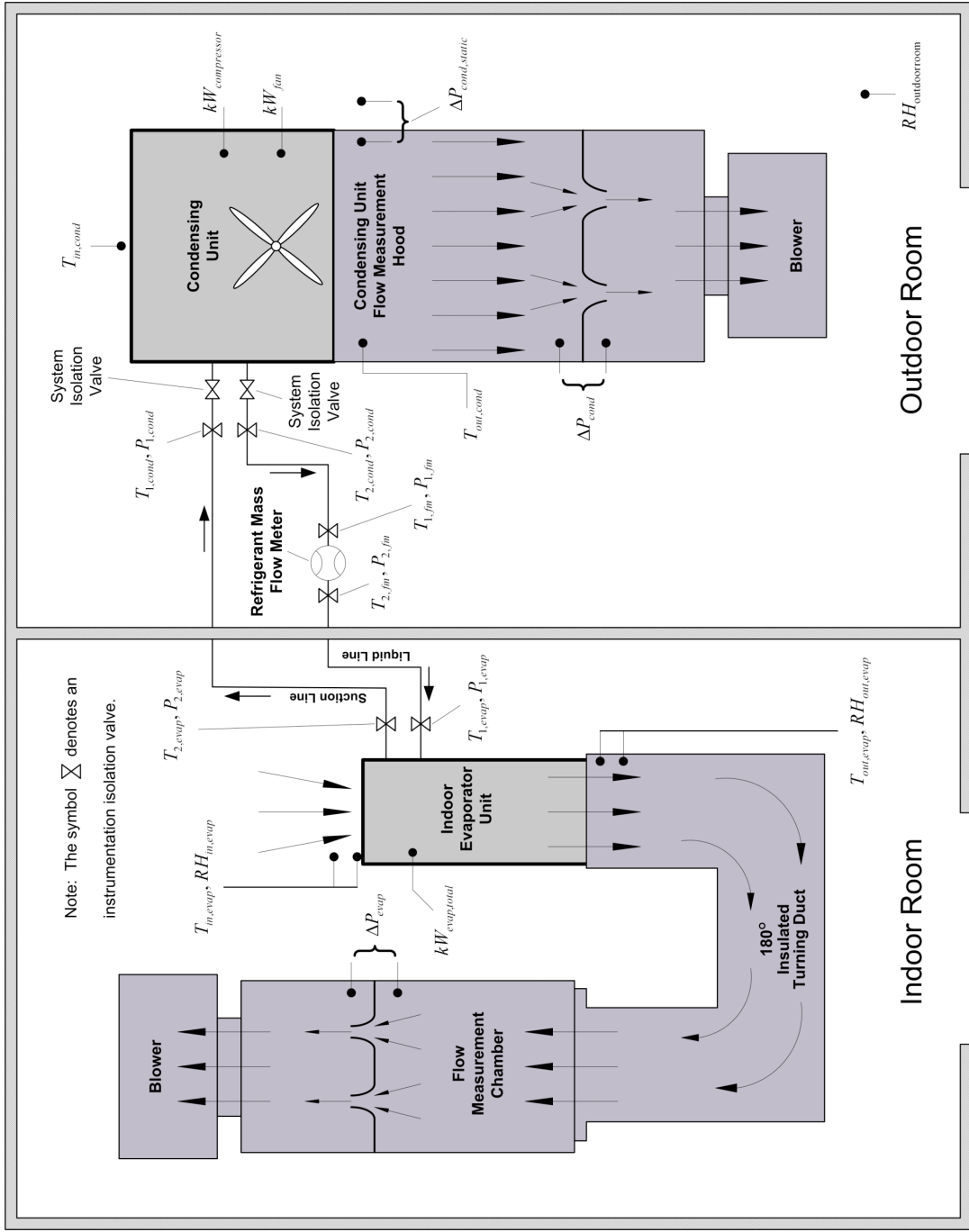
Figure 3.5 – Detailed Layout of the Test Points in the Psychrometric Rooms.

Table 3.2 – Complete Listing and Description of the Test Points.

Test Point Name	Test Point Description
$T_{1,evap}$	Evaporator Liquid Line Refrigerant Temperature
$T_{2,evap}$	Evaporator Suction Line Refrigerant Temperature
$T_{1,cond}$	Condenser Suction Line Refrigerant Temperature
$T_{2,cond}$	Condenser Liquid Line Refrigerant Temperature
$T_{1,fm}$	Flow Meter Inlet Refrigerant Temperature
$T_{2,fm}$	Flow Meter Outlet Refrigerant Temperature
$T_{in,evap}$	Evaporator Air Inlet Temperature
$T_{out,evap}$	Evaporator Air Outlet Temperature
$T_{in,cond}$	Condenser Air Inlet Temperature
$T_{out,cond}$	Condenser Air Outlet Temperature
$P_{1,evap}$	Evaporator Liquid Line Refrigerant Pressure
$P_{2,evap}$	Evaporator Suction Line Refrigerant Pressure
$P_{1,cond}$	Condenser Suction Line Refrigerant Pressure
$P_{2,cond}$	Condenser Liquid Line Refrigerant Pressure
$P_{1,fm}$	Flow Meter Inlet Refrigerant Pressure
$P_{2,fm}$	Flow Meter Outlet Refrigerant Pressure
$RH_{in,evap}$	Evaporator Air Inlet Relative Humidity
$RH_{out,evap}$	Evaporator Air Outlet Relative Humidity
$RH_{outdoor\ room}$	Outdoor Room Relative Humidity
$\dot{m}_r$	Refrigerant Mass Flow Rate
ΔP_{evap}	Evaporator Nozzle Chamber Pressure Differential
ΔP_{cond}	Condenser Nozzle Chamber Pressure Differential
$\Delta P_{cond,static}$	Condenser Air Outlet Static Pressure
$kW_{evap,total}$	Total Evaporator Unit Electrical Power Load
kW_{comp}	Compressor Electrical Power Load
kW_{fan}	Condenser Fan Electrical Power Load

CHAPTER IV

EXPERIMENTAL PROCEDURE

Different procedures were used for the cycling, evaporator airflow, and the condenser coil fouling studies. The American Refrigeration Institute (ARI) Standard 210/240 (ARI, 2003) was the basis for testing conditions used in all experiments. Throughout all testing, the indoor room temperature was held constant at 80°F (26.7°C) dry-bulb (db) while the outdoor room temperature was maintained at 82°F (27.8°C) db, 85°F (29.4°C) db, 95°F (35°C) db, or 105°F (40.6°C) db, depending on the experiment. For the cycling experiments, the indoor room relative humidity was varied between 40% and 60%, or kept below 20%. For the evaporator airflow and condenser coil fouling experiments, the indoor room humidity conditions were held constant at 67°F (19.4°C) wet-bulb (wb). For reference, the cooling test conditions imposed by ARI Standard 210/240 used in this research are presented in Table 4.1.

Table 4.1 – Selected Conditions from ARI Standard 210/240.

Test	Indoor Conditions		Outdoor Conditions	
	Dry Bulb Temperature	Wet Bulb Temperature	Dry Bulb Temperature	Wet Bulb Temperature[*]
Test A	80°F (26.7°C)	67°F (19.4°C)	95°F (35.0°C)	NR
Test B	80°F (26.7°C)	67°F (19.4°C)	82°F (27.8°C)	NR
Test C	80°F (26.7°C)	<57°F (13.9°C)	82°F (27.8°C)	NR
Test D	80°F (26.7°C)	<57°F (13.9°C)	82°F (27.8°C)	NR

---

[*] For ARI Standard 210/240, the measurement of outdoor room wet bulb temperature is not required (NR) when testing air-cooled condensers that do not evaporate condensate.

UNIT INSTALLATION

The air-side, refrigerant-side, and electrical connections to the evaporator in the indoor room were installed according to the guidelines provided by the manufacturer. The same evaporator was used for all testing and its configuration did not change once installed.

Because the condenser coil fouling study involved frequently changing condensers between tests, the general procedure used to install, configure, and remove a condenser is discussed. The refrigerant-side and electrical connections to each condenser tested in the outdoor room were installed according to the guidelines provided by the manufacturer of each unit. The air-side connections for each condenser described in Chapter III were made to interface with the airflow test section in the outdoor room. In both rooms, all air-side connections where made to the corresponding airflow test sections with insulated fiberglass duct board and thoroughly sealed with HVAC-rated foil tape. All refrigerant-side connections were made with refrigeration-grade copper tubing and sealed with high-strength brazing alloy.

Before each test, a condenser was installed in the outdoor room and high-pressure nitrogen gas at approximately 300 psig (21.7 bar) was used to pressure test the refrigerant line junctions for leaks. A vacuum pump was used to continuously evacuate the refrigerant lines for a minimum of 45 minutes to remove any residual moisture. At this point, the system was isolated while still under vacuum and each system was charged with a predetermined amount of refrigerant (See Table 3.1). The amount of refrigerant charge was measured on a mass basis with a calibrated electronic refrigerant scale.

After testing with a particular condenser was complete, a recovery device was used to retrieve the refrigerant from the system and the condenser was disconnected from the test set-up. The recovered refrigerant was not used again in future testing.

SYSTEM CYCLING

The cycling tests were performed with a single three ton (10.5 kW) condensing unit (Unit D, as described in Chapter III) that was factory-matched to the evaporator used in all testing. The condensing unit used HCFC-22 refrigerant with a scroll compressor. The unit had a rated SEER of 11.5 and a pin fin coil. The amount of refrigerant used in the system with this condenser in place (see Table 4.2) was determined by running a series of 30 minute steady-state tests[†] with varying amounts of charge until 10ºF (6.1ºC) of refrigerant subcooling was achieved. The relevant specifications for this condensing unit are shown in Table 4.2.

All tests conducted in the cycling study were performed at an indoor temperature of 80°F (26.7°C) db and an outdoor temperature of 95°F (35°C) db. Relative humidities of 40%, 50%, and 60% were used for the indoor moisture conditions. Three series of tests were conducted, with one series for each of the three moisture conditions. Each series of tests consisted of four individual 30 minute tests, all conducted at the indoor relative humidity corresponding to that series. The difference between the individual tests within each series was the cycle time, or the split between the amount of time that the air conditioning system spent in the "on" and "off" state. Table 4.3 shows the testing conditions and cycle time for each series of tests.

[†] Testing conditions were those imposed by ARI Standard 210/240 Test A.

Table 4.2 –Specifications for Condensing Unit D.

Specification	Unit D
Nominal Capacity (tons)	3
Compressor Type	Scroll
Condenser Coil Fin Type	Pin
Condenser Coil Density (fins/in.)	24
Condenser Coil Face Area (ft^2)	15.86
Condenser Fan Capacity (ft^3/min)	2500

Table 4.3 – Summary of Testing for the Cycling Study.

40% RH Indoor Series		50% RH Indoor Series		60% RH Indoor Series	
Test	On Time/Off Time	Test	On Time/Off Time	Test	On Time/Off Time
1	6 min / 24 min	1	6 min / 24 min	1	6 min / 24 min
2	10 min / 20 min	2	10 min / 20 min	2	10 min / 20 min
3	15 min / 15 min	3	15 min / 15 min	3	15 min / 15 min
4	20 min/ 10 min	4	20 min/ 10 min	4	20 min/ 10 min

Before a series of tests was started, the system was operated for a minimum of one hour at steady-state in the appropriate testing conditions. After this initial run at steady-state, the entire air conditioning system, including the airflow through the evaporator, was shut down for up to 30 minutes. During this time, the appropriate testing conditions were maintained in the indoor and outdoor rooms. After the shutdown period, data acquisition began and the first test in the series (Test 1, as shown in Table

4.3) was initiated by starting the air conditioning system. The air conditioner was run for the amount of time specified by the "on time" listings in Table 4.3 (6 minutes for Test 1) and then shut down. The appropriate testing conditions were maintained and data was recorded for the entire 30 minute testing period. After a test was completed, data acquisition was stopped and testing conditions were maintained while preparations were made to run the next test. The next test in the series followed the previous test and the time between shutdown for one test and restart at the onset of the next test was a minimum of 20 minutes.

Another set of cooling tests were conducted on this set-up to determine the coefficient of degradation for the air conditioning system. These tests were based on ARI Standard 210/240 Tests C and D. Test C was a steady-state dry coil test with indoor room conditions of 80°F (26.7°C) db and < 57°F (13.9°C) wb[**] and an outdoor room condition of 82°F (27.8°C) db. Test D was a cycling dry coil test totaling 30 minutes in duration with the same indoor and outdoor room conditions as Test C and a cycle time of 6 minutes on and 24 minutes off. The procedure used to conduct these tests was very similar to that used in the cycling tests previously described. Before data were taken for these dry coil tests, the system was operated for a minimum of one hour at steady-state in the testing conditions imposed by Tests C and D. For Test C, steady-state data were collected for a minimum of 30 minutes. The system was then shut down for approximately 30 minutes while testing conditions where maintained. After the shutdown period, the data acquisition began and Test D was initiated by starting the air

[**] The ARI Standard 210/240 states that the indoor wet-bulb temperature for tests C and D shall be sufficiently low so as to prevent any condensate from forming on the surface of the evaporator coils during the test. In practice, the relative humidity was maintained at or below 20%.

conditioning system. The system was run for 6 minutes and then shut down. Data were recorded for the entire 30 minute testing period.

EVAPORATOR AIRFLOW

The evaporator airflow tests were conducted with the same evaporator and condenser used in the cycling study. The relevant specifications for the evaporator unit are reproduced in Table 4.4.

Table 4.4 - Specifications for Evaporator used in All Testing.

Specification	Evaporator Unit
Expansion Device	0.071 inch (1.8 mm) Orifice
Evaporator Coil Type	Plate Fin
Evaporator Coil Configuration	Diagonal Updraft
Testing Orientation	Horizontal Left
Evaporator Coil Density, fins/in. (fins/cm)	14 (5.51)
Evaporator Coil Face Area, ft^2 (m^2)	2.86 (0.266)
Rated Evaporator Fan Power, hp (kW)	1/3 (0.25)
Rated Evaporator Airflow, ft^3/min (m^3/min)	1200 (34)

The indoor conditions for the evaporator airflow tests were performed in accordance with ARI Standard 210/240 Test A (see Table 4.1). The outdoor conditions were maintained at either 85°F (29.4°C) db, 95°F (35°C) db, or 105°F (40.6°C) db. Three series of steady-state tests were conducted in total, with one series for each of these three outdoor temperatures. Each series of tests consisted of eight individual 30 minute tests, all conducted at the outdoor temperature corresponding to that series. The difference between the individual tests within each series was the evaporator airflow

rate, which varied from $600 \, ft^3/min$ to $1650 \, ft^3/min$ in $150 \, ft^3/min$ increments. The airflow through the evaporator section was controlled by adjusting the exhaust damper on the assist blower connected to the indoor airflow test section. The evaporator airflow rates used in each test are presented in Table 4.5.

Table 4.5 – Summary of Testing for Evaporator Airflow Study.

85°F (29.4°C) db Outdoor Series		95°F (35°C) db Outdoor Series		105°F (40.6°C) db Outdoor Series		Deviation from Rated Airflow Condition	
Test	Evaporator Airflow Rate ft^3/min (m^3/min)	Test	Evaporator Airflow Rate ft^3/min (m^3/min)	Test	Evaporator Airflow Rate ft^3/min (m^3/min)		
1	600 (17)	1	600 (17)	1	600 (17)	-50.0 %	Low Airflow Tests
2	750 (21.2)	2	750 (21.2)	2	750 (21.2)	-37.5 %	
3	900 (25.5)	3	900 (25.5)	3	900 (25.5)	-25.0 %	
4	1050 (29.7)	4	1050 (29.7)	4	1050 (29.7)	-12.5 %	
5	1200 (34)	5	1200 (34)	5	1200 (34)	0.0 %	
6	1350 (38.2)	6	1350 (38.2)	6	1350 (38.2)	+12.5 %	High Airflow Tests
7	1500 (42.5)	7	1500 (42.5)	7	1500 (42.5)	+25.0 %	
8	1650 (46.7)	8	1650 (46.7)	8	1650 (46.7)	+37.5 %	

Before a series of tests was started, the system was operated for a minimum of one hour at steady-state in the appropriate testing conditions and rated evaporator airflow. Then, the first test was conducted by collecting 30 minutes of steady-state data. After the first test was complete, the damper on the assist blower was adjusted to the airflow rate of the next test. Before the next test began, the system was operated in steady-state with the new airflow rate for a minimum of 30 minutes. The next test was

then initiated and 30 minutes of steady-state data were collected. This process was repeated for each series shown in Table 4.5.

CONDENSER COIL FOULING

The condenser coil fouling study used a total of six condensing units divided into three groups (groups A, B, and C), with each group consisting of two units that were identical in brand, make, and model. Each condenser was rated at three tons (10.5 kW) and all were comparably energy-rated. The relevant specifications of each unit used in the condenser coil fouling study have been reproduced in Table 4.6.

Table 4.6 – Specifications for Condensing Units used in Coil Fouling Study.

Specification	Group A		Group B		Group C	
	A1	A2	B1	B2	C1	C2
Nominal Capacity, tons (kW)	3 (10.5)		3 (10.5)		3 (10.5)	
Compressor Type	Scroll		Scroll		Scroll	
Condenser Coil Fin Type	Pin		Plate		Plate	
Condenser Coil Density, fins/in. (fins/cm)	24 (9.45)		25 (9.84)		22 (8.66)	
Condenser Coil Face Area, ft^2 (m^2)	15.86 (1.47)		14.90 (1.38)		11.41 (1.06)	
Condenser Fan Capacity ft^3/min (m^3/min)	2500 (70.8)		2800 (79.3)		2510 (71.1)	

At the onset of the experiment, all six units listed in Table 4.6 were brand new, had never been operated in an outdoor environment, and were delivered with an unknown factory charge of refrigerant (R-22). Each unit was initially operated in

steady-state conditions[††] while refrigerant was added to or removed from the unknown factory charge until approximately 10ºF (6.1ºC) of subcooling was established. After proper charge for each unit was established, two baseline tests were conducted on each of the six units. The first baseline test used the conditions of ARI Standard 210/240 Test A and the second baseline test used those of Test B (see Figure 4.1). Before data was collected, each system was operated for a minimum of one hour at steady-state in the appropriate testing conditions. When each test started, one hour of steady-state data were collected.

After the baseline tests were completed, the units were placed in the outdoor runtime area described in Chapter III. Power was applied to only the fans of each unit (the compressors were disconnected) and the units were allowed to accumulate 2000 hours (approximately 2.5 months) of continuous run time in this controlled outdoor environment.

At the end of the first 2000 hour period, the units were brought back into the psychrometric rooms for testing. At this point, the first testing cycle was considered complete and the second testing cycle began. Two tests were conducted on each of the six units, again based on ARI Standard 210/240 Tests A and B. After this round of testing was complete, the coils of the #2 units in each group (i.e. units A2, B2, and C2) were cleaned[***] and each of these three units were immediately retested again using Tests A and B. After testing was completed, all six units were placed back in the outdoor runtime area for a second 2000 hour period. When this second 2000 hour period

---

[††] Room conditions were those imposed by ARI Standard 210/240 Test A.
[***] The cleaning techniques used on each unit utilized a non-acid based foaming coil cleaner applied in accordance with the manufacturer's cleaning instructions.

had elapsed, the second testing cycle was considered complete and the third testing cycle began. All units were tested and the #2 units were cleaned and retested in the manner previously described and then placed back in the outdoor runtime area for a final 4000 hour period. When this 4000 hour period had elapsed, the third testing cycle was considered complete and the fourth and final testing cycle began. The units were again tested, cleaned, and retested. The net result of these four cycles was a total of 8000 hours of outdoor runtime for the condenser fans. The duration of each complete cycle in relation to the others can be seen in Figure 4.1.
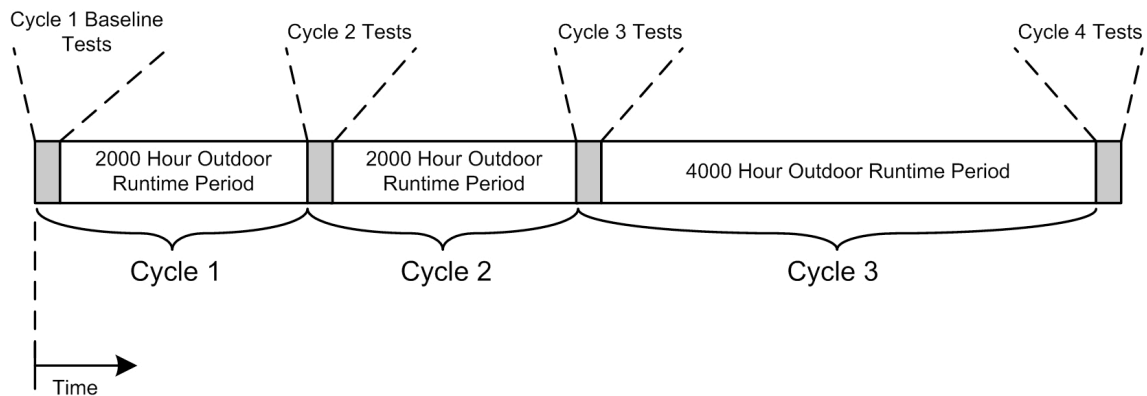
Figure 4.1 – Timeline of Testing Cycles for the Coil Fouling Study.

The pads used to hold the condensing units in the outdoor area were arranged and numbered as shown in Figure 4.2. Once the experiment began, the pads remained in their original places and retained these identifying numbers throughout the remainder of the experiment. The initial placement of the units on these pads in the outdoor runtime area is described in Table 4.7.
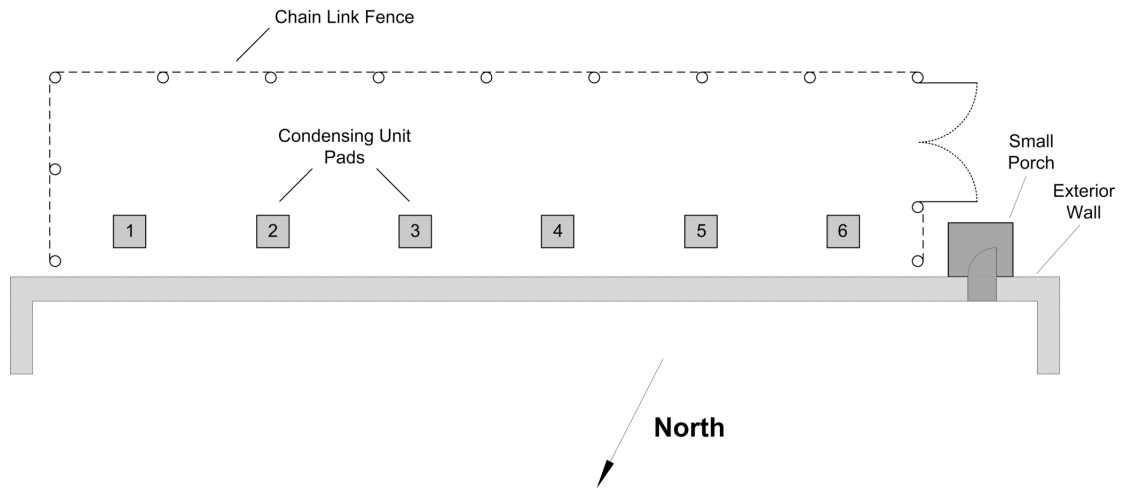
Figure 4.2 – Arrangement and Identification of Condenser Pads used in Outdoor Runtime Area.

Table 4.7 – Initial Placement of Condensing Units.

Initial Placement – Cycle 1	
Pad Number	**Condensing Unit**
1	A1
2	A2
3	B1
4	B2
5	C1
6	C2

After testing for a given cycle was completed, the units were not placed back on the same pads in the outdoor runtime area; rather, they were shifted from one testing cycle to the next. The placement of the condensing units for the second and third cycles is shown in Tables 4.8 and 4.9 and illustrated for all three cycles in Figure 4.3.

Table 4.8 – Condensing Unit
Placement for Cycle 2.

Cycle 2 Placement	
Pad Number	Condensing Unit
1	C2
2	A1
3	A2
4	B1
5	B2
6	C1

Table 4.9 – Condensing Unit
Placement for Cycle 3.

Cycle 3 Placement	
Pad Number	Condensing Unit
1	C1
2	C2
3	A1
4	A2
5	B1
6	B2

Cycle 1

Chain Link Fence

Condensing Units

| A1 | A2 | B1 | B2 | C1 | C2 |

Small Porch

Exterior Wall

North

Cycle 2

Chain Link Fence

Condensing Units

| C2 | A1 | A2 | B1 | B2 | C1 |

Small Porch

Exterior Wall

North

Cycle 3

Chain Link Fence

Condensing Units

| C1 | C2 | A1 | A2 | B1 | B2 |

Small Porch

Exterior Wall

North
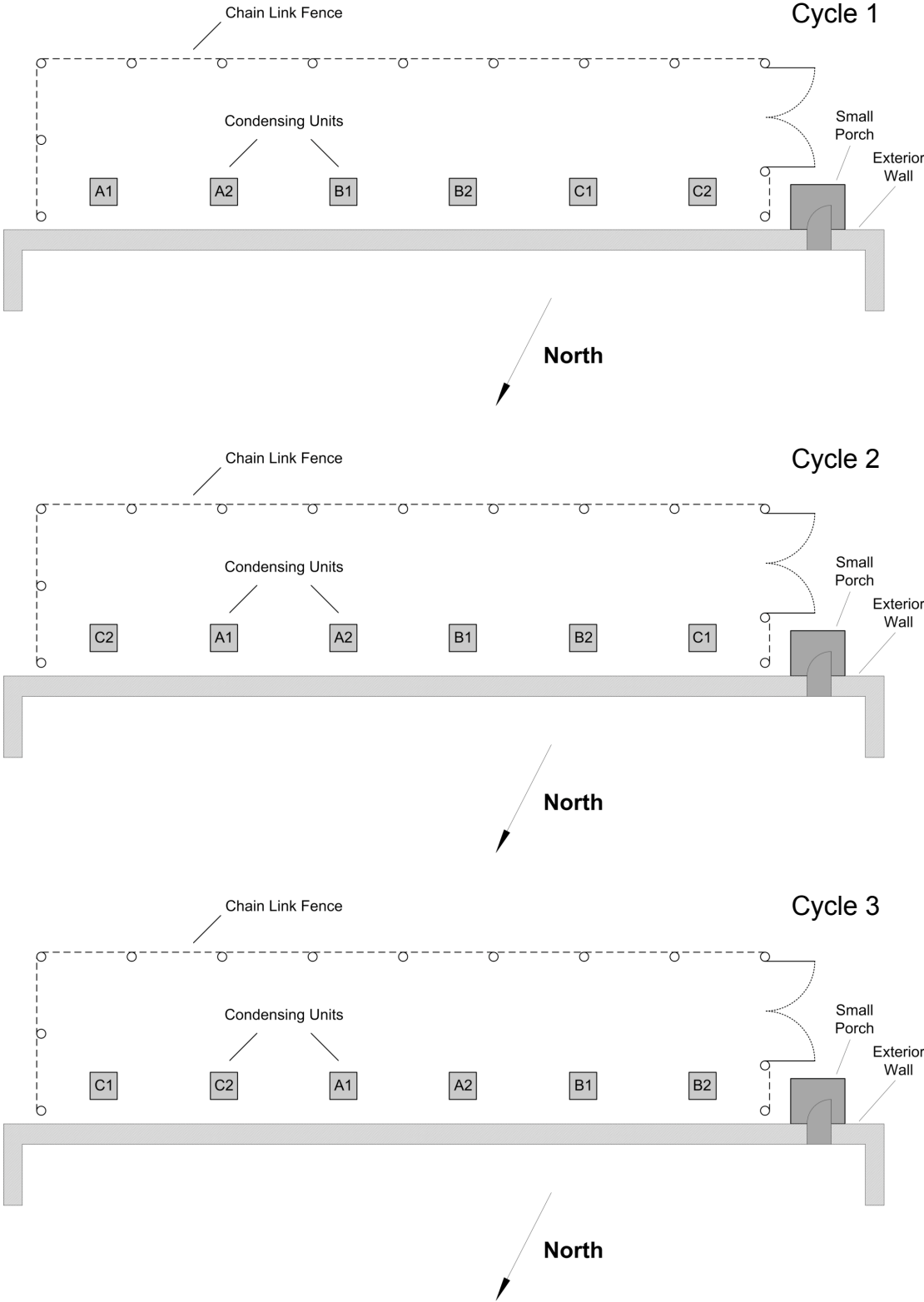
Figure 4.3 – Schematic of Condensing Unit Placement for Each Testing Cycle.

CHAPTER V
EXPERIMENTAL RESULTS FOR THE EFFECTS OF SYSTEM CYCLING ON THE DEHUMIDIFICATION PERFORMANCE OF AN AIR CONDITIONING SYSTEM

The cycling tests were performed with a single three ton (10.5 kW) condenser (unit D, described in Chapter IV) and a factory-matched evaporator. The system had a rated seasonal energy efficiency ratio (SEER) of 11.5, used HCFC-22 refrigerant, and utilized a 0.071 inch (1.8 mm) orifice for an expansion device. An initial series of baseline tests[*] were conducted to determine the refrigerant charge required to achieve a refrigerant subcooling of 10ºF (6.1ºC). The refrigerant charge used in the system throughout the cycling tests was 7.10 lbm (3.22 kg). Table 5.1 lists the major specifications for this condenser.

Table 5.1 – Specifications for Condensing Unit D.

Specification	Unit D
Nominal Capacity, tons (kW)	3 (10.6)
Compressor Type	Scroll
Condenser Coil Type	Pin Fin
Condenser Coil Density, fins/in. (fins/cm)	24 (9.6)
Condenser Coil Face Area, ft^2 (m^2)	15.86 (1.47)
Condenser Fan Capacity, ft^3/min (m^3/min)	2500 (70.8)

---

[*] Testing conditions were those imposed by ARI Standard 210/240 Test A.

For each series of tests conducted, the evaporator was exposed to indoor relative humidities of 40%, 50%, or 60% while the indoor and outdoor temperatures were held constant at 80°F (26.7°C) db and 95°F (35°C) db, respectively. Each series of tests consisted of four individual 30 minute tests all conducted at the indoor relative humidity corresponding to that series. The difference between the individual tests within each series was the length of the cycle time (Table 5.2).

Table 5.2 – Summary of Testing for the Cycling Study.

40% RH Indoor Series		50% RH Indoor Series		60% RH Indoor Series	
Test	**On Time/Off Time**	**Test**	**On Time/Off Time**	**Test**	**On Time/Off Time**
1	6 min / 24 min	1	6 min / 24 min	1	6 min / 24 min
2	10 min / 20 min	2	10 min / 20 min	2	10 min / 20 min
3	15 min / 15 min	3	15 min / 15 min	3	15 min / 15 min
4	20 min/ 10 min	4	20 min/ 10 min	4	20 min/ 10 min

System performance was characterized by cyclic capacity, cyclic coefficient of performance (COP), cyclic sensible heat factor (SHF), and total moisture removed. The degradation coefficient was also calculated and reported (see Appendix B)

INSTANTANEOUS CAPACITY AND MOISTURE REMOVAL RATE

The instantaneous capacity of the system was based evaporator air-side measurements. The instantaneous moisture removal rate was calculated from the expression

$$\dot{m}_{w,rmv} = \dot{m}_a \left(W_1 - W_2 \right) \qquad (5.1)$$

where $\dot{m}_a$ is the mass flow rate of the air through the evaporator unit and W_1 and W_2 are the humidity ratios of the air entering and leaving the evaporator, respectively. A negative value for $\dot{m}_{w,rmv}$ indicated that moisture was being added to the air.

For all tests performed, the instantaneous capacity and moisture removal rate showed similar profiles. The instantaneous total capacities and moisture removal rates for tests performed at the 50% RH condition are presented in Figure 5.1 and 5.2.
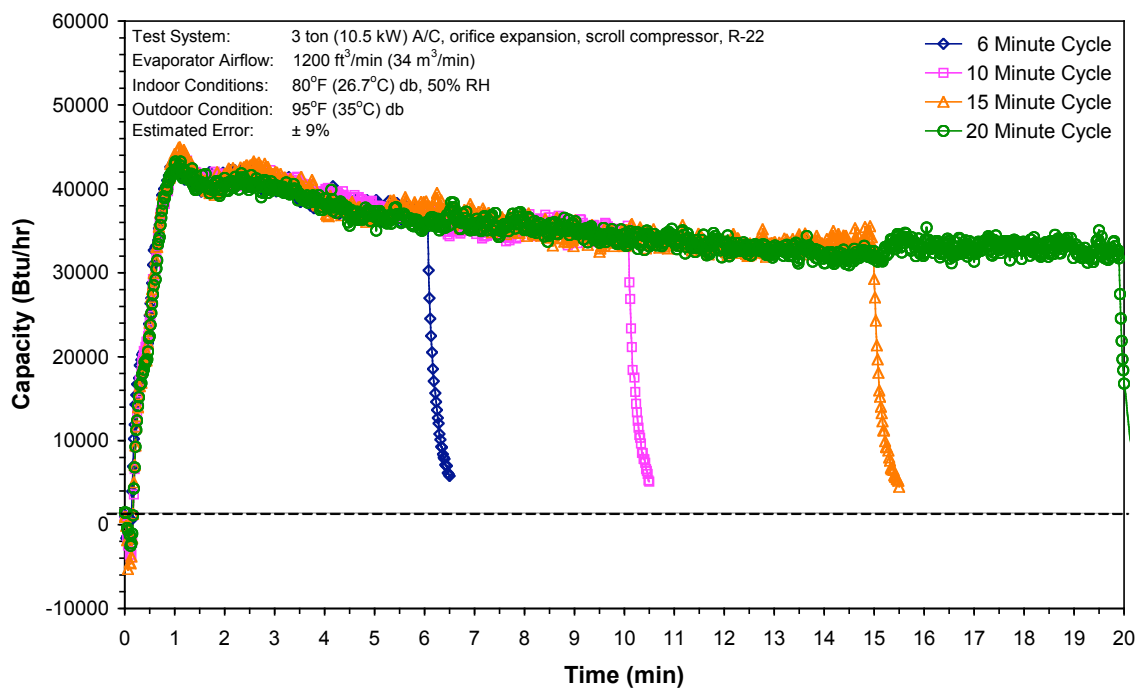
Figure 5.1 – Instantaneous Total Capacity at 50% Indoor Relative Humidity.
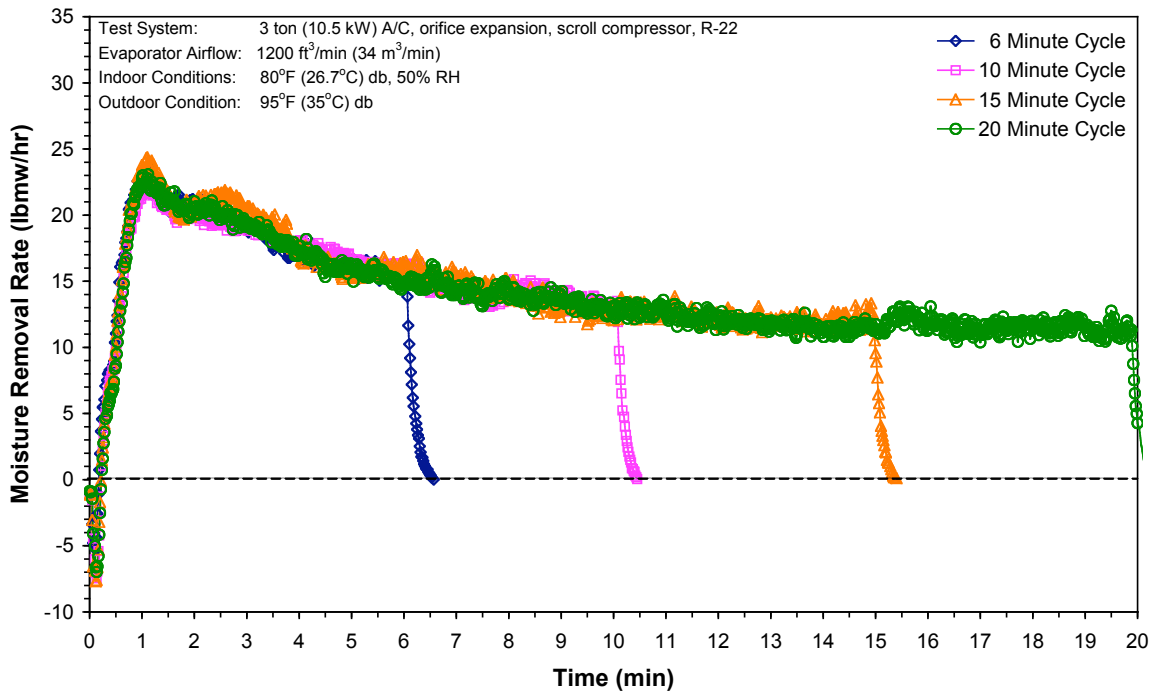
Figure 5.2 – Instantaneous Moisture Removal Rate at 50% Indoor Relative Humidity.

For each cycle in Figure 5.1, the instantaneous total capacity of the system was negative during approximately the first 8 seconds of start-up. After this time, the instantaneous capacity increased quickly to a maximum value of 45,000 Btu/hr (13.2 kW) one minute after startup and then slowly settled towards an average steady-state capacity of 33,000 Bth/hr (9.7 kW) as time increased. The response of the instantaneous moisture removal rate shown in Figure 5.2 was similar to that of the total capacity. The instantaneous moisture removal rate was negative for approximately the first 15 seconds of the cycle and then quickly increased to a maximum value of 24.4 lbmw/hr (11.4 kgw/hr) one minute after startup. It then approached a steady-state moisture removal rate of 11.6 lbmw/hr (5.26 kgw/hr). The profiles for each individual cycle in Figures 5.1 and 5.2 essentially form a single profile that is characteristic of the air conditioner for the given humidity condition. Similar profiles were seen for the 40% and 60% relative

humidity cases. The observed peak in total capacity and moisture removal at approximately 1 minute after startup is discussed in Appendix C.

The indoor chamber humidity conditions affected the total capacity and moisture removal rate of the system. The instantaneous capacity and moisture removal rate profiles for the 40% and 60% RH conditions followed the same general trends as those shown in Figures 5.1 and 5.2, but each humidity condition had different maximum and steady-state values. For the 40% condition, the maximum instantaneous capacity was 41,100 Btu/hr (12.0 kW) one minute after startup with a steady-state capacity of 29,200 Btu/hr (8.6 kW). The maximum instantaneous moisture removal rate for the 40% RH condition was 18.9 lbmw/hr (8.57 kgw/hr) one minute after startup with a steady-state value of 5.78 lbmw/hr (2.62 kgw/hr). For the 60% RH condition, the maximum instantaneous capacity was 50,000 Btu/hr (14.7 kW) one minute after startup and the steady-state capacity was 34,000 Btu/hr (9.98 kW). The maximum instantaneous moisture removal rate for the 60% RH condition was 32.3 lbmw/hr (14.7 kgw/hr) one minute after startup and the steady-state moisture removal rate was 15.7 lbmw/hr (7.12 kgw/hr). The maximum and steady-state values of instantaneous total capacity and moisture removal rate for all tests are summarized in Figures 5.3 and 5.4.

The maximum and steady-state total capacity and moisture removal rate increased with indoor humidity. The maximum and steady-state instantaneous total capacity and moisture removal rate shown in Figures 5.1 and 5.2 had a relatively constant offset throughout all testing.
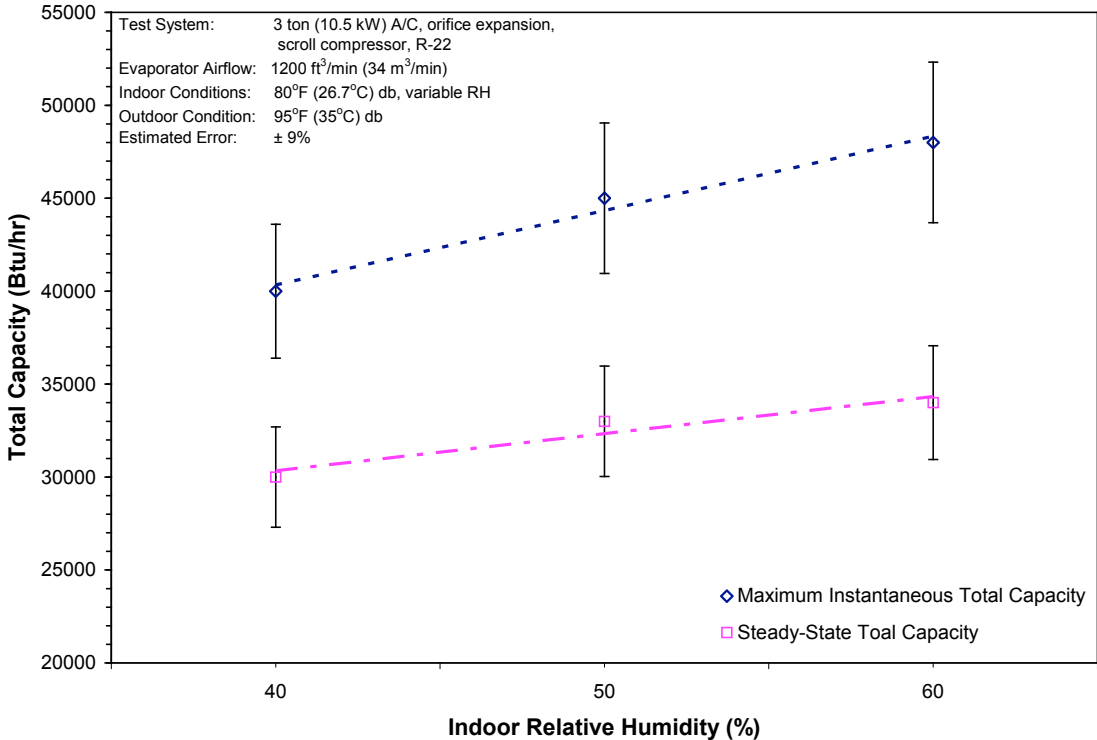
Figure 5.3 – Maximum and Steady-State Total Capacity for Each Test Series.
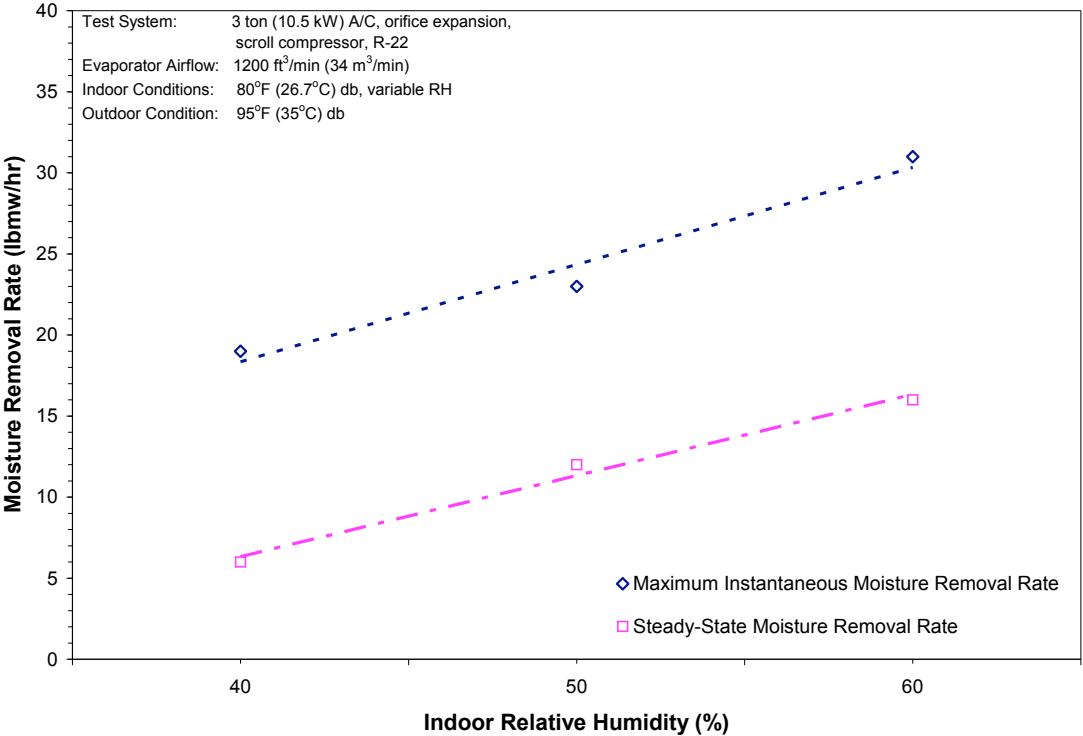
Figure 5.4 – Maximum and Steady-State Moisture Removal Rate for Each Test Series.

NEGATIVE CAPACITY AND MOISTURE REMOVAL RATE

Some insight into the negative instantaneous total capacities and moisture removal rates observed in Figures 5.1 and 5.2 was obtained by considering the state of the evaporator coil during the off-cycle and the response time of the system. The evaporator coil was wet with condensate at the end of each cycling test and some of this moisture remained on the surface of the coil during the off cycle. When the system was shut off, dehumidification stopped as airflow over the coil ceased and the coil surface temperature increased above the air dew point temperature. During the off-cycle, the coil was not dry; some of the moisture condensed out of the air stream just prior to the end of the previous cycle remained on the surface of the coil (the rest of this moisture drained off during the off-cycle). At the onset of the next cycle, full airflow was reestablished over the coil over at least 10 seconds before the coil surface temperature dropped below the air dew point temperature. The resulting "re-evaporation" occurred until all of the retained moisture was evaporated or the coil surface temperature dropped below the air dew point temperature. Therefore, during the first part of start-up, the net latent effect of the air conditioning system was actually *humidification*, which resulted in negative total capacities during the first 8 seconds of the cycles shown in Figure 5.1 and negative moisture removal rates during the first 13 seconds of those shown in Figure 5.2. This is shown in Figure 5.5 with the breakdown of instantaneous sensible and latent capacity superimposed onto the moisture removal rate of the system during the 15-minute cycling test at the 50% RH condition.
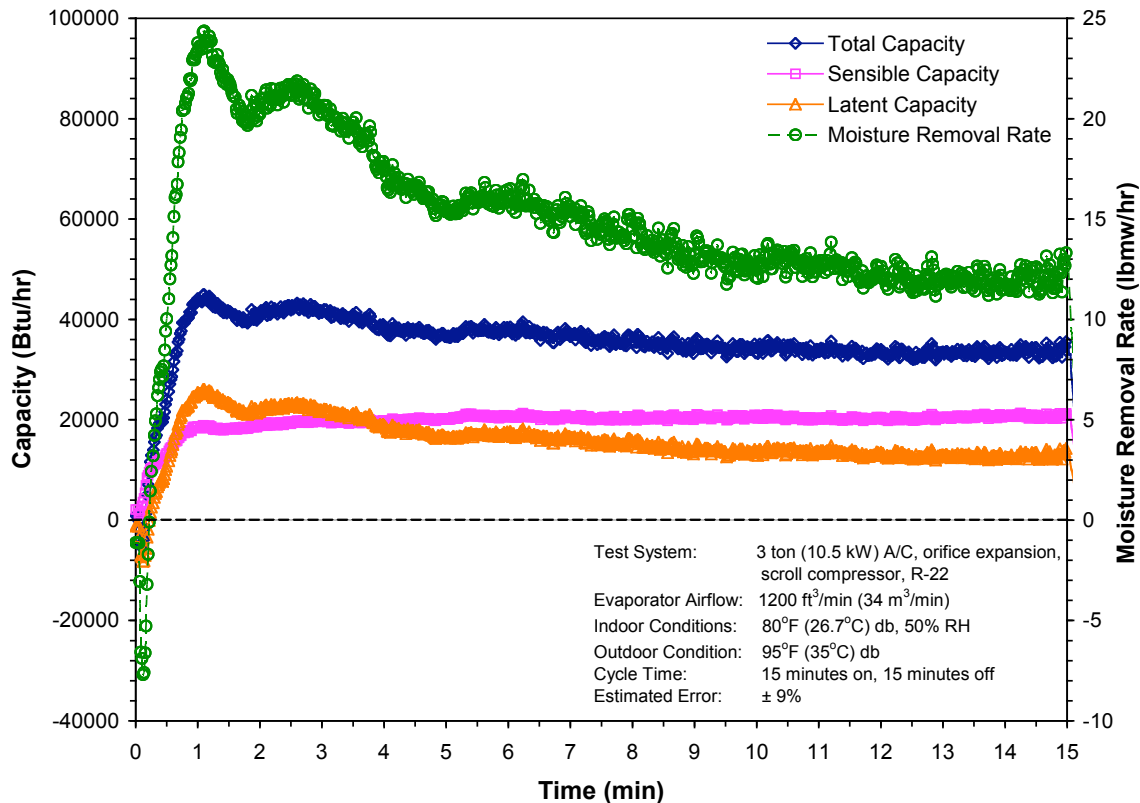
Figure 5.5 – Total, Sensible, and Latent Capacities and Moisture Removal
Rate for a 15 Minute Cycle at 50% Indoor Relative Humidity.

The instantaneous latent capacity drove the total capacity into negative values

during few seconds of startup while the sensible capacity was still small. After about 8

seconds, the total capacity increased to zero. At approximately 13 seconds after startup,

the latent capacity became positive. This was also verified by observing that the

moisture removal rate of the system became positive at approximately 13 seconds as

well (see Figure 5.2 and Figure 5.5). All other cycling tests showed results similar to

those presented in Figure 5.5. Dehumidification began between 5 and 30 seconds after

startup for almost all tests, depending on indoor humidity conditions.

The negative latent capacity and moisture removal rate shown in Figure 5.5 indicated that humidification was occurring until 13 seconds after startup. Because moisture was added to the air stream during the first 13 seconds of the cycle, additional time was required after dehumidification began for the system to remove a net positive amount of moisture. The total moisture removed from the air stream over the course of the cycle was calculated by integrating the instantaneous moisture removal rate given by Eq. 5.1 over the cycle time,

$$m_{w,total} = \int_{t_{on}}^{t_{off}} \dot{m}_{w,rmv} dt \tag{5.2}$$

where $\dot{m}_{r,rmv}$ is the moisture removal rate calculated from Eq. 5.1 and t_{on} and t_{off} are the on and off times of the cycle, respectively. The total moisture removed was calculated for the 15 minute cycle at 50% RH considered previously and is shown in Figure 5.6[**]. All other tests showed results that were similar to Figure 5.6. For the data shown in Figure 5.6, the total moisture removed became zero approximately 24 seconds after startup; this was the amount of time (referred to as the moisture removal break-even time) that the air conditioner required to remove the moisture added to the air stream during the first 13 seconds of the cycle. The moisture removal break-even time for all tests is presented in Figure 5.7.

The results presented in Figure 5.7 show that, in general, the indoor relative humidity did have an impact on the amount of time it took for the test air conditioning system to reach a break-even time with regards to dehumidification. This observation is consistent with the results presented in Figures 5.3 and 5.4. Those figures showed that

---

[**] The horizontal and secondary vertical axes are magnified to show the details present in the early part of the cycle.

the instantaneous and maximum total capacity and moisture removal rate of the test air conditioner was higher for increasing indoor humidity conditions. A system operating at a higher capacity and moisture removal rate would be able to remove moisture from the air stream faster than the same system operating at a lower capacity; hence, the shorter break-even times for the higher humidity conditions shown in Figure 5.7.
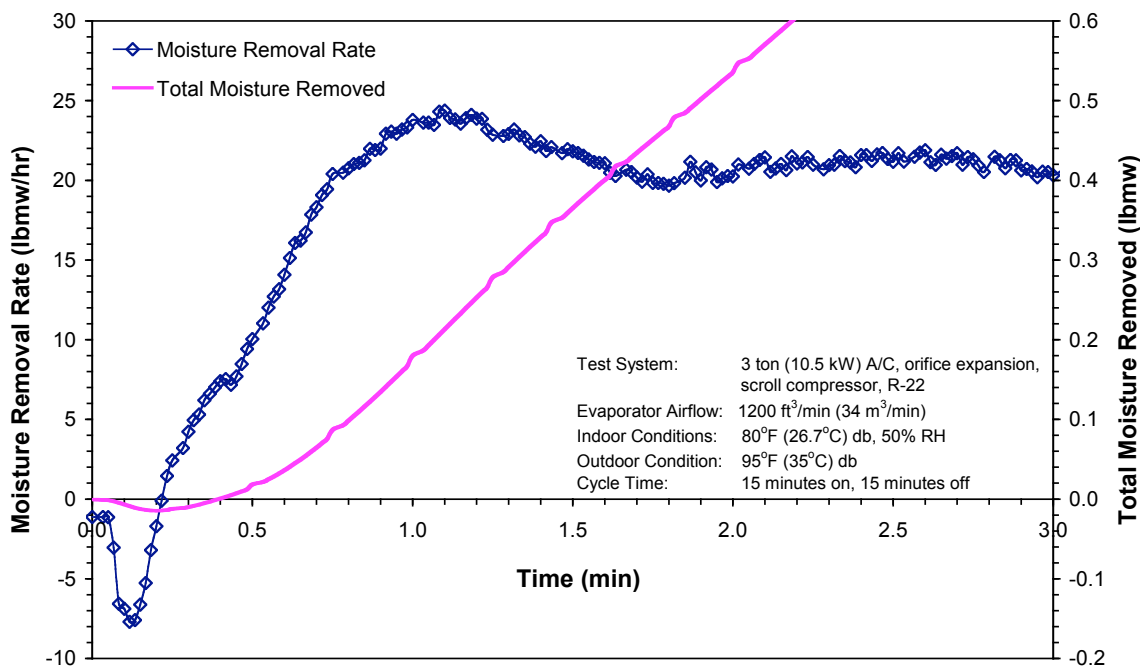
Figure 5.6 – Moisture Removal Rate and Total Moisture Removal for a 15 Minute Cycle at 50% Indoor Relative Humidity.
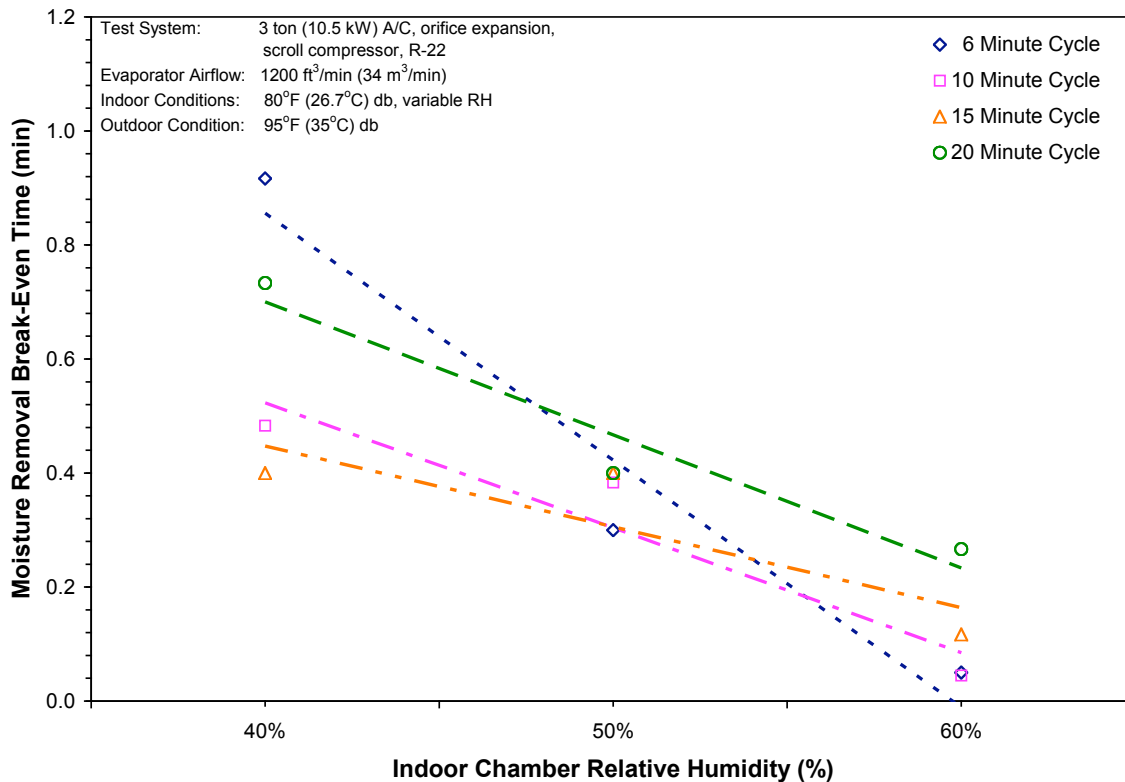
Figure 5.7 – Moisture Removal Break-Even Time for All Cycling Tests.

TOTAL MOISTURE REMOVED

To further generalize the effects of cycle time and indoor humidity on the dehumidification capacity of the system, the total moisture removed from the air stream over the course of a given cycle was computed by evaluating Eq. 5.2 for each test. The results are displayed in Figure 5.8.

As the cycle time increased, the total moisture removed increased for all three humidity conditions. The increase in total moisture removed with cycle time was approximately linear all humidity conditions. This simply shows that more moisture was removed for higher humidity conditions and longer cycle times.
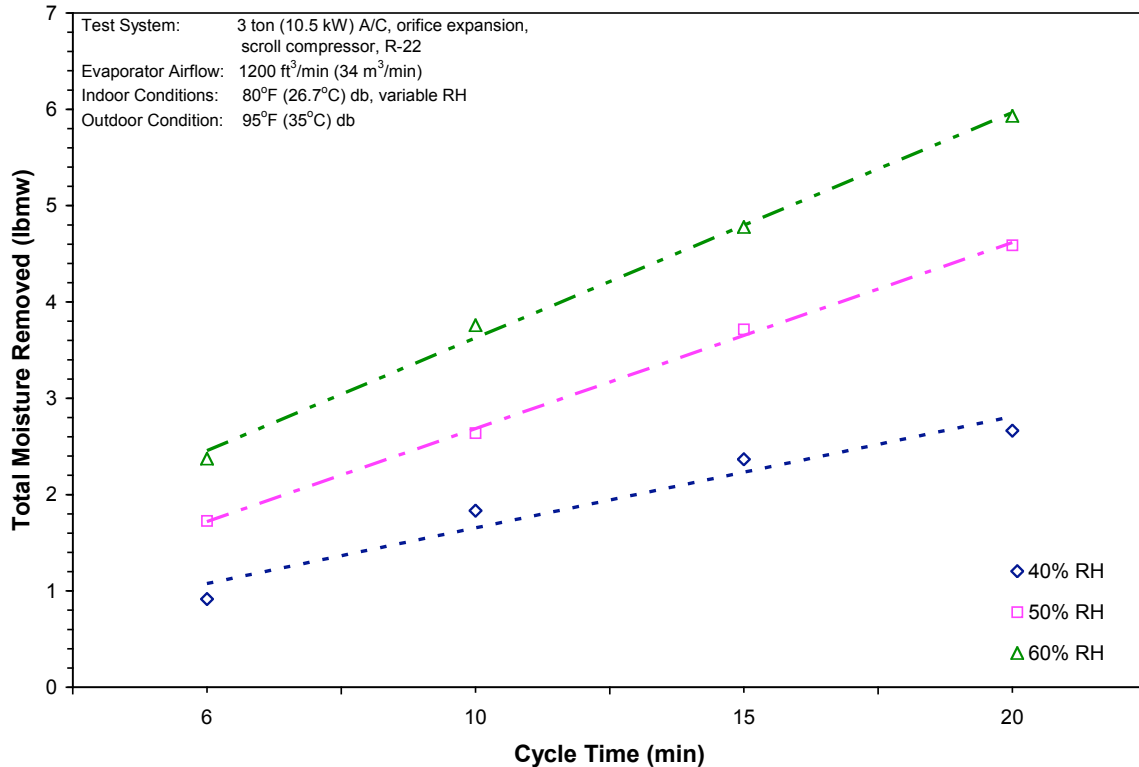
Figure 5.8 – Total Moisture Removed versus Cycle Time for Various Indoor Relative Humidities.

CYCLIC CAPACITY

To obtain a figure that expressed an average system capacity for a given cycle, the instantaneous capacity was integrated over the cycle and then normalized to the cycle time. This gave a time-integrated average capacity for each test conducted in the cycling tests:

$$\dot{Q}_{ave,cyclic} = \frac{\int_{t_{on}}^{t_{off}} \dot{Q}_{inst} dt}{\Delta t_{cycle}} \tag{5.3}$$

where $\dot{Q}_{inst}$ an instantaneous capacity of the system (total, sensible, or latent), t_{on} is the time the cycle begins, t_{off} is the time the cycle ends, and $\Delta t_{cycle} = t_{off} - t_{on}$. This time-

integrated average capacity is referred to as the cyclic total, sensible, or latent capacity of the system. The cyclic total, sensible, and latent capacities for all tests, based on Eq. (5.3), are shown in Figures 5.9, 5.10, and 5.11, respectively.

In general, the cyclic total capacity decreased with an increase in cycle time. For the 40% RH condition, the cyclic total capacity peaked at 33,200 Bth/hr (9.7 kW) for the 10 minute cycle, then decreased for larger cycles. The cyclic total capacity also generally increased as the indoor relative humidity increased. For all tests, the maximum cyclic total capacity was observed to be 41,350 Btu/hr (12.1 kW) for the 6 minute cycle at the 60% RH condition.

The cyclic sensible capacity increased with an increase in cycle time for all but the 60% RH indoor humidity condition. For the 60% RH condition, the cyclic sensible capacity increased from 16,000 Btu/hr (4.7 kW) for the 6 minute cycle to 17,200 Btu/hr (5.04 kW) for the 10 minute cycle. The cyclic sensible capacity essentially stayed constant from the 10 to 15 minute cycle and then decreased to 15,700 Btu/hr (4.6 kW) for the 20 minute cycle. The cyclic sensible capacity increased as the indoor relative humidity decreased.

On average, the cyclic latent capacity decreased with an increase in cycle time. For the 40% RH condition, the cyclic latent capacity peaked at 11,800 Btu/hr (3.5 kW) for the 10 minute cycle. The cyclic latent capacity increased as the indoor relative humidity increased.
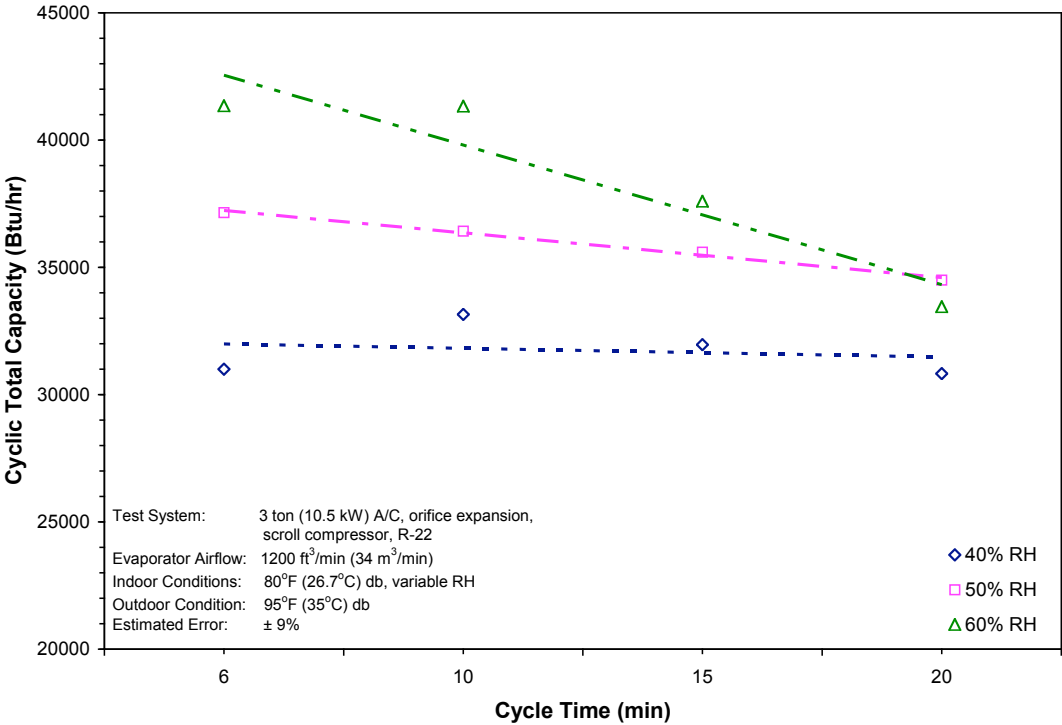
Figure 5.9 – Cyclic Total Capacity versus Cycle Time for Various Indoor Relative Humidities.
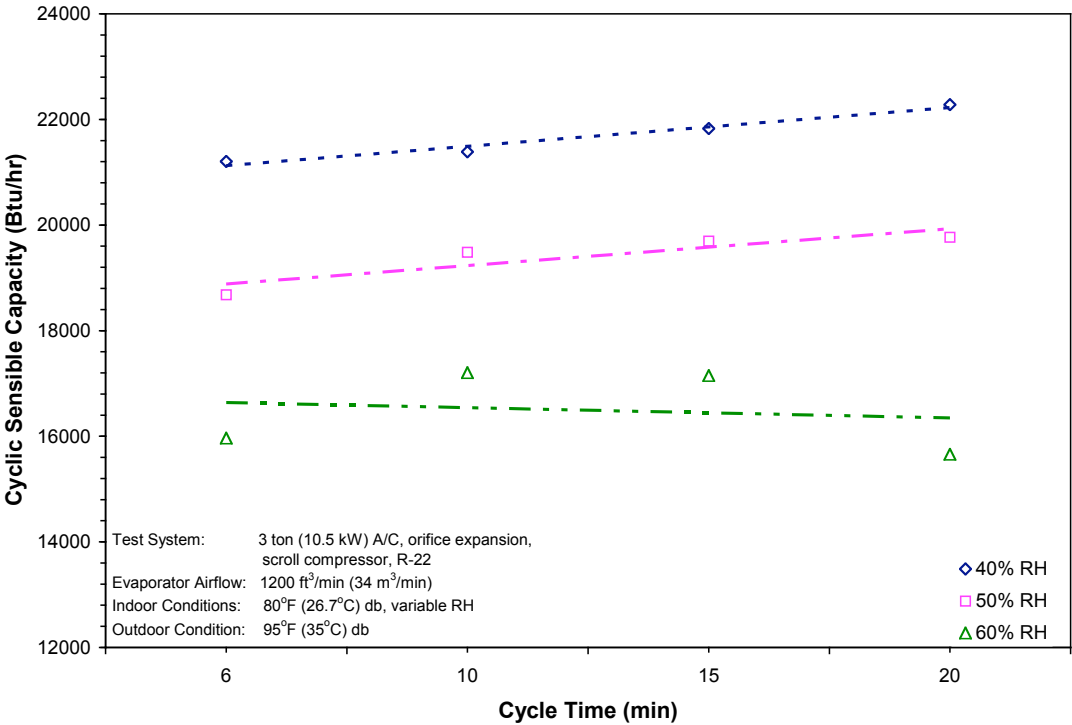
Figure 5.10 – Cyclic Sensible Capacity versus Cycle Time for Various Indoor Relative Humidities.
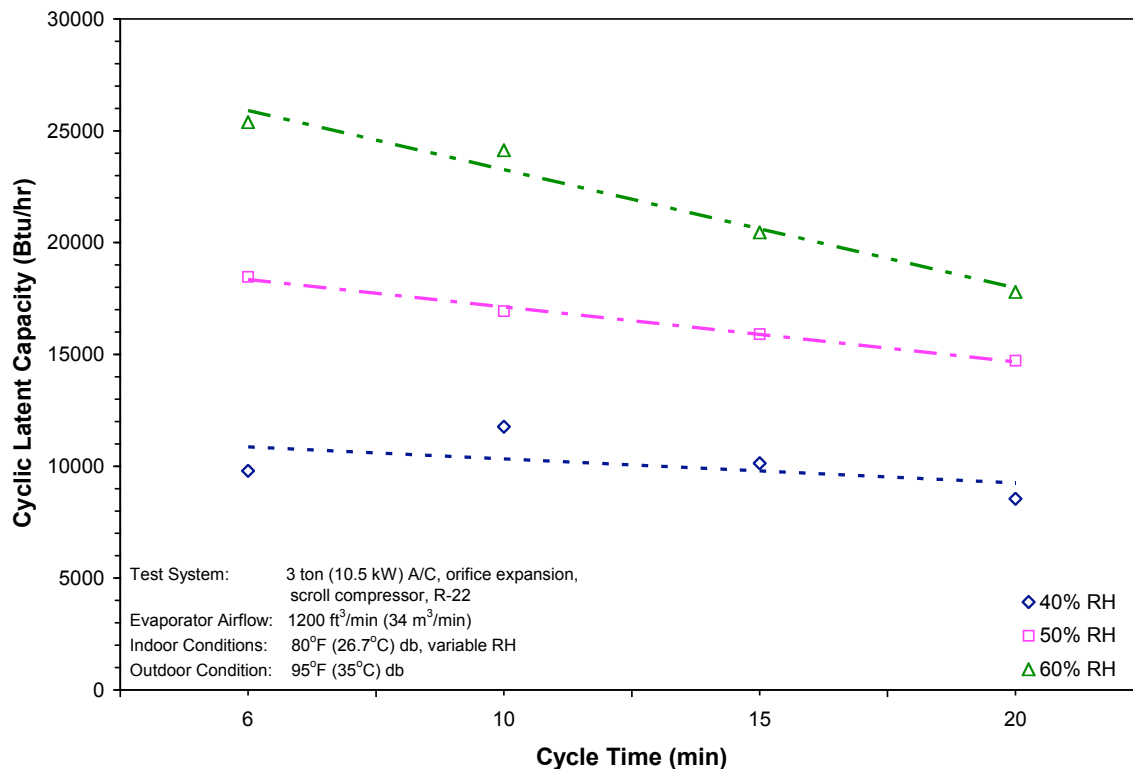
Figure 5.11 – Cyclic Latent Capacity versus Cycle Time for Various Indoor
Relative Humidities.

CYCLIC COEFFICIENT OF PERFORMANCE (COP)

Another variable used to measure the performance of the system was the cyclic

coefficient of performance (COP). The definition of the COP for the cyclic case was

modified to incorporate the instantaneous capacity and power consumption of the system

measured during the transient tests. The conventional definition of the COP is expressed

as the dimensionless ratio of cooling capacity to power consumed. The cyclic COP was

based on the total amount of energy transferred over a given cycle instead of steady-state

energy transfer rates. The definition of the cyclic COP is

$$COP_{cyclic} = \frac{\int_{t_{on}}^{t_{off}} \dot{Q}_{total} dt}{\int_{t_{on}}^{t_{off}} \dot{W}_{elec} dt}$$

(5.4)

where $\dot{Q}_{total}$ is the instantaneous total capacity of the system and $\dot{W}_{elec}$ is the measured instantaneous electrical power used to operate the system. The cyclic COP, based on Eq. 5.4, is shown in Figure 5.12
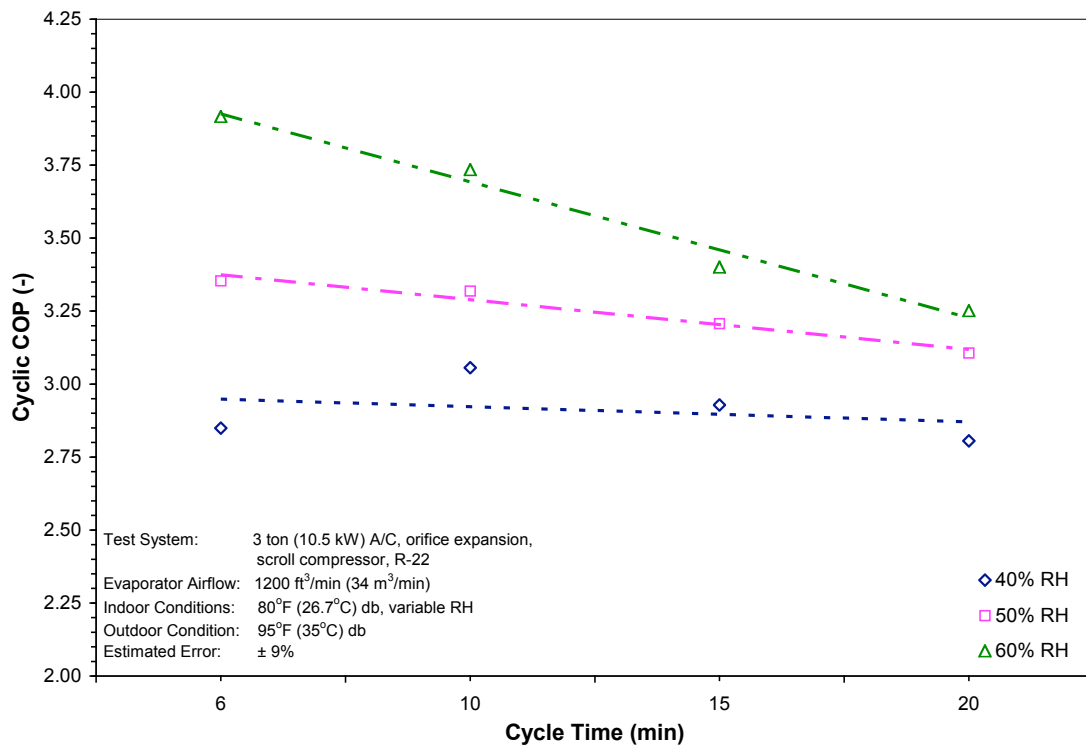
Figure 5.12 – Cyclic COP versus Cycle Time for Various Indoor Relative Humidities.

The cyclic COP decreased with an increase in cycle time for all but the 40% RH indoor humidity condition. For the 40% RH condition, the cyclic COP peaked at 3.06 for the 10 minute cycle. The cyclic COP showed increased as indoor relative humidity

increased. For all tests, the maximum COP was 3.92 and occurred at the 60% RH condition for the 6 minute cycle time.

CYCLIC SENSIBLE HEAT FACTOR (SHF)

The cyclic sensible heat factor (SHF) was another variable used to measure the performance of the system. The definition of the SHF for the cyclic case was modified to incorporate the instantaneous sensible and latent capacities of the system calculated from the transient tests. The definition of the cyclic SHF was based on the total amount of energy transferred over a given cycle instead of steady-state energy transfer rates. The expression for the cyclic SHF is of the form

$$ SHF_{cyclic} = \frac{\int_{t_{on}}^{t_{off}} \dot{Q}_{sensible}dt}{\int_{t_{on}}^{t_{off}} \dot{Q}_{total}dt} \tag{5.5} $$

where $\dot{Q}_{sensible}$ is the instantaneous sensible capacity of the system and $\dot{Q}_{total}$ is the instantaneous total capacity of the system. The cyclic SHF, based on Eq. 5.5, is shown in Figure 5.13.

The cyclic SHF generally increased with an increase in cycle time. The exception was for the 40% RH condition, where the cyclic SHF dropped to a minimum of 0.645 for the 10 minute cycle. The cyclic SHF decreased as the indoor chamber relative humidity increased, indicating that a larger fraction of the system's capacity was devoted to moisture removal at higher humidity conditions.
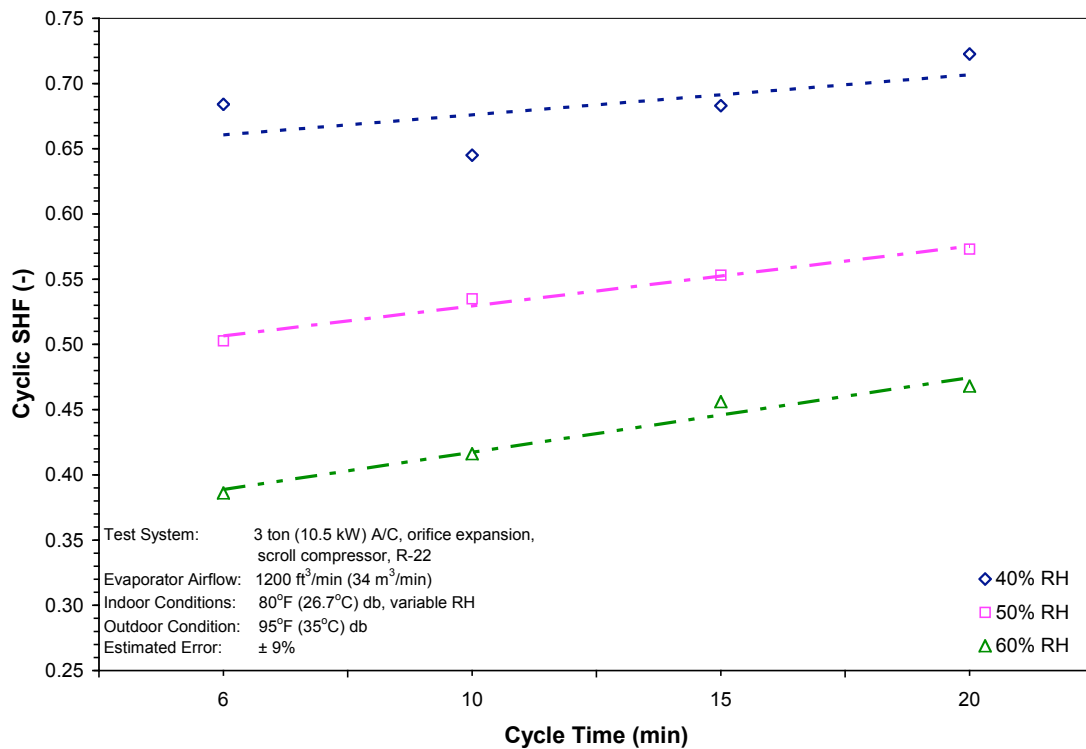
Figure 5.13 - Cyclic SHF versus Cycle Time for Various Indoor Relative Humidities.

SUMMARY OF EXPERIMENTAL RESULTS

Although a total of 12 tests were conducted in this study, a general characterization of the transient behavior of air conditioners was not possible. However, the effects of cycling on several overall performance variables were quantified. The following discussion summarizes the results of this study.

For all tests, moisture removal rate was negative at startup due to the evaporation of moisture retained on the coil during the off cycle. Sensible capacity was never negative and began to increase almost immediately after startup. Dehumidification began after the moisture removal rate became positive, but the net effect of

dehumidification was delayed by the time (the moisture removal break-even time) required to remove a net positive amount of moisture from the air stream. The moisture removal break-even time varied from 5 to 55 seconds after startup and generally decreased with increasing humidity. Cycle run time had no effect on moisture removal break-even time. The total moisture removed, given by Eq. (5.2), increased with increasing cycle time and indoor humidity.

The overall performance of the test air conditioner was quantified with the cyclic total, sensible, and latent capacities, the cyclic coefficient of performance (COP), and the cyclic sensible heat factor (SHF). In general, the cyclic total and latent capacities decreased with an increase in cycle time, but increased with indoor humidity. The cyclic sensible capacity decreased with an increase in indoor humidity, but increased with cycle time for all but the 60% RH condition. The cyclic COP generally decreased with an increase in cycle time, but increased with indoor humidity for all tests. On average, the cyclic SHF increased linearly with cycle run time but decreased with an increase in indoor humidity.

Certain aspects of this study are consistent with previous investigations into the cyclic dehumidification performance of air conditioners. The negative moisture removal rates observed after startup (Figures 5.2, 5.5, and 5.6) were also observed by Katipamula (1989). For his study, dehumidification began 60 to 150 seconds after startup whereas in the present study, dehumidification began 3 to 30 seconds after startup. The faster latent response of the air conditioner used in this study can be at least partly attributed to the fact that Katipamula's work was based on a heat pump operating in cooling mode. Heat pumps typically employ an accumulator to help prevent liquid slugging in the

compressor. Therefore, a heat pump could be expected to respond slower at startup because it will take additional time for liquid refrigerant to be evacuated from the accumulator. The test air conditioner used in this study did not have an accumulator.

Other aspects of this study were not entirely consistent with previous research concerning cyclic dehumidification performance. Katipamula (1989) showed that the cyclic efficiency of his test system increased with system run time and percent on-time. Henderson *et al.* (2003) reported that the SHF of their system decreased towards the steady-state value with increasing run-time fraction. For this study, cyclic efficiency (Figure 5.12) decreased while cyclic SHF (Figure 5.13) increased with increasing cycle time. However, the peaks in total capacity and moisture removal rate observed one minute after startup in this study (Figures 5.1, 5.2, and 5.5) were not observed in the other investigations. Above-normal total capacities during the early part of the cycle accounted for the higher cyclic efficiencies seen for shorter cycle times. Above-normal latent capacities during this same period accounted for the lower SHFs seen for shorter cycle times.

The results of this study characterized a number of important trends relating to the cyclic performance of the test air conditioner:

1. Moisture was added to the air stream during startup. Dehumidification began between 5 and 30 seconds after startup, but net positive dehumidification did not begin until 10 to 60 seconds after startup for most tests. This indicates that if a cycle is less than 1 minute, moisture may be added to the air.

2. The peak in latent capacity one minute after startup led to reduced cyclic SHFs for the shorter cycles (Figure 5.13). This simply indicated that the shorter cycles had more dehumidification capacity than the longer cycles. However, the total moisture removed increased steadily with increasing cycle time (Figure 5.8). In practice, longer cycles may be required for better overall dehumidification performance.

CHAPTER VI

EXPERIMENTAL RESULTS FOR THE EFFECTS OF EVAPORATOR AIRFLOW ON THE PERFORMANCE OF AN AIR CONDITIONING SYSTEM

The evaporator airflow tests were conducted with a single three ton (10.5 kW) condenser (unit D, described in Chapter IV) and a factory-matched evaporator. The evaporator coil was a 3-row, single slab coil with a rated airflow of 1200 ft^3/min (34 m^3/min). An initial series of baseline tests[*] were conducted to determine the refrigerant charge required to achieve refrigerant subcooling of 10ºF (6.1ºC). This was the refrigerant charge used in the system throughout the evaporator airflow tests. The relevant specifications for the evaporator used in this study are listed in Table 6.1.

Table 6.1 – Specifications for Evaporator used in Evaporator Airflow Study.

Specification	Evaporator Unit
Expansion Device	0.071 inch (1.8 mm) Orifice
Evaporator Coil Type	Plate Fin
Evaporator Coil Configuration	Diagonal Updraft
Testing Orientation	Horizontal Left
Evaporator Coil Density, fins/in. (fins/cm)	14 (5.51)
Evaporator Coil Face Area, ft^2 (m^2)	2.86 (0.266)
Rated Evaporator Fan Power, hp (kW)	1/3 (0.25)
Rated Evaporator Airflow, ft^3/min (m^3/min)	1200 (34)

---

[*] Testing conditions were those imposed by ARI Standard 210/240 Test A.

For each series of tests, the outdoor temperature was held constant at 85°F
(29.4°C) db, 95°F (35°C) db, or 105°F (40.6°C) db while indoor conditions were held
constant at 80°F (26.7°C) and 67°F (19.4°C) wb. Each series of tests consisted of eight
individual 30 minutes tests conducted at the outdoor temperature corresponding to that
series. The difference between the individual tests within each series was the evaporator
airflow rate, which varied from 600 ft^3/min (17 m³/min) to 1650 ft^3/min (46.7 m³/min)
in 150 ft^3/min (4.2 m³/min) increments. A summary of the evaporator airflow rates
used for all testing is shown in Table 6.2.

Table 6.2 – Summary of Testing for Evaporator Airflow Study.

85°F (29.4°C) db Outdoor Series		95°F (35°C) db Outdoor Series		105°F (40.6°C) db Outdoor Series		Deviation from Rated Airflow Condition	
Test	Evaporator Airflow Rate ft^3/min (m^3/min)	Test	Evaporator Airflow Rate ft^3/min (m^3/min)	Test	Evaporator Airflow Rate ft^3/min (m^3/min)		
1	600 (17)	1	600 (17)	1	600 (17)	-50.0 %	Low Airflow Tests
2	750 (21.2)	2	750 (21.2)	2	750 (21.2)	-37.5 %	
3	900 (25.5)	3	900 (25.5)	3	900 (25.5)	-25.0 %	
4	1050 (29.7)	4	1050 (29.7)	4	1050 (29.7)	-12.5 %	
5	1200 (34)	5	1200 (34)	5	1200 (34)	0.0 %	
6	1350 (38.2)	6	1350 (38.2)	6	1350 (38.2)	+12.5 %	High Airflow Tests
7	1500 (42.5)	7	1500 (42.5)	7	1500 (42.5)	+25.0 %	
8	1650 (46.7)	8	1650 (46.7)	8	1650 (46.7)	+37.5 %	

The variables used to measure the performance of the system for these tests were
total, sensible, and latent capacities, energy efficiency ratio (EER), and sensible heat

factor (SHF). Other variables reported include the system power consumption, condenser discharge pressure and temperature, evaporator suction pressure, and the air-side temperature differential across the evaporator coil.

CAPACITY

The sensible capacity of the system was based on evaporator air-side measurements. The latent capacity of the system was based on the mass of the condensate collected during a given test. Total capacity was simply the summation of sensible and latent capacities. The total, sensible, and latent capacity for all tests are shown in Figures 6.1, 6.2, and 6.3, respectively.
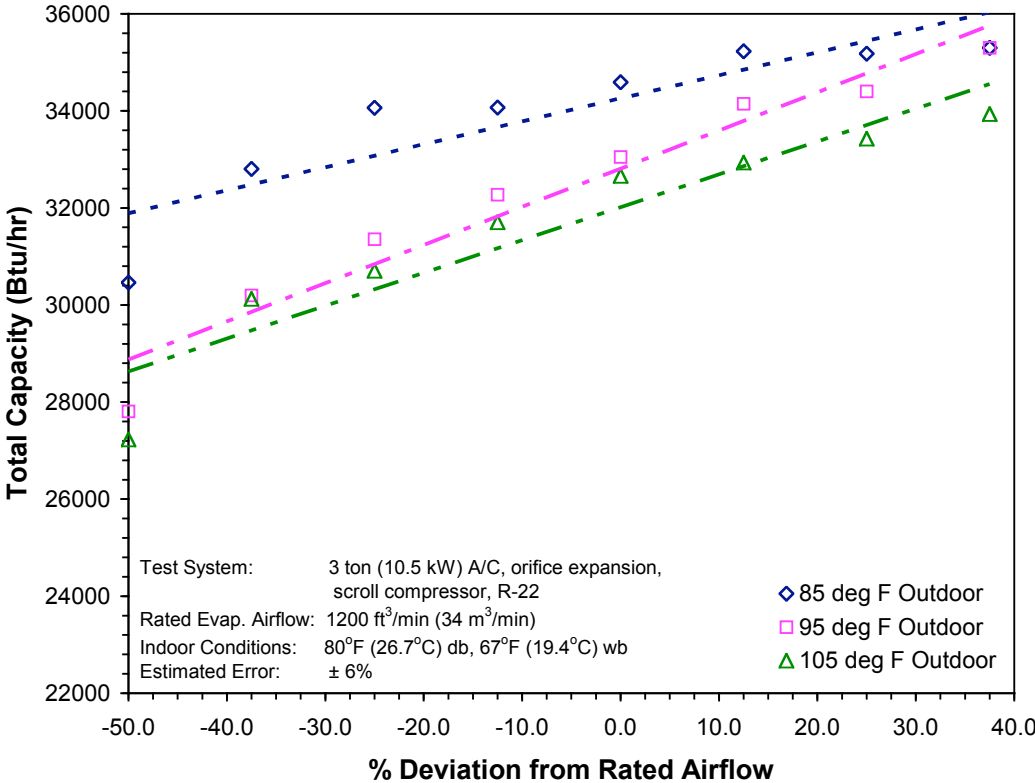
Figure 6.1 – Total Capacity for All Evaporator Airflow Tests.
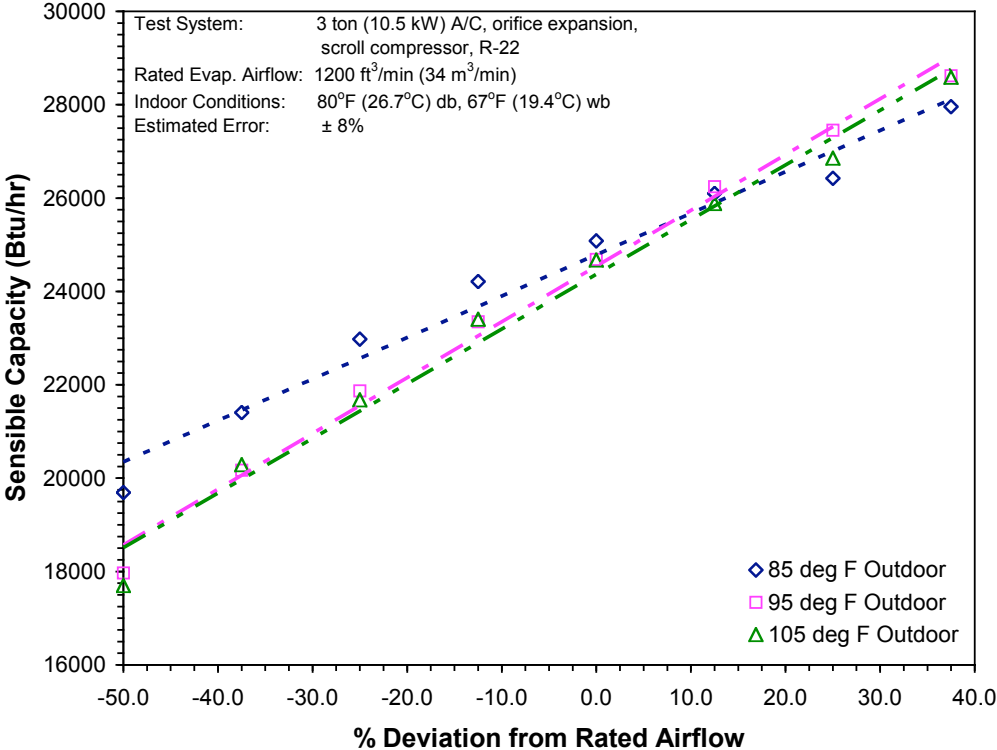
Figure 6.2 – Sensible Capacity for All Evaporator Airflow Tests.
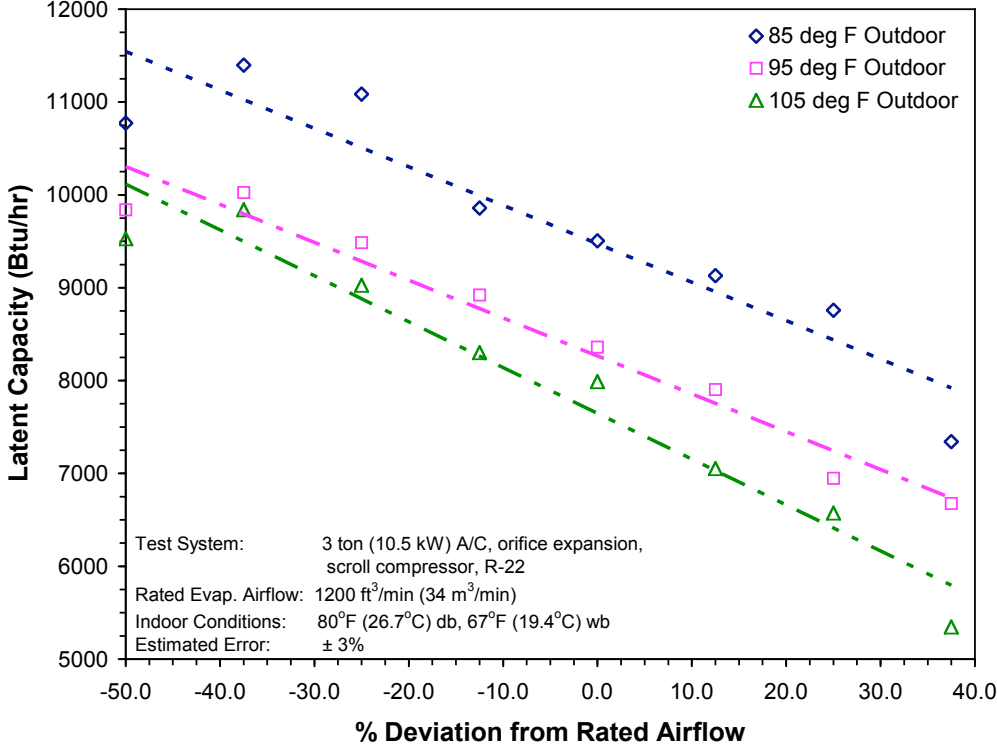
Figure 6.3 – Latent Capacity for All Evaporator Airflow Tests.

The total capacity increased with an increase in evaporator airflow. For a fixed amount of airflow through the evaporator, the total capacity increased as outdoor temperature decreased. The sensible capacity also increased as airflow increased. An interesting observation was at 50% reduced airflow, the sensible capacity for the 85°F (29.4°C) db outdoor condition was almost 10% higher than for the 95°F (35°C) db and 105°F (40.6°C) db outdoor conditions. As airflow increased, the difference between the sensible capacities for the three outdoor conditions decreased to less than 5%. The latent capacity reached a maximum for a 37.5% reduction in airflow for all three outdoor conditions and then decreased as airflow increased.

The total capacity decreased by an average of 18% for a 50% reduction below rated airflow. The total capacity increased by an average of 7% for a 37.5% increase above rated airflow. The latent capacity was also affected by deviations in evaporator airflow from the rated condition. In general, a 37.5% reduction below rated airflow increased latent capacity by about 20%. A 37.5% increase above rated airflow decreased the latent capacity of the system by an average of about 35%.

ENERGY EFFICIENCY RATIO (EER)

Figure 6.4 shows the EER values for all evaporator airflow tests. The EER was relatively constant over the range of airflows considered except for the case of 50% reduced airflow, where it decreased. The curves shown in Figure 6.4 indicate that system efficiency was not greatly affected by evaporator airflow except for cases below 40% of the rated condition. For a fixed amount of airflow through the evaporator, the EER decreased as outdoor temperature increased. The difference between EER values for each outdoor condition was essentially constant over the range of airflow rates

considered. In general, the difference between the 85°F (29.4°C) db and 95°F (35°C) db

outdoor conditions was about 23% while the difference between the 95°F (35°C) db and

105°F (40.6°C) db outdoor conditions was about 12%.
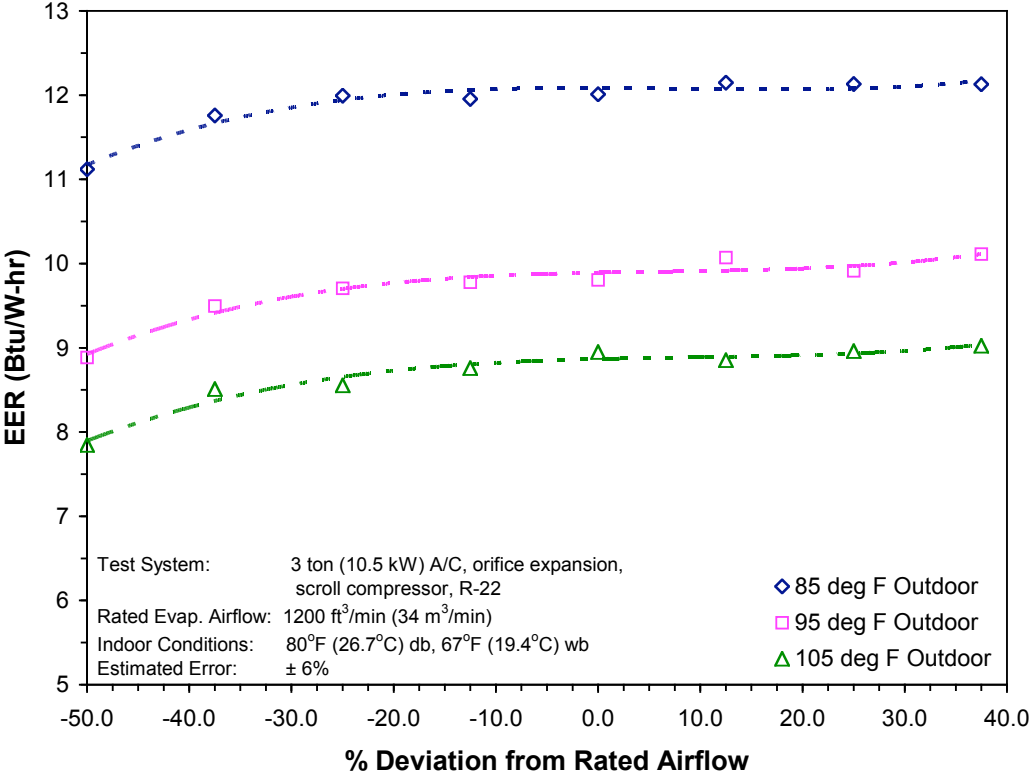
Figure 6.4 – EER for All Evaporator Airflow Tests.

SENSIBLE HEAT FACTOR (SHF)

Figure 6.5 shows the SHF values for all evaporator airflow tests. The SHR

increased with an increase in evaporator airflow. On average, a 50% reduction in

evaporator airflow resulted in a 15% reduction in the SHF while a 37.5% increase in

evaporator airflow resulted in a 10% increase in the SHF. The SHF showed a slight

dependence on outdoor temperature, but for a given airflow rate, the largest difference between the SHF for any two tests was only 7%. These results indicate that evaporator airflow had a greater effect on the dehumidification capacity of the test air conditioner than the outdoor temperatures considered in this study.
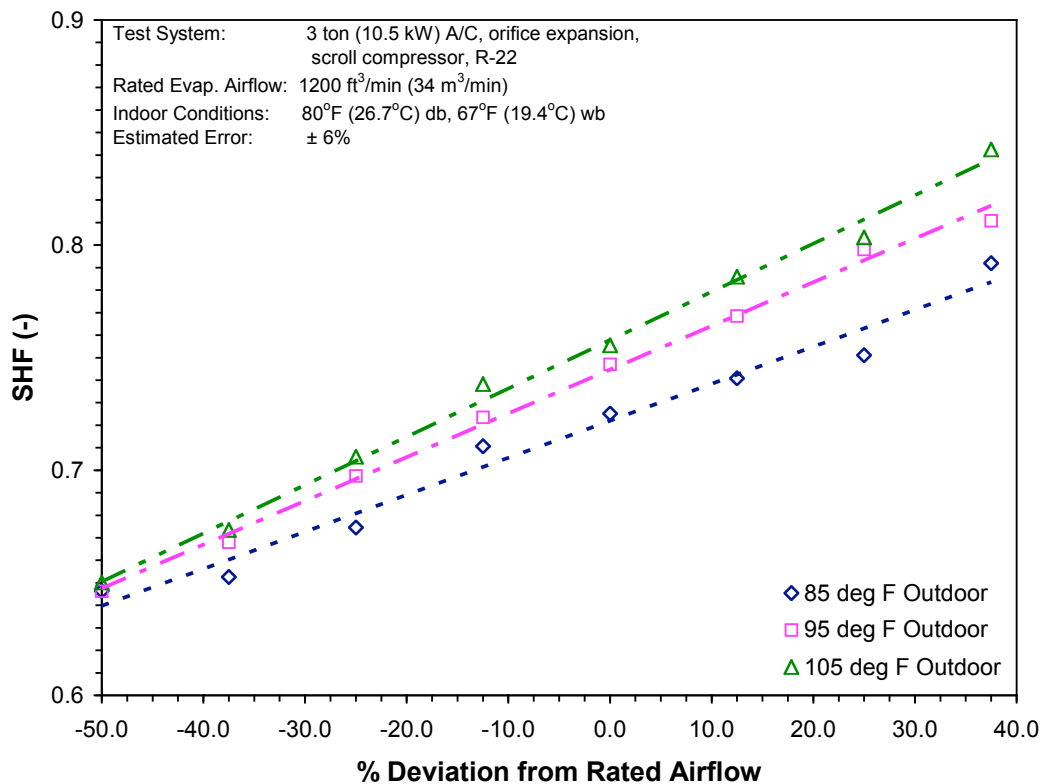
Figure 6.5 – SHF for All Evaporator Airflow Tests.

POWER CONSUMPTION

Figure 6.6 shows the power consumption of the system (evaporator and condenser) for all evaporator airflow tests. The system power consumption increased by an average of 9% from the lowest to highest evaporator airflow rate. System power consumption also increased with an increase in outdoor temperature. In general, power

consumption increased about 17% from the 85°F (29.4°C) db to the 95°F (35°C) db outdoor condition. System power increased by an average of 10% from the 95°F (35°C) db to the 105°F (40.6°C) db outdoor condition. Figure 6.7 shows the power consumption of the condenser only. Condenser power consumption increased by an average of 5% from the lowest to highest evaporator airflow rate. The average difference in condenser power consumption between the three outdoor temperature conditions was about 13%.
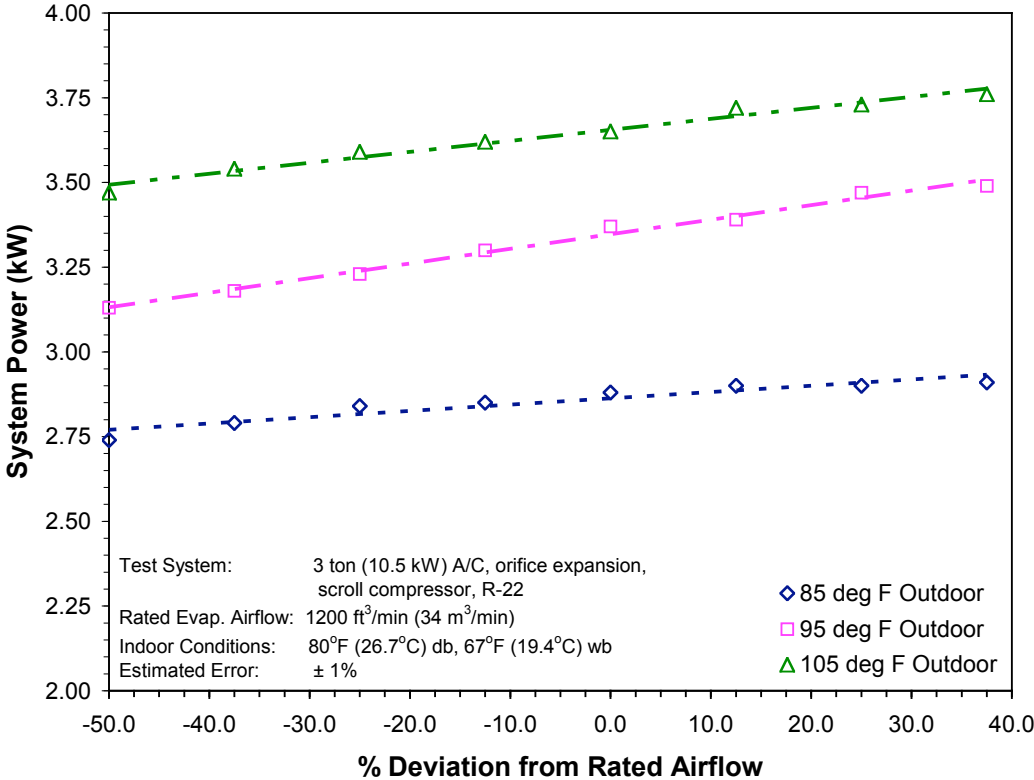
Figure 6.6 – System Power Consumption for All Evaporator Airflow Tests.
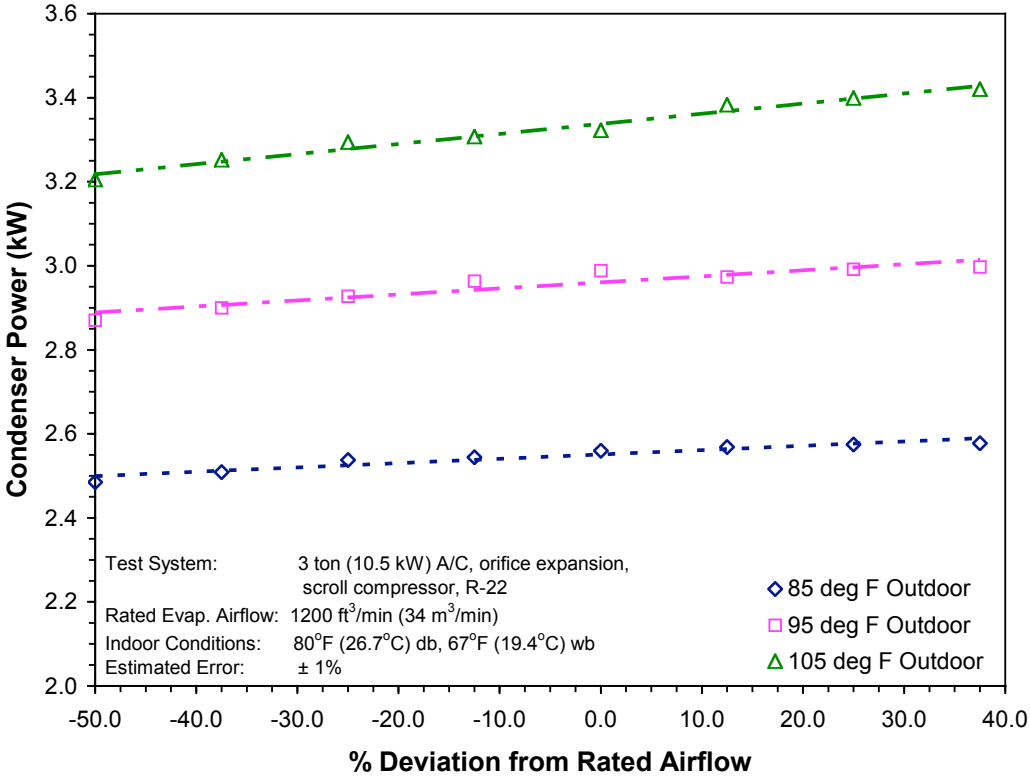
Figure 6.7 – Condenser Power Consumption for All Evaporator Airflow Tests.

CONDENSER DISCHARGE PRESSURE AND TEMPERATURE

The condenser refrigerant discharge pressure is shown in Figure 6.8 for all evaporator airflow tests. The discharge pressure increased slightly for an increase in evaporator airflow rate. In general, the discharge pressure increased by about 4% from the lowest to highest evaporator airflow rate. Discharge pressure increased with outdoor temperature to a greater extent. The average increase in discharge pressure from the 85°F (29.4°C) db to 95°F (35°C) db and from the 95°F (35°C) db to 105°F (40.6°C) db outdoor condition was about 16%.
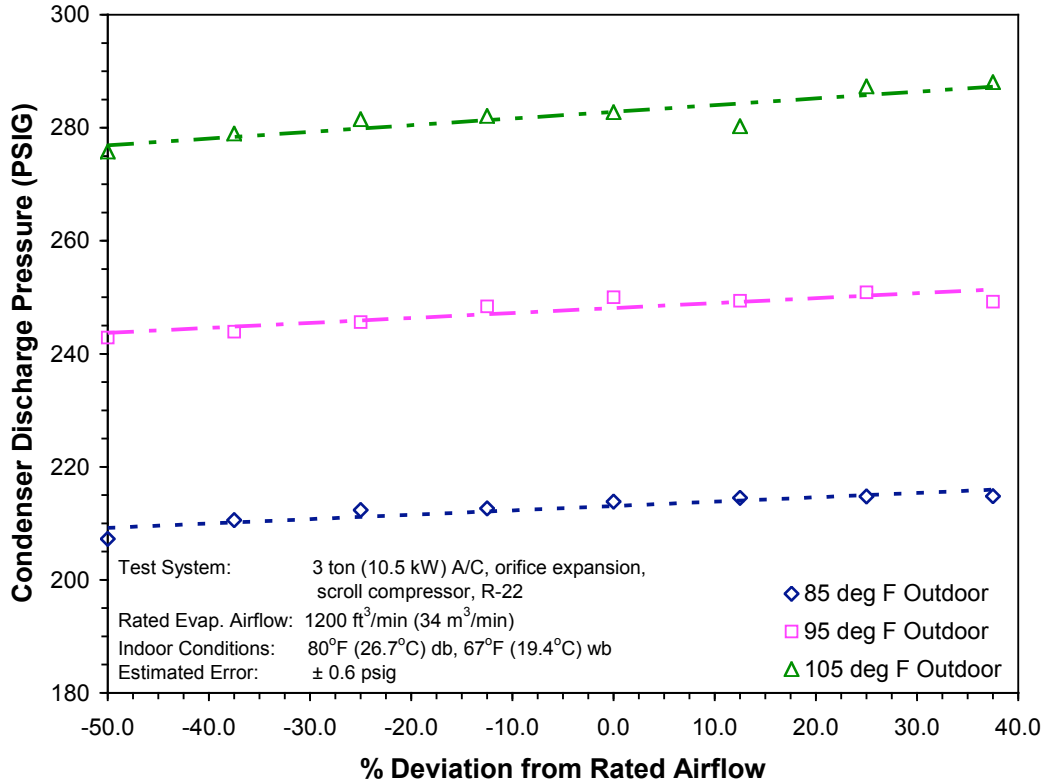
Figure 6.8 – Condenser Refrigerant Discharge Pressure for All Evaporator
Airflow Tests.

Figure 6.9 shows the condenser refrigerant discharge temperature. The discharge temperature was essentially independent of evaporator airflow, but was affected by outdoor temperature. On average, an increase in outdoor temperature of 10°F (5.6°C) resulted in an 11°F (6.1°C) increase in discharge temperature.
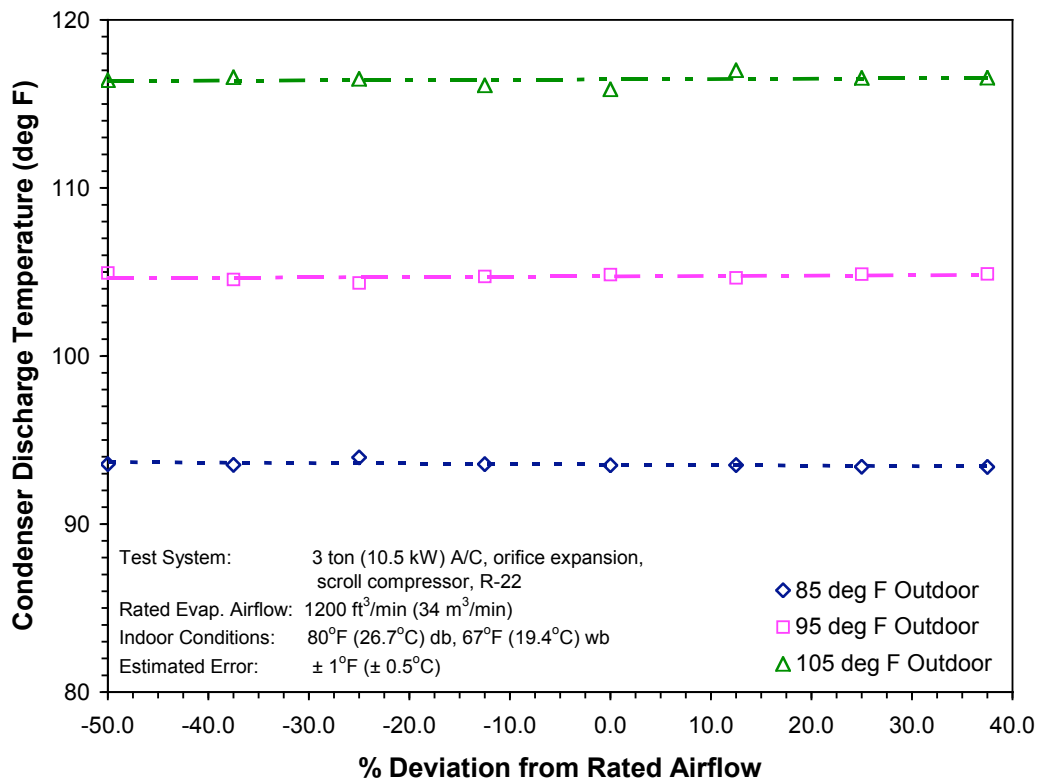
Figure 6.9 – Condenser Refrigerant Discharge Temperature for All
Evaporator Airflow Tests.

EVAPORATOR SUCTION PRESSURE

Figure 6.10 shows the evaporator refrigerant suction pressure for all evaporator airflow tests. The suction pressure increased nonlinearly for an increase in evaporator airflow rate. Suction pressure also increased with an increase in outdoor temperature. An interesting observation was that the suction pressures for the 95°F (35°C) db and 105°F (40.6°C) db outdoor conditions were essentially the same at 50% reduced airflow, but slowly diverged as evaporator airflow increased. The suction pressure for the 85°F (29.4°C) db outdoor condition was about 8% lower than for the 95°F (35°C) db outdoor condition for all airflow rates. An important observation was that for the 85°F (29.4°C) db outdoor condition, the suction pressure at 50% reduced evaporator airflow was
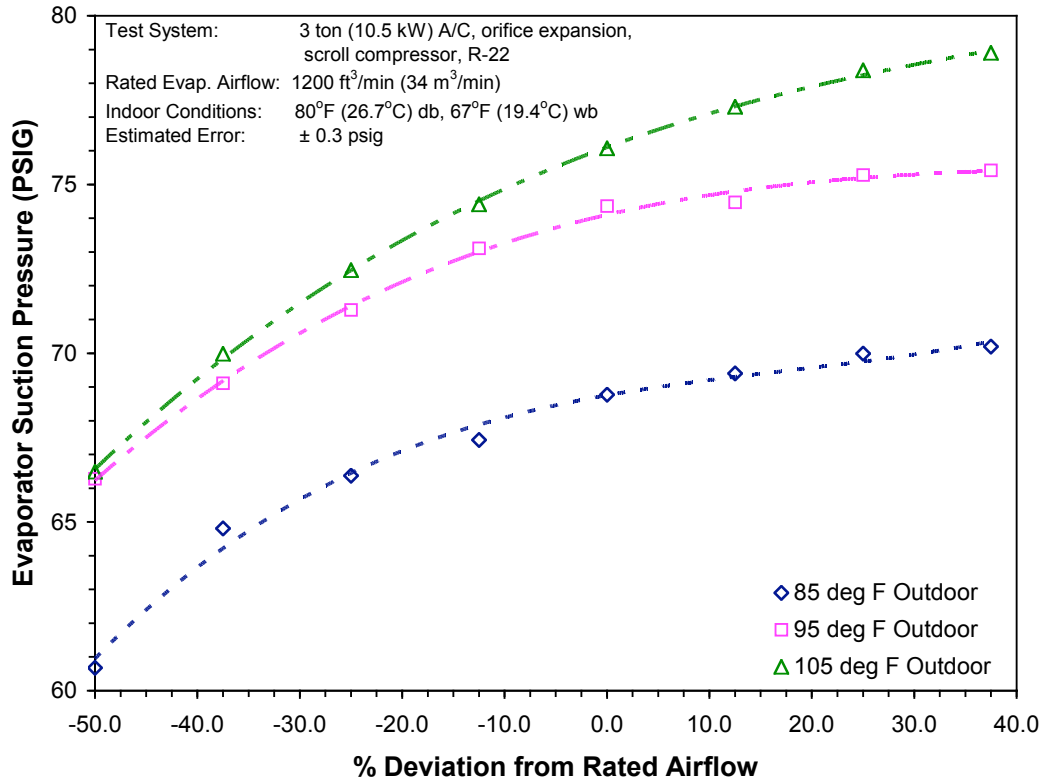
Figure 6.10 – Evaporator Refrigerant Suction Pressure for All Evaporator
Airflow Tests.

around 61 psig (5.2 bar), which corresponded to an evaporating (saturation) temperature
of about 34°F (1.1°C). This indicates that evaporator coil frosting is likely to occur for
evaporator airflow rates and outdoor temperatures just slightly lower than the range
considered in this study.

EVAPORATOR AIR TEMPERATURE DIFFERENTIAL

The air-side temperature differential across the evaporator coil is shown in Figure
6.11. The air temperature differential decreased as evaporator airflow increased. The
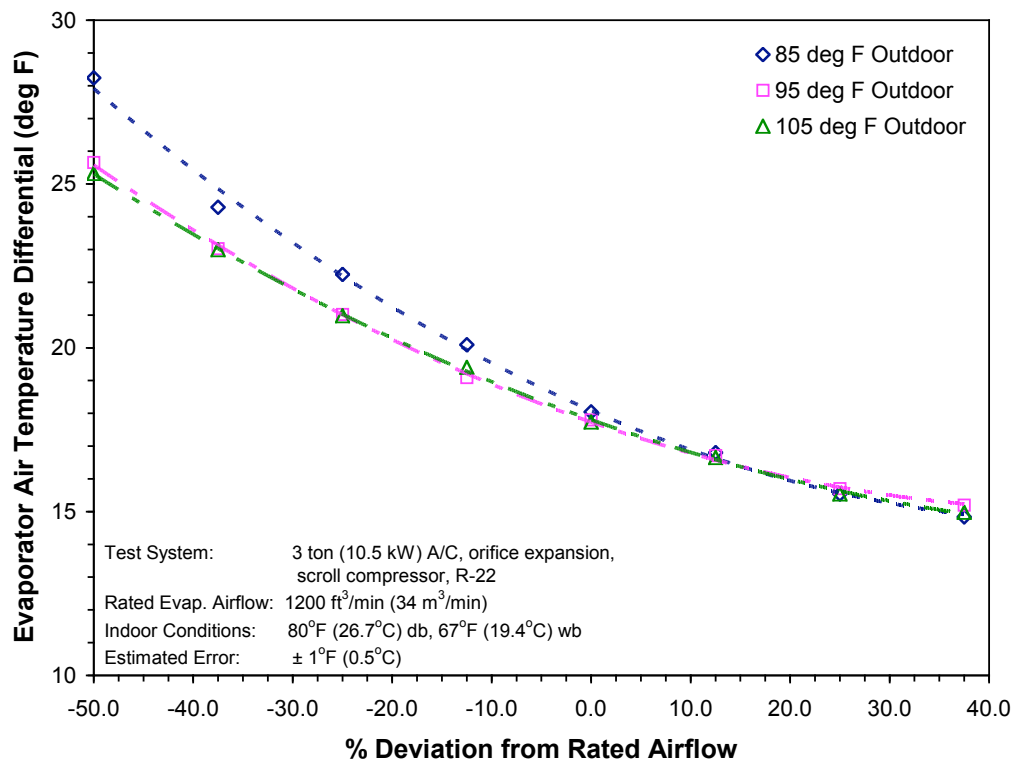
Figure 6.11 – Evaporator Air Temperature Differential for All Evaporator
Airflow Tests.

temperature differential for the 95°F (35°C) db and the 105°F (40.6°C) db outdoor

conditions were within 2% for all airflow rates. For airflow rates at or above rated

airflow, the temperature differentials for all three outdoor conditions were within 3%.

Another interesting observation was that for airflow rates below rated airflow, the

temperature differential curve for the 85°F (29.4°C) db outdoor condition diverged from

the other two curves. For the 85°F (29.4°C) db outdoor condition at 50% reduced

airflow, the air-side evaporator temperature differential was approximately 10% higher

than for the other two outdoor conditions.

SUMMARY OF EXPERIMENTAL RESULTS

Total and sensible capacity increased whereas latent capacity decreased for an increase in evaporator airflow. Overall, an increase in outdoor temperature had little effect on sensible capacity, but was seen to increase latent capacity. The EER remained relatively constant for all evaporator airflow rates except the lowest, for which it decreased. The SHF increased for increases in both evaporator airflow and outdoor temperature, but evaporator airflow had a larger effect. System power consumption increased slightly with an increase in evaporator airflow and increased to a greater extent with an increase in outdoor temperature. The condenser refrigerant discharge pressure and temperature were essentially constant over the range of evaporator airflows considered, but increased substantially with an increase in outdoor temperature. The evaporator suction pressure increased with an increase in both evaporator airflow and outdoor temperature. The evaporator air temperature differential decreased as evaporator airflow increased, but overall was affected little by outdoor temperature.

The results of this study are generally consistent with previous research conducted for low evaporator airflow conditions. For a 50% reduction in evaporator airflow, Palani *et al*. (1992) observed that the total capacity of a residential air conditioner decreased by as much as 15%. An average of an 18% reduction in total capacity was observed in this study for the same reduction in evaporator airflow. Rodriguez *et al.* (1996) quantified a 7% reduction in SHF for a 50% reduction in evaporator airflow for one system with a thermostatic expansion valve (TXV) and another system with an orifice expansion device. For the present study, the SHF decreased by an average of 15% for the same reduction in evaporator airflow. The greater reduction in SHF observed for the present study as compared to other research

could be because the test systems used by Rodriguez *et al.* (1996) were actually heat pumps operating in cooling mode. This indicates that the dehumidification performance of air conditioners may be slightly more sensitive to evaporator airflow than heat pumps.

The results of this study highlighted several operating characteristics of the test air conditioner under various evaporator airflow conditions:

1. Evaporator airflow can be as low as 40% below the rated condition without significantly impacting system efficiency (EER). Extrapolation of the curves in Figure 6.4 indicates that system efficiency would also not be greatly affected for airflow rates 40% above the rated condition or higher. This implies that sizeable efficiency losses in residential installations are not generally caused by improperly configured evaporator airflow.

2. Increasing evaporator airflow can increase total and sensible capacity, but at the expense of latent capacity. The latent capacity can decrease more than 35% for airflow rates 40% above the rated condition. Therefore a system operating with higher than rated evaporator airflow will remove more net heat energy, but dehumidification performance will be poorer.

3. Reducing evaporator airflow can reduce the SHF, but if the airflow is too low, the evaporating temperature in the coil may decrease below freezing. For a given airflow rate, evaporating temperature also decreased with outdoor temperature. Therefore evaporator coil icing may result for low airflow rates and outdoor temperatures.

CHAPTER VII

EXPERIMENTAL RESULTS FOR THE EFFECTS OF CONDENSING COIL

FOULING ON THE PERFORMANCE OF AN AIR CONDITIONING SYSTEM

The condensing coil fouling tests were conducted with a total of six condensing units divided into three groups. A naming convention of groups A, B, and C was used, with each group consisting of a #1 and #2 unit. Within each group, the #1 and #2 units were identical in make, model, and brand and each group was comprised of units made by a different manufacturer. The #1 unit in each group served as the control unit and was never cleaned while each #2 unit was subjected to periodic cleaning throughout the study. All testing was completed using the same evaporator and expansion device as used in the cycling and evaporator airflow experiments presented in Chapters V and VI. The major specifications for the six condensers used in this study are shown in Table 7.1.

Table 7.1 – Specifications for Condensing Units used in Coil Fouling Study.

Specification	Group A		Group B		Group C	
	A1	A2	B1	B2	C1	C2
Nominal Capacity, tons (kW)	3 (10.5)		3 (10.5)		3 (10.5)	
Compressor Type	Scroll		Scroll		Scroll	
Condenser Coil Fin Type	Pin		Plate		Plate	
Condenser Coil Density, fins/in. (fins/cm)	24 (9.45)		25 (9.84)		22 (8.66)	
Condenser Coil Face Area, ft^2 (m^2)	15.86 (1.47)		14.90 (1.38)		11.41 (1.06)	
Condenser Fan Capacity ft^3/min (m^3/min)	2500 (70.8)		2800 (79.3)		2510 (71.1)	

At the beginning of the experiment, all six test units were brand new and were delivered with an unknown factory charge of refrigerant (R-22). Each unit was initially operated in steady-state conditions[*] while refrigerant was added to or removed from the unknown factory charge until approximately 10ºF (6.1ºC) of subcooling was established. To establish a datum for future tests, two 1-hour steady-state baseline tests[†] were conducted on each unit before they were placed in an outdoor environment. After the baseline tests were completed, the units were placed in the outdoor runtime area described in Chapter III. The fans of each unit were operated continuously for approximately 2000 hours and then the units were brought back into the laboratory for the next round of testing. All six units were first retested[†] and then each #2 unit was cleaned[**] and immediately retested. The units were then placed back into the outdoor runtime area and the process was repeated two additional times. The last outdoor runtime period was approximately 4000 hours. The duration of each testing cycle in relation to the others is shown in Figure 7.1. A detailed description of the testing cycles and conditions can be found in Chapter IV.
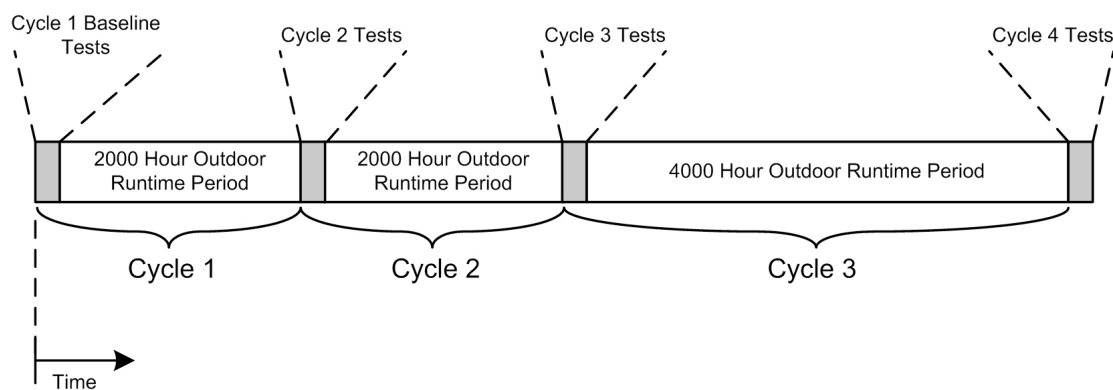
Figure 7.1 – Timeline of Testing Cycles for the Coil Fouling Study.

[*] Room conditions were those imposed by ARI Standard 210/240 Test A. See Chapter IV.
[†] ARI Standard 210/240 Tests A and B. See Chapter IV.
[**] The cleaning techniques used on each unit utilized a non-acid based foaming coil cleaner applied in accordance with the manufacturer's cleaning instructions.

The variables used to measure the performance of each unit were total capacity, energy efficiency ratio (EER) and sensible heat factor (SHF). Other variables reported include the system power consumption, condenser discharge pressure, and evaporator suction pressure. Airflow through the condenser was not calculated directly but was considered from the pressure differential measured across the condenser airflow chamber nozzles.

CAPACITY

The total capacity of the system was determined from the summation of air-side sensible and latent capacities. Sensible capacity was determined from air-side measurements in the evaporator and latent capacity was based on the mass of condensate collected during a given test. The total capacities for groups A, B, and C are shown in Tables 7.2, 7.3, and 7.4, respectively.

Table 7.2 – Total Capacity for Units in Group A.

Testing Cycle / Total Outdoor Runtime (hrs)	Total Capacity (Btu/hr) Estimated Error = ± 6%		
	Unit A1	Unit A2	
	---	Pre-Cleaning	Post-Cleaning
1 / 0	31,479	32,503	---
2 / 2000	33,374	33,075	32,782
3 / 4000	32,819	32,446	32,264
4 / 8000	30,362	33,704	33,133

Table 7.3 – Total Capacity for Units in Group B.

Testing Cycle / Total Outdoor Runtime (hrs)	Total Capacity (Btu/hr) Estimated Error = ± 6%		
	Unit B1	Unit B2	
	---	Pre-Cleaning	Post-Cleaning
1 / 0	32,256	32,173	---
2 / 2000	33,756	33,431	34,194
3 / 4000	34,255	33,558	33,673
4 / 8000	30,712	27,006	28,517

Table 7.4 – Total Capacity for Units in Group C.

Testing Cycle / Total Outdoor Runtime (hrs)	Total Capacity (Btu/hr) (±6% error) Estimated Error = ± 6%		
	Unit C1	Unit C2	
	---	Pre-Cleaning	Post-Cleaning
1 / 0	32,936	32,615	---
2 / 2000	33,840	34,014	33,950
3 / 4000	34,002	34,040	34,321
4 / 8000	26,184	28,099	28,717

The total capacities shown in Tables 7.2 through 7.4 are for the results of ARI Standard 210/240 Test A (ARI, 2003). The results for ARI Standard 210/240 Test B were similar and are not included in the present discussion. The total capacity for all three groups remained relatively constant until the last testing cycle was reached (8000 hours total outdoor runtime). The total capacity for unit A1 (Table 7.2) decreased by about 8% at 8000 hours total runtime compared to capacities measured for previous testing cycles. The total capacity for unit A2, before and after cleaning, varied less than 3% over all outdoor runtimes considered. Total capacity for unit B1 (Table 7.3) also decreased by about 8% at 8000 hours total runtime compared to capacities measured in earlier testing cycles. The total capacity for unit B2 was seen to decrease by up to 23% at 8000 hours. The total capacity for units C1 and C2 (Table 7.4) decreased by about 30% and 20% at 8000 hours, respectively.

One of the goals of this study was to determine if regular coil cleaning actually improved performance. The #2 units in each group were tested, cleaned, and then retested after each outdoor runtime period was completed. The differences in performance of a unit before and after cleaning are presented in Tables 7.2 through 7.4 as the pre-cleaning and post-cleaning capacities for the #2 units. In almost all cases, the post-cleaning capacities were slightly higher than the pre-cleaning capacities. For units A2, B2, and C2, total capacity before and after cleaning for total outdoor runtimes of 2000 and 4000 hours differ by less than 1%. For a total outdoor runtime of 8000 hours, the post-cleaning capacities of units A2, B2, and C2 differ from the pre-cleaning capacities by no more than 6%.

At first glace, the total capacity results indicate that coil fouling in the last test cycle, which was 4000 hours as opposed to the previous 2000 hour cycles, may have had more of an impact on system performance. However, the total capacity of the control (#1) units decreased inconsistently with the total capacity of the cleaned (#2) units. Because the control units were never cleaned for the duration of the experiment, they would be expected to experience more of a performance drop due to fouling over the course of the experiment. But for group B, the total capacity of the control unit (B1) decreased less than that of the cleaned unit (B2) at 8000 hours of total outdoor runtime. For group C, the total capacity of the control unit (C1) decreased more than that of the cleaned unit (C2) at the same amount of outdoor runtime. This indicates that factors other than coil fouling may also have contributed to the notable decrease in total capacity observed for the last testing cycle. An important observation is that in general, cleaning the condensing coils between cycles did slightly affect the performance of the air conditioners, but the measurable effect was within the uncertainty of the air-side capacity calculations (see Appendix A).

ENERGY EFFICIENCY RATIO (EER)

Tables 7.5, 7.6, and 7.7 show the EER values for groups A, B, and C, respectively. The EER for group A varied by no more than 7% over all outdoor runtimes considered. The EER for group B showed more variation, with an increase of around 14% for the control unit (B1) between the zero and 4000 hours total runtime mark. At 8000 hours total runtime, the EER of the control unit decreased to values comparable to the baseline values and the cleaned unit (B2) showed a 20% decrease in pre-cleaned EER from previous values. The EER values of group C showed a similar

pattern to group B, but the EER of the control unit (C1) decreased more than the cleaned unit (C2) after 8000 hours of total runtime.

Cleaning slightly affected the efficiency of the units. In general, the EER for a unit was slightly higher after cleaning than before. The largest increase in EER after cleaning for any unit was about 8% for the cycle 4 test performed on unit B2. All other increases in EER after cleaning were less than 5%, which is within the uncertainty of the air-side capacity calculations. Therefore, the periodic coil cleaning performed in this study did not appear to have a meaningful effect on the efficiency of most of the air conditioners.

Table 7.5 – EER for Units in Group A.

Testing Cycle / Total Outdoor Runtime (hrs)	EER (Btu/W-hr) Estimated Error = ± 6%		
	Unit A1	Unit A2	
	---	Pre-Cleaning	Post-Cleaning
1 / 0	9.8	9.9	---
2 / 2000	10.4	10.2	10.1
3 / 4000	10.0	9.4	9.5
4 / 8000	9.4	10.1	10.0

Table 7.6 – EER for Units in Group B.

Testing Cycle / Total Outdoor Runtime (hrs)	EER (Btu/W-hr) Estimated Error = ± 6%		
	Unit B1	Unit B2	
	---	Pre-Cleaning	Post-Cleaning
1 / 0	9.5	9.5	---
2 / 2000	10.6	10.0	10.5
3 / 4000	10.8	10.2	10.3
4 / 8000	9.9	8.5	9.1

Table 7.7 – EER for Units in Group C.

Testing Cycle / Total Outdoor Runtime (hrs)	EER (Btu/W-hr) Estimated Error = ± 6%		
	Unit C1	Unit C2	
	---	Pre-Cleaning	Post-Cleaning
1 / 0	10.5	10.1	---
2 / 2000	10.8	10.6	10.6
3 / 4000	10.8	10.6	10.8
4 / 8000	8.8	9.3	9.5

SENSIBLE HEAT FACTOR (SHF)

Tables 7.8, 7.9, and 7.10 show the SHF values for groups A, B, and C, respectively. For all tests, the SHR varied little with an increase in outdoor runtime or with cleaning. The largest variation in SHF between any two tests for a given group was less than 3% in all cases. This indicates that coil fouling or cleaning did not significantly affect the dehumidification capacity of any of the test systems.

Table 7.8 – SHF for Units in Group A.

Testing Cycle / Total Outdoor Runtime (hrs)	SHF (-) Estimated Error = ± 6%		
	Unit A1	Unit A2	
	---	Pre-Cleaning	Post-Cleaning
1 / 0	0.78	0.73	---
2 / 2000	0.77	0.78	0.78
3 / 4000	0.75	0.79	0.77
4 / 8000	0.74	0.75	0.75

Table 7.9 – SHF for Units in Group B.

Testing Cycle / Total Outdoor Runtime (hrs)	SHF (-) Estimated Error = ± 6%		
	Unit B1	Unit B2	
	---	Pre-Cleaning	Post-Cleaning
1 / 0	0.75	0.76	---
2 / 2000	0.76	0.77	0.75
3 / 4000	0.76	0.76	0.76
4 / 8000	0.74	0.78	0.77

Table 7.10 – SHF for Units in Group C.

Testing Cycle / Total Outdoor Runtime (hrs)	SHF (-) Estimated Error = ± 6%		
	Unit C1	Unit C2	
	---	Pre-Cleaning	Post-Cleaning
1 / 0	0.75	0.75	---
2 / 2000	0.77	0.76	0.75
3 / 4000	0.75	0.75	0.76
4 / 8000	0.78	0.77	0.76

POWER CONSUMPTION

System power consumption for groups A, B, and C is shown in Tables 7.11, 7.12, and 7.13, respectively. For all tests, power consumption varied somewhat with outdoor runtime or unit cleaning. For a given unit, the largest variation in power consumption between any two tests was about 9%. The largest decrease in power consumption after cleaning was less than 3% and occurred for unit B2 at 2000 hours of total runtime.

Table 7.11 – System Power Consumption for Units in Group A.

Testing Cycle / Total Outdoor Runtime (hrs)	System Power Consumption (kW) Estimated Error = ± 1%		
	Unit A1	Unit A2	
	---	Pre-Cleaning	Post-Cleaning
1 / 0	3.21	3.29	---
2 / 2000	3.20	3.25	3.24
3 / 4000	3.26	3.44	3.40
4 / 8000	3.24	3.34	3.32

Table 7.12 – System Power Consumption for Units in Group B.

Testing Cycle / Total Outdoor Runtime (hrs)	System Power Consumption (kW) Estimated Error = ± 1%		
	Unit B1	Unit B2	
	---	Pre-Cleaning	Post-Cleaning
1 / 0	3.41	3.38	---
2 / 2000	3.19	3.35	3.26
3 / 4000	3.16	3.28	3.26
4 / 8000	3.09	3.18	3.12

Table 7.13 – System Power Consumption for Units in Group C.

Testing Cycle / Total Outdoor Runtime (hrs)	System Power Consumption (kW) Estimated Error = ± 1%		
	Unit C1	Unit C2	
	---	Pre-Cleaning	Post-Cleaning
1 / 0	3.15	3.22	---
2 / 2000	3.13	3.20	3.19
3 / 4000	3.16	3.21	3.19
4 / 8000	2.98	3.01	3.02

CONDENSER DISCHARGE PRESSURE

Tables 7.14, 7.15, and 7.16 show the condenser refrigerant discharge pressure for groups A, B, and C, respectively. For all tests, the discharge pressure was highest at 4000 hours of total outdoor runtime. The lowest discharge pressures generally occurred

at 8000 hours of total runtime. Cleaning had a minimal impact on discharge pressure.
In most cases, the change in discharge pressure before and after cleaning was less than
1% and never varied by more than 4%.

Table 7.14 – Condenser Refrigerant Discharge Pressure for
Units in Group A.

Testing Cycle / Total Outdoor Runtime (hrs)	Condenser Discharge Pressure (psig) Estimated Error = ± 0.6 psig		
	Unit A1	Unit A2	
	---	Pre-Cleaning	Post-Cleaning
1 / 0	244.5	254.4	---
2 / 2000	243.2	246.1	245.5
3 / 4000	248.8	264.3	261.8
4 / 8000	252.1	256.2	253.5

Table 7.15 – Condenser Refrigerant Discharge Pressure for
Units in Group B.

Testing Cycle / Total Outdoor Runtime (hrs)	Condenser Discharge Pressure (psig) Estimated Error = ± 0.6 psig		
	Unit B1	Unit B2	
	---	Pre-Cleaning	Post-Cleaning
1 / 0	234.9	233.4	---
2 / 2000	229.7	229.7	228.1
3 / 4000	237.6	241.2	239.5
4 / 8000	227.8	219.3	219.4

Table 7.16 – Condenser Refrigerant Discharge Pressure for
Units in Group C.

Testing Cycle / Total Outdoor Runtime (hrs)	Condenser Discharge Pressure (psig) Estimated Error = ± 0.6 psig		
	Unit C1	Unit C2	
	---	Pre-Cleaning	Post-Cleaning
1 / 0	237.6	239.4	---
2 / 2000	233.6	236.0	228.1
3 / 4000	240.1	241.2	238.8
4 / 8000	227.6	220.5	221.5

EVAPORATOR SUCTION PRESSURE

The evaporator refrigerant suction pressure for groups A, B, and C are shown in Tables 7.17, 7.18, and 7.19, respectively. Suction pressure varied little for all tests up to 4000 hours of total outdoor runtime. However, at 8000 hours of total runtime, the suction pressures decreased from the previous values by up to 35%. Cleaning slightly increased the suction pressure for units B2 and C2 at the 8000 hour mark, but the difference was less than 4% in both cases.

The lower suction pressures observed for the tests conducted after 8000 hours of total runtime are concurrent with the lower total capacities observed in Tables 7.2 through 7.4. The lowest value of suction pressure was approximately 55 psig (4.8 bar) for unit C2 at 8000 hours of total runtime, which corresponded to an evaporating (saturation) temperature of about 30°F (-1.1°C).

Table 7.17 – Evaporator Refrigerant Suction Pressure for
Units in Group A.

Testing Cycle / Total Outdoor Runtime (hrs)	Evaporator Suction Pressure (psig) Estimated Error = ± 0.3 psig		
	Unit A1	Unit A2	
	---	Pre-Cleaning	Post-Cleaning
1 / 0	74.6	75.8	---
2 / 2000	73.7	74.0	74.8
3 / 4000	73.7	76.1	76.3
4 / 8000	70.0	74.4	74.2

Table 7.18 – Evaporator Refrigerant Suction Pressure for
Units in Group B.

Testing Cycle / Total Outdoor Runtime (hrs)	Evaporator Suction Pressure (psig) Estimated Error = ± 0.3 psig		
	Unit B1	Unit B2	
	---	Pre-Cleaning	Post-Cleaning
1 / 0	76.3	75.4	---
2 / 2000	74.2	74.2	75.0
3 / 4000	74.3	75.3	75.2
4 / 8000	66.8	59.1	61.5

Table 7.19 – Evaporator Refrigerant Suction Pressure for
Units in Group C.

Testing Cycle / Total Outdoor Runtime (hrs)	Evaporator Suction Pressure (psig) Estimated Error = ± 0.3 psig		
	Unit C1	Unit C2	
	---	Pre-Cleaning	Post-Cleaning
1 / 0	75.1	74.7	---
2 / 2000	73.8	74.1	74.6
3 / 4000	74.4	74.5	74.4
4 / 8000	55.3	59.6	60.8

CONDENSER AIRFLOW CHAMBER PRESSURE DIFFERENTIAL

Airflow through each condenser was not calculated directly, but considered from the pressure differential across the condenser flow chamber nozzles. The pressure differential across the flow chamber nozzles for groups A, B, and C are shown in Tables 7.20, 7.21, and 7.22. The pressure differential decreased slightly with increasing outdoor runtime for almost all units. In general, cleaning tended to increase the pressure differential, indicating that condenser airflow was increased by cleaning. The most noticeable changes in pressure differential occurred for units B1 and B2, which showed a considerable decrease in airflow between 4000 and 8000 hours total runtime compared to the other units.

Table 7.20 – Condenser Flow Chamber Pressure Differential
for Units in Group A.

Testing Cycle / Total Outdoor Runtime (hrs)	Condenser Flow Chamber ΔP (in. H_2O) Estimated Error = $\pm$ 0.005 in. H_2O		
	Unit A1	Unit A2	
	---	Pre-Cleaning	Post-Cleaning
1 / 0	0.724	0.692	---
2 / 2000	0.726	0.709	0.736
3 / 4000	0.724	0.750	0.725
4 / 8000	0.697	0.727	0.758

Table 7.21 – Condenser Flow Chamber Pressure Differential
for Units in Group B.

Testing Cycle / Total Outdoor Runtime (hrs)	Condenser Flow Chamber ΔP (in. H_2O) Estimated Error = $\pm$ 0.005 in. H_2O		
	Unit B1	Unit B2	
	---	Pre-Cleaning	Post-Cleaning
1 / 0	1.361	1.423	---
2 / 2000	1.273	1.366	1.378
3 / 4000	1.310	1.340	1.396
4 / 8000	1.080	1.210	1.372

Table 7.22 – Condenser Flow Chamber Pressure Differential
for Units in Group C.

Testing Cycle / Total Outdoor Runtime (hrs)	Condenser Flow Chamber ΔP (in. H_2O) Estimated Error = ± 0.005 in. H_2O		
	Unit C1	Unit C2	
	---	Pre-Cleaning	Post-Cleaning
1 / 0	0.639	0.610	---
2 / 2000	0.613	0.589	0.622
3 / 4000	0.642	0.614	0.625
4 / 8000	0.622	0.594	0.625

SUMMARY OF EXPERIMENTAL RESULTS

Total capacity, EER, and evaporator refrigerant suction pressure were essentially constant for the first 4000 hours of outdoor runtime, but decreased considerably by the 8000 hour mark for most units. Cleaning was observed to increase total capacity and EER slightly, but the improvements were within the uncertainty of the calculated air-side capacities. In general, SHF, system power consumption, and condenser refrigerant discharge pressure were constant for the duration of the experiment and showed very little response to cleaning.

The significant drop in total capacity, EER, and suction pressure for most units at the 8000 hour mark indicate that factors other than coil fouling may have contributed to performance degradation for this testing cycle. The fact that coil cleaning in each of these cases did not significantly enhance performance reinforces this hypothesis. One

explanation for this discrepancy may be that the effective refrigerant charge used in most of the units varied enough between the third and last set of tests to result in a measurable performance drop. This could possibly be attributed to unavoidable changes in the test apparatus, such as refrigerant tubing length, between the third and last tests.

Overall, the results of this study show that for the units considered, condensing coil cleaning can produce small increases in performance and efficiency. However, the amount of benefit provided by coil cleaning can not be quantified with the present data. The only independent variable for this study was the amount of time each condenser was exposed to an outdoor environment. Because outdoor conditions can vary considerably over time and location, coil fouling can not necessarily be correlated to outdoor exposure time.

CHAPTER VIII

CONCLUSIONS AND RECOMMENDATIONS

Cycling did not significantly affect the instantaneous dehumidification performance of the test air conditioner used in the cycling study. However, cycling did affect overall performance and efficiency. A common observation for all testing was that the moisture removal rate was negative during the first 3 to 30 seconds after startup and net dehumidification occurred between 5 and 55 seconds after startup. As indoor humidity increased, the time required for net dehumidification to begin decreased. Cycle time did not appear to affect the time required to reach net dehumidification. Several overall performance variables were quantified, and they showed a dependency on both cycle time and indoor relative humidity. The cyclic total and latent capacity generally decreased with increasing cycle time and increased with indoor humidity. The cyclic sensible capacity showed an opposite response, increasing with cycle time and decreasing with increasing indoor humidity. The cyclic coefficient of performance (COP) decreased with increasing cycle time, but increased with indoor humidity. The cyclic sensible heat factor (SHF) increased with cycle time, but decreased with increasing indoor humidity.

Compared to previous research conducted on transient startup performance, it appears that dehumidification in air conditioners may respond faster than heat pumps during startup. The results of the cycling study showed that cyclic total and latent capacity were higher for shorter cycle times. This indicates that, on average, heat energy was removed at a greater rate for the shorter cycles compared to the longer cycles. However, this does not necessarily indicate that dehumidification performance is better

for shorter cycles because longer cycles remove more total moisture. Other results of the cycling study showed that for cycles shorter than one minute, moisture may be added to the space. Thus, preventing air conditioner short-cycling may help to maintain comfort conditions.

Evaporator airflow affected the overall performance of the test air conditioner used in the evaporator airflow study. Total and sensible capacity increased with airflow, but latent capacity decreased with increasing airflow. Total, sensible, and latent capacity were all higher for lower outdoor temperatures. System efficiency for the evaporator airflow study was measured by the energy efficiency ratio (EER), which was affected little by airflow but did increase with a reduction in outdoor temperature. The SHF increased with both evaporator airflow and outdoor temperature.

Several performance characteristics were derived from the results of the evaporator airflow study. Evaporator airflow was seen to vary by about ±40% from the rated condition without significantly affecting system efficiency. This indicates that some fairly substantial installation and configuration errors could occur in the field without seriously impacting the efficiency of an air conditioner. However, the capacity of the system was more sensitive to evaporator airflow. Higher evaporator airflow resulted in higher total capacity, but at the expense of latent capacity. Therefore, higher evaporator airflow may remove more net heat energy from a space, but the rise in humidity levels may negate any associated benefit. For slightly reduced airflow rates (about 10% below rated airflow), latent capacity increased by an average of about 7% whereas the total capacity decreased by less than 3%. Thus more dehumidification could be obtained without seriously reducing total capacity by simply lowering

evaporator airflow slightly below the rated condition. As evaporator airflow decreased below the rated condition, the evaporator refrigerant suction pressure decreased rapidly. The evaporating temperatures associated with these lower suction pressures decreased towards the freezing point of water as airflow decreased. Therefore, if evaporator airflow is too low, coil frosting may occur.

Outdoor runtime did not have a statistically meaningful effect on the overall performance of the six condensing units used in the coil fouling study. Total capacity and EER were essentially constant for the first 4000 hours, but decreased considerably for most units after 8000 hours of outdoor runtime was accumulated. The large drop in capacity and EER for the last testing cycle was attributed to incorrect refrigerant charging and unavoidable changes made to the test set-up between the third and fourth testing cycles. On average, airflow through the condenser (considered by the pressure differential across the condenser flow chamber nozzles) decreased slightly with increasing outdoor runtime. In general, cleaning between testing cycles slightly increased total capacity and EER, but the measured benefit was within the uncertainty of the calculated air-side capacities. For almost all tests, cleaning improved airflow through the condenser. The SHF did not appear to be affected by coil fouling or cleaning.

Comparing the pre-cleaned to post-cleaned performance and efficiency of the units in the coil fouling experiment indicated that coil cleaning generally provided slight improvements in performance and efficiency. However, because of the uncertainties associated with the various measurements made, the amount of benefit obtained from cleaning could not be truly quantified. The changes in performance and efficiency for a

given unit as a function of outdoor runtime were less consistent. Because the experimental set-up required slight modifications between any two testing cycles, comparing the performance of a unit to previous testing cycles was less meaningful than comparing the pre-cleaned to post-cleaned performance for a given testing cycle.

There are a number of ways that future work could enhance the three studies conducted in this research. These recommendations are summarized below.

In regards to the cycling study, a more complete understanding of transient dehumidification performance during startup could be obtained with a comprehensive model of the air-side energy and mass transport processes. Also, all of the data collected for the cycling study were based on a test air conditioner that used a standard orifice as an expansion device and one specific type of evaporator coil. A thermostatic expansion valve (TXV) or a capillary tube would almost certainly respond differently than an orifice. And evaporator coils with different fin densities (spacing) and surface characteristics may retain moisture differently than the coil considered in the cycling study. Therefore, future work should investigate the effects that various expansion devices and other evaporator coil geometries have on the startup dehumidification performance of air conditioners. One last recommendation for future work in transient dehumidification performance deals with instrument response time. For the cycling study, all data were acquired at a frequency of 1 reading per second. The thermocouples[*] and pressure transducers used to measure air-side and refrigerant-side temperatures and pressures all had response times that were less than 1 second. Air-side moisture measurements were made with thin-film polymer humidity sensors located

---

[*] Based on example calculations from pp 217-218 in Incropera and DeWitt, 1996.

upstream and downstream of the evaporator coil. These humidity sensors had a reported response time of about 10 seconds. A more detailed investigation into this matter revealed that the reported response time of 10 seconds was determined in still air conditions. The manufacturer of the humidity sensors verified that the response of the sensors would be significantly faster in forced airflow conditions, but did not have any data that quantified how much faster the response would be. Therefore, future work dealing with transient dehumidification performance may need to address the issue of humidity sensor time response. A series of simple experiments in which the humidity sensor is exposed to a step change in humidity could be used to characterize the expected decrease in response time for various air stream velocities.

For the evaporator airflow study, only an orifice expansion device was considered. Future work in this area will need to determine how various types of expansion devices affect system performance under a range of evaporator airflow conditions. Also, only one type of evaporator coil configuration (i.e. coil orientation, placement in the air stream, etc.) was considered in the evaporator airflow study. Moisture drainage from an evaporator coil may vary markedly from one coil orientation to the next and coil placement may affect the air stream directly. Therefore, more work is recommended to determine the effects of evaporator coil configuration on system performance over a range of evaporator airflow conditions.

For the coil fouling study, the only independent variable was outdoor runtime. In practice, actual condenser coil fouling depends not only on outdoor runtime, but on other factors such as outdoor conditions and coil geometry. Because outdoor conditions can vary over time and location, coil fouling can not necessarily be correlated to outdoor

runtime. Future work in this area will need to include a more reliable way of controlling and measuring coil fouling. One recommendation is exposing the condenser to a continuously agitated mixture of standardized dusts[†] for a specified amount of time in a controlled environment. For diagnostics, optical microscopy could be used to evaluate the thickness of dust buildup on the coil surface at various points. In addition, more accurate condenser airflow measurements might be useful in characterizing the amount of fouling.

[†] e.g. ASHRAE synthetic dust or a combination of the ISO-12103-1 A1-A4 test dusts.

REFERENCES

ANSI/ISA, 1982. *Standard MC96.1, Temperature measurement thermocouples.* Washington, DC: American National Standards Institute.

ANSI/AMCA, 1999. *Standard 210-99, Laboratory methods of testing fans for aerodynamic performance rating.* Arlington Heights, IL: Air Movement and Control Association International, Inc.

ANSI/ASHRAE, 1986. *Standard 41.1-86, Standard method for temperature measurement.* Atlanta, GA: American Society of Heating, Refrigerating, and Air-Conditioning Engineers, Inc.

ARI, 2003. *Standard 210/240, Unitary air-conditioning and air-source heat pump equipment.* Arlington, VA: Air-Conditioning and Refrigeration Institute.

DOE, 1999. *Energy-Efficient Air Conditioning.* Golden, CO: National Renewable Energy Laboratory, U. S. Department of Energy.

EIA, 1999. *A Look at Residential Energy Consumption in 1997.* Washington, DC: Energy Information Administration, U. S. Department of Energy.

Greig, A. 1998. Technical Factors Accounting for Double-Digit Energy Efficiency Improvement Accruing from Cleaning and Treatment of HVAC/R Condenser Coils and Extended Unit Life. *Technical Paper and Support of HVAC/R.* Palm Coast, FL: Adsil, Inc.

Henderson, H. I., Shirey, D. B., and Raustad, R. A. 2003. "Understanding the Dehumidification Performance of Air-Conditioning Equipment at Part-Load Conditions." *Presented at the CIBSE/ASHRAE Conference.* Edinburgh, Scotland, September 24-26.

Incropera, F. P., and DeWitt, D. P. 1999. *Fundamentals of Heat and Mass Transfer.* 4th Edition. New York: Wiley.

Judge, J. F., and Radermacher, R. 1995. The Transient and Steady State Performance of R-22 and R-407C. *Heat Pump and Refrigeration Systems Design, Analysis and Applications – Proceedings of ASME.* AES-Vol. 34, pp 1-9. ASME International Mechanical Engineering Congress and Exposition, San Francisco, CA, November 12-17.

Katipamula, S. 1989. A study of the transient behavior during start-up of residential heat pumps. Ph. D. Dissertation. Texas A&M University, College Station.

Kim, M. H., and Bullard, C. W. 2001. Dynamic characteristics of a R-410A split air-conditioning system. *International Journal of Refrigeration.* 24: 652-659.

Kline, S. J., and McClintock, F. A. 1953. Describing uncertainties in single-sample experiments. *Mechanical Engineering*, 75 (1): 3-9.

McQuiston, F. C., Parker, J. D., and Spitler, J. D. 2000. *Heating, Ventilating, and Air Conditioning Analysis and Design.* 5th Edition. New York: Wiley.

Mulroy, W. J., and Didion, D. A. 1985. Refrigerant migration in a split-unit air conditioner. *ASHRAE Transactions*. 91 (1A): 193-206.

Murphy, W. E., and Goldschmidt, V. W. 1984. Transient response of air-conditioners – A qualitative interpretation through a sample case. *ASHRAE Transactions*. 90 (1B): 997-1008.

Muyshondt, A., Nutter, D., and Gordon, M. 1998. Investigation of a fin-and-tube surface as a contaminant sink. *ASHRAE IAQ '98*: 207-211.

Palani, M., O'Neal, D. L., and Haberl, J. 1992. The effect of reduced evaporator airflow on the performance of a residential central air conditioner. *Proceedings of the Eighth Annual Symposium on Improving Building Systems in Hot and Humid Climates.* Dallas, TX. May 13-14.

Rodriguez, A. 1995. Effect of refrigerant charge, duct leakage, and evaporator airflow on the high temperature performance of air conditioners and heat pumps. Master's Thesis. Texas A&M University, College Station.

Rodriguez, A., O'Neal, D., Davis, M., and Kondepudi, S. 1996. Effect of reduced evaporator airflow on the high temperature performance of air conditioners. *Energy and Buildings*. 24: 195-201.

Siegel, J. A., and Nazaroff, W. W. 2002. Modeling Particle Deposition on HVAC Heat Exchangers. Lawrence Berkeley National Laboratory, report no. LBNL 49339. Berkeley, California.

Wheeler, J. 2003. Function of the evaporator in the air-conditioning cycle." *Supply House Times,* March 2003.

APPENDIX A

AIR-SIDE CAPACITY UNCERTAINTY ANALYSIS: SAMPLE

CALCULATION

The total air-side capacity of the system was calculated based on evaporator air-side, condensate, and electrical power measurements. To determine how the uncertainty associated with each of these measurements propagated through the calculation of total air-side capacity, an uncertainty analysis was conducted, based on the method of Kline and McClintock (1953). According to this method, the uncertainty interval for a calculated variable that is a function of n independent variables, $R = R(x_1, x_2, ..., x_n)$, can be expressed as

$$w_R^2 = \left(\frac{\partial R}{\partial x_1} w_1 \right)^2 + \left(\frac{\partial R}{\partial x_2} w_2 \right)^2 + ... + \left(\frac{\partial R}{\partial x_n} w_n \right)^2 \tag{A.1}$$

where $w_1, w_2 ... w_n$ are the uncertainties of each independent variable $x_1, x_2, ..., x_n$, and w_R is the uncertainty of the calculated variable R.

The air-side capacity was calculated from an energy balance on the evaporator, given here as

$$\dot{Q}_{total,AS} = \dot{Q}_s + \dot{Q}_l - \dot{W}_{fan,evap} \tag{A.2}$$

where $\dot{Q}_{total,AS}$ is the total air-side capacity, $\dot{Q}_s$ is the sensible air-side capacity, $\dot{Q}_l$ is the air-side latent capacity, and $\dot{W}_{fan,evap}$ is the electrical power consumed by the evaporator

fan. Applying Eq. (A.1), the uncertainty associated with the total air-side capacity can be expressed as

$$w_{\dot{Q}_{total,AS}}^2 = \left(\frac{\partial \dot{Q}_{total,AS}}{\partial \dot{Q}_s} w_{\dot{Q}_s} \right)^2 + \left(\frac{\partial \dot{Q}_{total,AS}}{\partial \dot{Q}_l} w_{\dot{Q}_l} \right)^2 + \left(\frac{\partial \dot{Q}_{total,AS}}{\partial \dot{W}_{fan,evap}} w_{\dot{W}_{fan,evap}} \right)^2 \qquad (A.3)$$

where $w_{\dot{Q}_s}$, $w_{\dot{Q}_l}$, and $w_{\dot{W}_{fan,evap}}$ are the uncertainties in the air-side sensible, latent, and evaporator fan power measurements, respectively. Evaluating the partial derivatives in Eq. (A.3), it can be shown that

$$w_{\dot{Q}_{total,AS}}^2 = w_{\dot{Q}_s}^2 + w_{\dot{Q}_l}^2 + w_{\dot{W}_{fan,evap}}^2 \qquad (A.4)$$

In order to evaluate the uncertainty of the total air-side capacity, the uncertainty of the sensible capacity, latent capacity, and evaporator fan power must first be evaluated. The sensible capacity was calculated from the formula

$$\dot{Q}_s = \frac{\dot{V}}{v} c_p \left(T_{in} - T_{out} \right) \qquad (A.5)$$

Where $\dot{V}$ is the volumetric airflow rate, v is the specific volume of the air at the temperature used to calculate $\dot{V}$, c_p is the specific heat at constant pressure of air, T_{in} is the evaporator air inlet dry-bulb temperature, and T_{out} is the evaporator air outlet dry-bulb temperature. Using the ideal gas equation of state, Eq. (A.5) can be expressed as

$$\dot{Q}_s = \frac{P_a \dot{V}}{R_a T_{out}} c_p \left(T_{in} - T_{out} \right) \qquad (A.6)$$

where P_a is the partial pressure of air and R_a is the ideal gas constant for air.

For the steady-state tests, the latent capacity was based on the mass flow rate of condensate measured during a given testing cycle, which can be expressed as

$$\dot{Q}_l = \dot{m}_{cond} h_{fg,w} \tag{A.7}$$

where $\dot{m}_{cond}$ is the mass flow rate of the condensate and $h_{fg,w}$ is the enthalpy of vaporization for pure water evaluated at the inlet air dew point temperature. In practice, $\dot{m}_{cond}$ was determined by measuring the mass of condensate accumulated during a given testing period. As a result, the condensate mass flow rate in Eq. (A.7) can be expressed as an average value, which gives the latent capacity in the form of

$$\dot{Q}_l = \frac{\Delta m}{\Delta t}\bigg|_{cond} h_{fg,w} \tag{A.8}$$

where Δm is the mass of condensate measured over the time interval Δt.

To find the uncertainties associated with the sensible and latent capacities, Eq. (A.1) is applied to Eq. (A.6) and Eq. (A.8), respectively, which yields

$$w_{\dot{Q}_s}^2 = \left(\frac{\partial \dot{Q}_s}{\partial P_a} w_{P_a}\right)^2 + \left(\frac{\partial \dot{Q}_s}{\partial \dot{V}} w_{\dot{V}}\right)^2 + \left(\frac{\partial \dot{Q}_s}{\partial T_{in}} w_{T_{in}}\right)^2 + \left(\frac{\partial \dot{Q}_s}{\partial T_{out}} w_{T_{out}}\right)^2 \tag{A.9}$$

and

$$w_{\dot{Q}_l}^2 = \left(\frac{\partial \dot{Q}_l}{\partial \Delta m} w_{\Delta m}\right)^2 + \left(\frac{\partial \dot{Q}_l}{\partial \Delta t} w_{\Delta t}\right)^2 + \left(\frac{\partial \dot{Q}_l}{\partial h_{fg,w}} w_{h_{fg,w}}\right)^2 \tag{A.10}$$

The measurement of electrical power for the evaporator fan was a fundamental measurement in this experiment. Therefore, the uncertainty associated with electrical power is simply the total accuracy of the instrument and is expressed as

$$w_{\dot{W}_{fan,evap}} = \pm \varepsilon \times \dot{W}_{measured} \qquad (A.11)$$

where ε is the relative accuracy of the instrument (in percent of the measured reading) and $\dot{W}_{measured}$ is the measured electrical power.

With the exception of the partial pressure of air, P_a, the uncertainties of each variable in Eq. (A.9) and Eq. (A.10) are known. The uncertainty of the airflow rate ($w_{\dot{V}}$) was taken to be ±1.4% of the calculated airflow rate (ANSI/AMCA, 1999). The uncertainties of the air inlet and outlet dry-bulb temperatures ($w_{T_{in}}$ and $w_{T_{out}}$) were taken to be ±1°F (±0.5°C), which are within the limits required by the ANSI Standard MC96.1 (ANSI/ISA, 1982). The uncertainty of the condensate mass ($w_{\Delta m}$) was taken to be ±0.01 lbmw (±0.005 kgw), which was the smallest division on the digital scale used to measure the mass. The uncertainty of the testing period time ($w_{\Delta t}$) was taken to be ±1 min. or ±0.017 hr. The uncertainty of the enthalpy of vaporization of pure water ($w_{h_{fg,w}}$) was calculated over a range of temperatures spanning ±1°F (±0.5°C) of the dew point temperature at a given condition, but the variation was found to be less than 0.03% and deemed negligible. The accuracy (ε) of the electrical power transducer used to measure evaporator fan power was taken to be ±1% of the measured power and was used in Eq. (A.11) to determine the uncertainty of the evaporator fan power measurement ($w_{\dot{W}_{fan,evap}}$).

The uncertainty of the partial pressure of air (w_{P_a}) was found by considering an psychrometric relationship

$$P_a = P_{atm} - \phi P_{w,sat} \tag{A.12}$$

where P_{atm} is the atmospheric or barometric pressure, ϕ is the relative humidity of the air, and $P_{w,sat}$ is the water vapor saturation pressure. Based on Eq. (A.1), the uncertainty of the partial pressure of air can be expressed as

$$w_{P_a}^2 = \left(\frac{\partial P_a}{\partial P_{atm}} w_{P_{atm}} \right)^2 + \left(\frac{\partial P_a}{\partial \phi} w_\phi \right)^2 + \left(\frac{\partial P_a}{\partial P_{w,sat}} w_{P_{w,sat}} \right)^2 \tag{A.13}$$

The uncertainty of the atmospheric pressure ($w_{P_{atm}}$) was taken to be ±0.05 in. Hg (±0.17 kPa) and the uncertainty of the relative humidity (w_ϕ) was taken to be ±2% (provided by the manufacturer of the instrument). The uncertainty of the water vapor saturation pressure ($w_{P_{w,sat}}$) was determined from the multiple-constant equation used to calculate saturation pressure as a function of dry-bulb temperature, given here as

$$P_{w,sat} = \exp\left[\frac{C_8}{T} + C_9 + C_{10}T + C_{11}T^2 + C_{12}T^3 + C_{13}\ln(T) \right] \tag{A.14}$$

where T is the dry-bulb temperature in deg R and $P_{w,sat}$ is in psia. The constants used in this equation are defined in Table A.1.

Table A.1 – Constants for
$P_{w,sat}$ Equation.

Equation Constant	Value
C_8	-10440.4
C_9	-11.2946
C_{10}	-0.02702
C_{11}	1.289e-5
C_{12}	-2.478e-9
C_{13}	6.54597

Applying Eq (A.1) to Eq. (A.14) at the evaporator outlet, the uncertainty of the water vapor saturation pressure ($w_{P_{w,sat}}$) was found to be ±0.0098 psia (±0.068 kPa). The uncertainty of the partial pressure of air (w_{P_a}) was found with Eq. (A.13) to be ±0.026 psia (±0.179 kPa).

A sample uncertainty calculation was performed on the data from the cycle 4 95°F (35°C) outdoor steady-state test[*] conducted on Unit A2 in the coil fouling study (see Chapter VII). The data shown in Table A.2 were used in the sample calculation and represent average values for the steady-state test.

---

[*] ARI Standard 210/240 Test A

Table A.2 – Selected Data for Unit A2 in Cycle 4.

Variable	Value
T_{in}	79.99°F (26.7°C)
T_{out}	62.23°F (16.8°C)
$\dot{V}$	1219 ft^3/min (34.5 m³/min)
Δm_{cond}	7.98 lbmw (3.62 kgw)
Δt_{cycle}	1.00 hr
ϕ_{in}	51.2% RH
ϕ_{out}	75.3% RH
P_{atm}	29.94 in Hg (101.4 kPa)
$\dot{W}_{fan,evap}$	0.38 kW
$\dot{Q}_{total,AS}$	33,700 Btu/hr (9.88 kW)

The data shown in Table A.2 was used with the previously defined uncertainties in Eqs. (A.9), (A.10), and (A.11) to determine the uncertainty in the total air-side capacity, given by Eq. (A.4). The uncertainty of the total air-side capacity was found to be

$$w_{\dot{Q}_{total,AS}} = \pm 1,957 \ \text{Btu/hr} \ (\pm 0.58 \, \text{kW})$$

Therefore, the total air-side capacity for one of the cycle 4 steady-state tests conducted on Unit A2 can be formally expressed as

$$\dot{Q}_{total,AS} = 33,700 \pm 1,957 \, \text{Btu/hr} \ (9.88 \pm 0.58 \, \text{kW})$$

The uncertainty in this case is about ±6% of the calculated total capacity and represents the amount by which the total air-side capacity could be expected to be in error for a given set of measurements.

An uncertainty analysis for the transient cycling tests was not conducted. However, it should be noted that the uncertainty in air-side capacity for the transient cycling tests would be expected to be slightly higher than for the steady-state tests conducted in the evaporator airflow and condenser coil fouling studies. This is because the calculation of instantaneous latent capacity for the cycling tests was based on measurements made with relative humidity sensors at each data point. The uncertainty of the relative humidity measurements ($w_{\phi} = \pm 2\%$) is higher than the uncertainties of condensate mass and time measurements used to calculate latent capacity for the other studies. A previous uncertainty analysis performed on a test set-up similar to the one used in the cycling tests showed that the overall uncertainty in the total air-side capacity was around ±9% (Rodriguez, 1995).

APPENDIX B

CALCULATION OF THE DEGRADATION COEFFICIENT FOR THE TEST

AIR CONDITIONER USED IN THE CYCLING STUDY

A set of standardized tests were conducted on the test air conditioner used in the cycling study to ascertain the overall degradation in performance due to cycling. These were dry coil tests based on ARI Standard 210/240 Tests C and D. Test C was a steady state dry coil test with indoor conditions of 80°F (26.7°C) db and < 57°F (13.9°C) wb[*] and an outdoor condition of 82°F (27.8°C) db. Test D was a cycling dry coil test totaling 30 minutes in duration with the same indoor and outdoor conditions as Test C and a cycle time of 6 minutes on and 24 minutes off.

The degradation coefficient was calculated from the expression given by

$$C_D = \frac{1 - \dfrac{EER_{cyc,dry}}{EER_{ss,dry}}}{1 - \dfrac{Q_{cyc,dry}}{Q_{ss,dry}}} \tag{B.1}$$

where $EER_{cyc,dry}$ is the cyclic dry coil energy efficiency ratio (EER), $EER_{ss,dry}$ is the steady-state dry coil EER, $Q_{cyc,dry}$ is the total amount of energy removed due to cooling for the 6 minute cycle, and $Q_{ss,dry}$ is the total amount of energy removed due to steady-state cooling over a 6 minute period. The formal definitions for these parameters are as follows (ARI, 2003):

---

[*] The ARI Standard 210/240 states that the indoor wet-bulb temperature for tests C and D shall be sufficiently low so as to prevent any condensate from forming on the surface of the evaporator coils during the test.

$$EER_{cyc,dry} = \frac{\int_{t_{on}}^{t_{off}} \dot{Q}_{cyc,dry}\,dt}{\int_{t_{on}}^{t_{off}} \dot{W}_{cyc,elec}\,dt} \tag{B.2a}$$

$$EER_{ss,dry} = \frac{\overline{\dot{Q}}_{ss,total}}{\overline{\dot{W}}_{ss,elec}} \tag{B.2b}$$

$$Q_{cyc,dry} = \frac{60 \times \overline{\dot{V}} \times C_{pa} \times \Gamma}{\left[V_a' \times (1 + W_a)\right]} \tag{B.2c}$$

$$Q_{ss,dry} = \overline{\dot{Q}}_{ss,dry} \times \left(t_{off} - t_{on}\right) \tag{B.2d}$$

where $\dot{Q}_{cyc,total}$ (Btu/hr) is the instantaneous capacity for the cycling dry coil test, $\dot{W}_{cyc,elec}$ ($Watts$) is the instantaneous total electrical power consumption for the cycling test, $\overline{\dot{Q}}_{ss,total}$ (Btu/hr) is the average total capacity for the dry coil steady-state test, $\overline{\dot{W}}_{ss,elec}$ ($Watts$) is the total electrical power consumption of the system for the steady-state test, t_{off} and t_{on} ($hours$) are the off and on times of the cycle used in Test D, $\overline{\dot{V}}$ (ft^3/min) is the average airflow rate through the evaporator for Test C, C_{pa} ($Btu/lb \cdot °F$) is the specific heat at constant pressure of the evaporator inlet air-water mixture per pound of dry air, V_a' (ft^3/lbm) is the average specific volume of the air-water mixture used to determine the airflow rate, W_a ($lbmw/lbma$) is the average air inlet humidity ratio, and Γ ($°F \cdot hr$) is defined as

$$\Gamma = \int_{t_{on}}^{t_{off}} \left[T_{in}(t) - T_{out}(t)\right] dt \tag{B.3}$$

where $T_{in}(t)$ and $T_{out}(t)$ are the instantaneous evaporator air inlet and outlet temperatures, respectively.

The part load factor (PLF) can be expressed as the ratio of cyclic to steady-state EER for the dry coil tests, given by

$$PLF = \frac{EER_{cyc,dry}}{EER_{ss,dry}} \tag{B.4}$$

and the cooling load factor (CLF) can be expressed as the ratio of the cyclic to steady-state capacity for the dry coil tests, given by

$$CLF = \frac{Q_{cyc,dry}}{Q_{ss,dry}} \tag{B.5}$$

where the terms on the right-hand-side of Eqs. B.4 and B.5 are evaluated from Eqs. B.2. Thus, the degradation coefficient given by Eq. B.1 can be alternately expressed as

$$C_D = \frac{1 - PLF}{1 - CLF} \tag{B.6}$$

The PLF and CLF for the test air conditioner were found to be 0.993 and 0.902, respectively. The degradation coefficient C_D, based on Eq. B.6, was found to be 0.069. This indicates that the part-load performance of the test air conditioner was not significantly affected by cycling. Physically, these numbers show that if the test air conditioner is operating at about 90% of full load at part-load conditions, the EER will be around 99% of the steady-state value.

APPENDIX C

CONSIDERATIONS ON THE PEAK IN INSTANTANEOUS CAPACITY AND MOISTURE REMOVAL RATE FOR THE CYCLING TESTS

Some insight into the capacity overshoot of the system displayed in Figures 5.1 and 5.2 was obtained by considering both the refrigerant and air side conditions present in the evaporator unit during startup. Of particular interest was the cause of the peak in instantaneous total capacity and moisture removal rate around one minute after start-up. In fact, the peak in total capacity is actually due to the peak in moisture removal rate. The variation in instantaneous latent capacity during startup caused the total capacity to peak concurrently with moisture removal rate at approximately one minute after startup (see Figure 5.5).

The evaporator used in the cycling tests used a three row, three circuit coil. For a multiple-row coil, the refrigerant conditions and mass flow rate in each row can vary markedly from the other rows, making it difficult to predict certain operating characteristics of the coil, such as local coil surface temperature. The complexity of this situation only increases when the refrigerant dynamics during startup is considered. In order to gain some insight into the phenomenon of capacity overshoot observed in the data, the complexity of the evaporator coil was reduced by assuming the coil to have only one flow path; that is, one row or one circuit.

The amount of refrigerant superheating at the outlet of an evaporator in steady-state operation can be used by manufacturers as an alternate charging criterion to help reduce the chance of liquid slugging in the compressor (McQuisiton *et at.,* 2000). The

evaporator coil of an air conditioning system that is charged to maintain a certain

amount of refrigerant superheating will consist of two distinct thermal regions in steady-

state operation. For the idealized single row coil considered in this discussion, these two

thermal regions can be viewed as a refrigerant evaporating section and a refrigerant

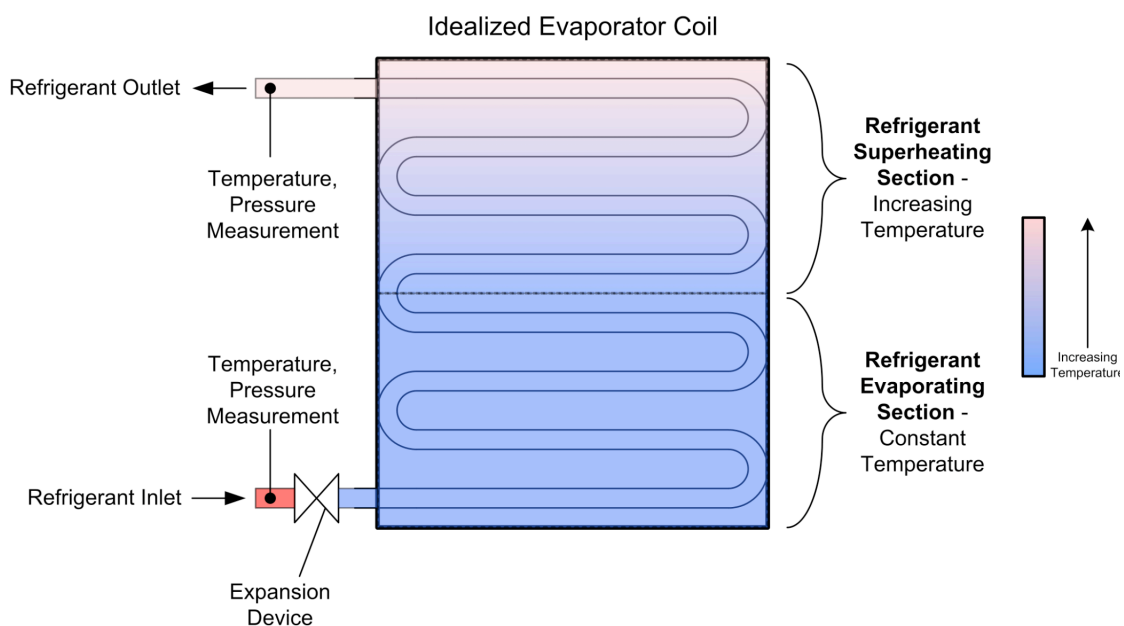superheating section. This concept is illustrated in Figure C.1.

Figure C.1 – Schematic of an Idealized Evaporator Coil.

The *refrigerant evaporating section* of the coil shown in Figure C.1 consists of a

lower section of the coil in which two-phase refrigerant is evaporated to saturated vapor.

As a result of the phase change, the coil surface temperature in this section is uniform

and near the saturation temperature of the refrigerant at the evaporator pressure. The

refrigerant superheating section of the coil consists of an upper section of the coil

beginning at the point where the refrigerant evaporating section ends. After this point,

the refrigerant is superheated gas and the coil surface temperature of the refrigerant

superheating section is not uniform, but increasing to the end of the coil, as shown in Figure C.1.

Depending on the degree of superheating, an upper portion of the coil in the refrigerant superheating section may rise above the air dew point temperature. In this case, that portion of the coil surface will be dry and not contribute to dehumidification. This is illustrated in Figure C.2.
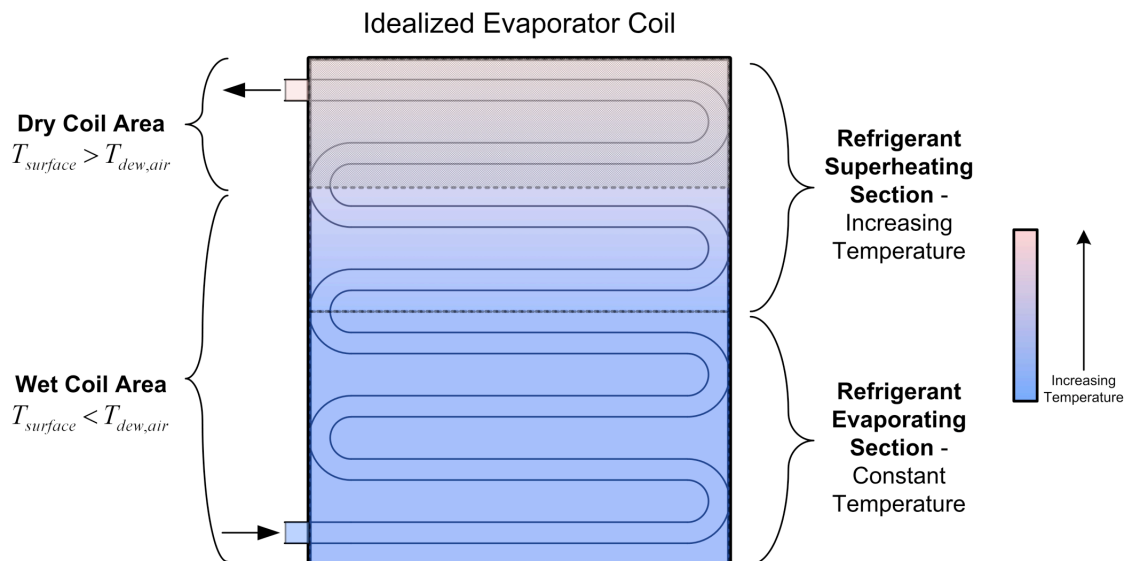

Figure C.2 – Wet and Dry Coil Areas for an Idealized Evaporator Coil.

During startup, the wet and dry coil areas, as well as the refrigerant evaporating and superheating sections, can vary in size due to refrigerant dynamics. In the case where refrigerant superheating results in a dry section of the coil, a higher refrigerant outlet temperature would correspond to a larger of dry coil area. These idealized parameters have been considered indirectly by studying the refrigerant conditions at the inlet and outlet of the evaporator during startup. The refrigerant saturation and outlet

temperatures, moisture removal rate, and air inlet dew point temperature for the evaporator during the 15-minute cycling test at the 50% RH condition are shown in Figure C.3. The refrigerant outlet temperature was measured at the point illustrated in Figure C.1. Note that the difference between the measured refrigerant outlet temperature and the saturation pressure is the degree of superheating.

Test System: 3 ton (10.5 kW) A/C, orifice expansion,
                            scroll compressor, R-22
Evaporator Airflow: 1200 ft^3/min (34 m^3/min)
Indoor Conditions: 80°F (26.7^{o}C) db, 50% RH
Outdoor Condition: 95°F (35°C) db
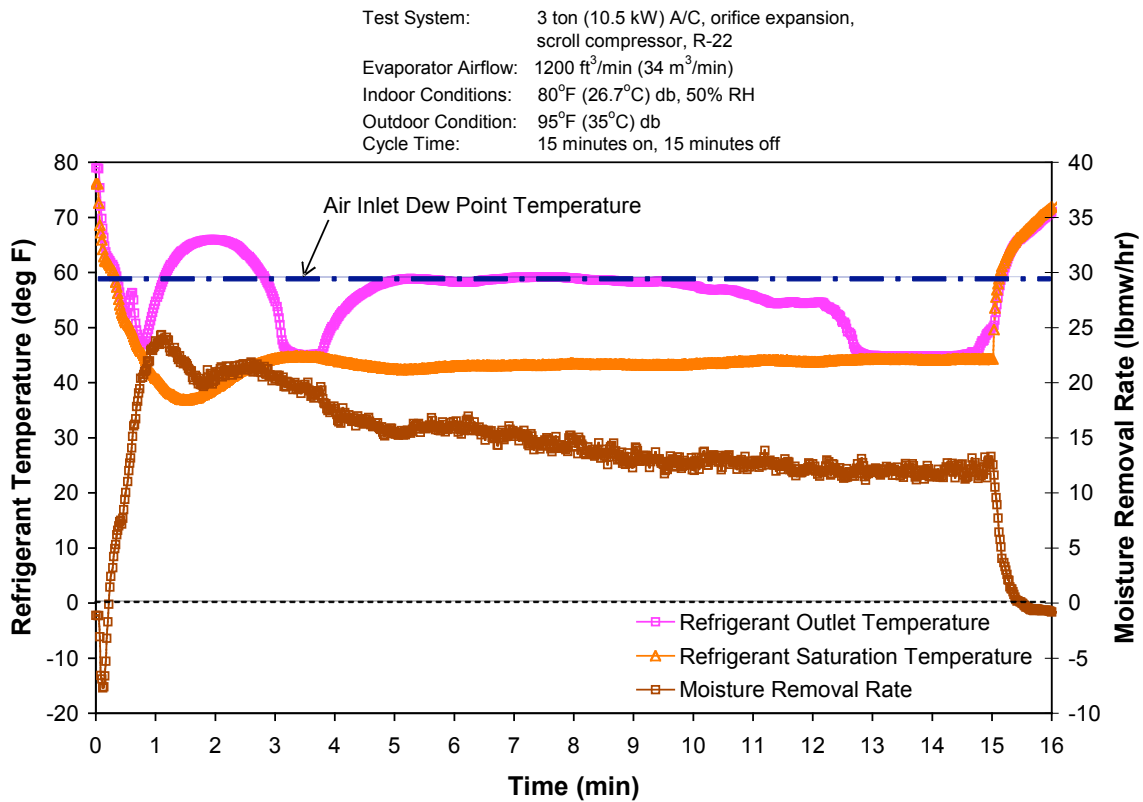Cycle Time: 15 minutes on, 15 minutes off

Figure C.3 – Evaporator Refrigerant Temperatures and Moisture Removal Rate
for a 15 Minute Cycle at 50% Indoor Relative Humidity

The first and largest peak in moisture removal rate in Figure C.3 coincided with when the refrigerant outlet temperature increased above the air dew point temperature. This indicates that at approximately 1 minute after startup, refrigerant superheating

reached a sufficient level to heat an upper portion of the coil above the air dew point temperature, which caused that portion to stop dehumidifying (i.e. the dry coil area shown in Figure C.2 began to increase from zero). The maximum refrigerant outlet temperature coincided with a localized minimum in the moisture removal rate at around 2 minutes. This indicates that at approximately 2 minutes after startup, the dry coil area had reached a maximum, which corresponds to the observed drop in dehumidification capacity at that time. A localized maximum occurred for the moisture removal rate at approximately 2.8 minutes after startup and was seen to coincide with when the refrigerant outlet temperature decreased below the air dew point temperature. This indicates that as the refrigerant outlet temperature decreased between 2 and 2.8 minutes after startup, more of the coil surface began to contribute to dehumidification (i.e. the dry coil area shown in Figure C.2 was decreasing). After 2.8 minutes, the refrigerant outlet temperature decreased below the air dew point temperature, indicating that the entire coil was providing some level of dehumidification (i.e. the dry coil area shown in Figure C.2 was zero). Between 3.2 and 3.8 minutes after startup, refrigerant superheating was zero, indicating that the entire coil surface temperature was uniform during this period. However, after 2.8 minutes the moisture removal rate began to steadily decrease towards the steady-state value, indicating that dehumidification capacity wasn't as strongly affected by instantaneous variations in coil surface temperature as during the first 2.8 minutes of the cycle. An explanation for the behavior seen after 2.8 minutes might be that since some moisture drains from the evaporator coil during the off-cycle, a certain amount of moisture must be accumulated during the next on-cycle before equilibrium is established and dehumidification reaches steady-state. The amount of moisture retention required to establish equilibrium would be dependent on the surface characteristics and geometry of the coil. While accumulation occurs, the

dehumidification capacity of the system would be enhanced, but decreasing towards a steady-state value. Thus, the dehumidification behavior can be described by refrigerant dynamics during the first 2.8 minutes of the cycle and partially explained by physical aspects of the coil during the later part of the cycle.

The refrigerant temperatures and moisture removal rate for all tests were similar to those shown in Figure C.3. The following observations were made for all tests:

1. The maximum moisture removal rate occurred at approximately 1 minute after startup and coincided with the time where the refrigerant outlet temperature increased above the air inlet dew point temperature.

2. The refrigerant outlet temperature decreased below the air inlet dew point temperature between 2.8 and 3 minutes after startup for, which coincided with the time the moisture removal rate began to decrease towards steady-state.

3. The moisture removal rate was not strongly affected by variations in coil surface temperature after about 2.8 minutes into the cycle.

VITA

Jeffrey Brandon Dooley was born on January 16, 1979 in Dallas, Texas, USA. He graduated from Lone Oak High School in 1997 and began undergraduate study at Texas A&M University-Commerce later that year. In 1999, he transferred to Texas A&M University in College Station and graduated with honors in 2002 with a Bachelor of Science degree in Mechanical Engineering. In 2003, he enrolled in the Master of Science program in the Department of Mechanical Engineering at Texas A&M University.

Mr. Dooley's permanent address is: 3711 FM 513 South, Lone Oak, TX, 75453.